Inferring and comparing structural parcellations of the human brain using diffusion MRI

Guillermo Alejandro Gallardo Diez

UNIVERSITÉ CÔTE D'AZUR

ÉCOLE DOCTORALE
SCIENCES ET TECHNOLOGIES DE L'INFORMATION ET DE LA COMMUNICATION

THÈSE DE DOCTORAT

Construction et Comparaison de Parcellisations Structurelles Cérébrale par Imagerie de Diffusion

Guillermo GALLARDO

Inria Sophia Antipolis – Méditerranée, Équipe-Projet Athéna

Présentée en vue de l'obtention du grade de docteur en Automatique et Traitement du Signal
et des Images **d'**Université Côte d'Azur

Dirigée par : Rachid Deriche
Co-encadrée par : Demian Wassermann

Date probable de soutenance :
21/12/2018

Devant le jury, composé de :
Olivier Coulon, Directeur de Recherche, CNRS, Aix-Marseille University - Rapporteur
Rachid Deriche, Directeur de Recherche, Inria Sophia Antipolis - Directeur
Bertrand Thirion, Directeur de Recherche, Inria Saclay IdF - Examinateur
Michel Thiebaut de Schotten, Directeur de Recherche, CNRS, ICM, Paris - Rapporteur
Ragini Verma, Professeur, SBIA, University of Pennsylvania - Examiner
Demian Wasserman, Chargé de Recherche, Inria Saclay IdF – Co-Encadrant
Alfred Anwander, Chargé de Recherche, Max Planck Institute for Human Cognitive and Brain Sciences, Germany

Contents

Résumé

Comprendre l'organisation de la connectivité structurelle du cerveau ainsi que comment celle-ci contraint sa fonctionnalité est une question fondamentale en neuroscience. L'avènement de l'Imagerie par Résonance Magnétique de diffusion (IRMd) a permit l'estimation de la connectivité des neurones in vivo. Dans cette thèse, nous profitons de ces avancées pour: étudier l'organisation structurelle du cerveau; étudier la relation entre la connectivité, l'anatomie et la fonction cérébrale; identifier les régions corticales correspondantes d'un sujet à un autre; et inférer la connectivité en présence de pathologie. Cette thèse contient trois contributions majeures. La première est un modèle pour la connectivité axonale et une technique efficace pour diviser le cerveau en régions de connectivité homogène. Cette technique de parcellisation permet de diviser le cerveau tant pour un seul sujet que pour une population. Les parcelles résultantes sont en accord avec les parcellations anatomiques, structurelles et fonctionnelles existant dans la littérature. La seconde contribution de cette thèse est une technique qui permet d'identifier les régions correspondantes d'un sujet à un autre. Cette technique, basée sur le transport optimal, offre une meilleure performance que les techniques courantes. La troisième contribution est une technique de segmentation, dite multi-atlas, pour identifier les faisceaux d'axones de la matière blanche de patients atteints d'une pathologie cérébrale. Comme les techniques existantes, notre approche utilise l'information spatiale provenant d'atlas de sujets sains, mais pondère celle-ci avec l'information d'IRMd du patient. Nous montrons que notre technique obtient de meilleurs résultats que les méthodes non pondérées.

Mots-clés: Parcellisations Structurelles, Imagerie de Diffusion

Abstract

Understanding how brain connectivity is organized, and how this constrains brain functionality is a key question of neuroscience. The advent of Diffusion Magnetic Resonance Imaging (dMRI) permitted the in vivo estimation of brain axonal connectivity. In this thesis, we leverage these advances in order to: study how the brain connectivity is organized; study the relationship between brain connectivity, anatomy, and function; find correspondences between structurally-defined regions of different subjects, and infer connectivity in the presence of a brain's pathology. We present three major contributions. Our first contribution is a model for the long-range axonal connectivity, and an efficient technique to divide the brain in regions with homogeneous connectivity. Our parceling technique can create both single-subject and groupwise structural parcellations of the brain. The resulting parcels are in agreement with anatomical, structural and functional parcellations extant in the literature. Our second contribution is a method to find correspondence between structural parcellations of different subjects. Based on Optimal Transport, it performs significantly better than the state-of-the-art ones. Our third contribution is a multi-atlas technique to infer the location of white-matter bundles in patients with a brain pathology. As existent techniques, our approach aggregates spatial information from healthy subjects, our novelty is to weight such information with the diffusion image of the patient. We show that our technique achieves better results than the non-weighted methods.

Key words: Structural Parcellation, Diffusion MRI

Dedications

To my family, with love

Introduction

Composed of billions of interconnected neurons, the brain is a highly complex biological machine. Untangling this network is the main goal of neuroscience, a task that has proven to be arduous. The problem is two fold. First, it is not feasible to characterize cellular function or axonal connectivity at the scale of the brain with current approaches. Second, even if we could characterize the neural network at a cellular level, studying it is unrealistic given the huge amount of neurons in the brain[1]. These current technical limitations highlight the need to abstract the complexity of the brain's neuronal network before studying it.

Brain parcellation is a way of dimensionality reduction. Parceling the brain allows us to abstract the interaction between billions of neurons into a tractable number of interacting regions. Accumulating evidence suggest that regions with distinct function or cytoarchitecture also possess distinct axonal connectivity[2;3;4;5]. Hence, understanding how the cortex is arranged based on its axonal connectivity could provide key information in unraveling brain organization.

Cerebral dissections[6;7;8], and the injection of chemical markers[9;10] used to be the only way to map brain axonal connectivity. Such methodologies are highly invasive and can only be used in post-mortem studies. Nowadays, the advent of Diffusion Magnetic Resonance Imaging (dMRI) allows to non-invasively quantify the diffusion of water molecules in live tissue as the white-matter. Under normal unhindered conditions, water particles diffuse randomly in a process known as Brownian motion. However, in the white matter, water molecules are constrained, and can only diffuse inside and along axonal bundles. Due to this phenomenon, dMRI is able to capture information about the structural organization of the brain. Building on top of this, tractography algorithms reconstruct white matter bundles in the brain, allowing to estimate the brain's axonal connectivity.

In this thesis, we leverage recent advances in dMRI and tractography algorithms in order to: study how the brain connectivity is organized; study the relationship between brain connectivity, anatomy, and function; find correspondences between structurally-defined regions of different subjects, and infer connectivity in the presence of a brain's pathology. We present three major contributions.

The first contribution is a parsimonious model for the long-range axonal connectivity (extrinsic connectivity), and an efficient technique to parcellate the brain in regions with homogeneous extrinsic connectivity[11]. Our connectivity model is based on histological results obtained in the macaque brain, and accounts for the across-subject variability in the human brain connectivity. Our parcellation technique uses a hierarchical clustering approach, letting us comprise multiple granularities of the same brain parcellation. Also, our technique can create both single subject and groupwise parcellations of the whole cortex, allowing to study brain connectivity at the single subject and at the population level. While our technique is solely based on the brain's structural connectivity, our resulting parcels are in agreement with anatomical, structural and functional parcellations extant in the literature. Our technique helps to lower the gap between structural connectivity and brain function, since some of our pure structural parcels show good overlapping with responses to functional tasks.

The second contribution is a technique to find correspondence between structural parcellations of different subjects[12]. Even when produced by the same technique, parcellations tend to differ in the number, shape, and spatial localization of parcels across subjects. Matching these parcels across subjects is an open problem in neuroscience. To solve it, we propose a parcel matching method based on Optimal Transport. We test its performance on different parcellations, and compare it against state of the art matching techniques. We show that our method achieves the highest number of correct matches. Our technique could help to study properties of structurally defined areas, when they do not have high spatial coherence across subjects. Also, it could help to understand the link between different brain atlases, and improve the comparisons of cortical areas between higher primates[13].

The third contribution is a multi-atlas technique to infer the location of white-matter bundles in patients with a brain pathology[14]. Lesions in the cortex or white matter disrupt the normal functioning of the brain. Some white matter pathologies, such as focal lesions or traumatic brain injury, hampers tractography, difficulting to infer which pathways are affected. We present a technique that infers the affected tracts by aggregating spatial information from healthy subjects while taking into account the diffusion information of the patient. Particularly, we register the tracts of each healthy subject to the patient, and make each healthy patient's 'vote' for a tract on each voxel of the DWI image of the patient. Our technique weights the vote of each subject based on how the voted pathway is supported by the patient's diffusion data, Meaning, if the diffusion data of our patient is consistent with the direction of the voted pathway, the vote has a higher weight. We show that our technique

achieves higher precision than Majority Voting[15] at the cost of having lower sensitivity.

Organization of this Thesis

This thesis is divided in two parts: Background and Contributions. In the Background chapters we give a brief introduction to neuroanatomy, non-invasive imaging techniques, and brain parcellation. In the Contributions chapters we introduce our parceling technique, our matching technique and our multi-atlas technique. We now present the outline of each chapter.

Part I: Background

Chapter 1: Introduction to Brain Cytoarchitecture, Neuroanatomy and Brain Function. In this chapter we cover the basic aspects of cellular composition, morphology and function of the human brain. We start with a brief introduction to the human nervous system, in order to understand the biological context of the brain. Then, we study the brain from both a microscopic and a macroscopic view. In the microscopic view, we explain the cellular composition of the brain and how it's organized. In the macroscopic view, we zoom out and make a review of the most important divisions and anatomical landmarks of the brain. Finally, we describe the functional role of some of these gross anatomical divisions.

Chapter 2: Introduction to Non-invasive Imaging Techniques. In this chapter, we start by introducing some concepts in nuclear physics and explain how they are applied in MRI to study the human brain. Then, we explain how modifying the acquisition sequences allows to study the physical process of diffusion, enabling to estimate the location of tracts in the white-matter. Finally, we make a brief introduction to how to detect brain activation in response to functional or cognitive tasks in the brain using Functional MRI.

Chapter 3: Mapping the Brain: A review of brain parcellations. Neuroscientists have long thought of the brain as a mosaic of interconnected regions. As of today, it's not clear that a unique and universal division of the human brain exists. Different modalities have been used to study the brain, deriving in different parcellations. In this chapter, we review parcellations created based on different criteria. We briefly explain the methodologies behind them, and discuss in which case to use them.

Part II: Contributions

Chapter 4: Groupwise Structural Parcellation of the Whole Cortex: A Logistic Random Effects Model Based Approach In this chapter, we propose a parsimonious model for the extrinsic connectivity and an efficient parceling technique based on clustering of tractograms. Our parcellation technique allows the creation of single subject and groupwise parcellations of the whole cortex. We show that our technique creates parcellations in agreement with anatomical, structural and functional parcellations extant in the literature.

Chapter 5: Solving the Cross-Subject Parcel Matching Problem using Optimal Transport. In this chapter, we propose a parcel matching method based on Optimal Transport. We test its performance by matching parcels of the Desikan atlas, parcels based on a functional criteria and structural parcels. We compare our technique against three other ways to match parcels which are based on the Euclidean distance, the cosine similarity, and the Kullback-Leibler divergence. Our results show that our method achieves the highest number of correct matches.

Chapter 6: Inferring the Localization of White–Matter Tracts using Diffusion Driven Label Fusion In this chapter, we introduce a label-fusion technique to infer the location of brain pathways on a target subject by aggregating information of template subjects. Our technique adds diffusion-based weights to a Majority Voting scheme. The weigh of each vote is based on how the voted pathway is supported by the target's diffusion data. Meaning, if the diffusion data of our target is consistent with the direction of the voted pathway, the vote has a higher weight. We show that our technique achieves higher precision than Majority Voting at the cost of having lower sensitivity.

Bibliography

[1] G. Gong, Y. He, L. Concha, C. Lebel, D. W. Gross, A. C. Evans, and C. Beaulieu, "Mapping anatomical connectivity patterns of human cerebral cortex using in vivo diffusion tensor imaging tractography," *Cereb. Cortex*, vol. 19, no. 3, pp. 524–536, 2009.

[2] R. E. Passingham, K. E. Stephan, and R. Kötter, "The anatomical basis of functional localization in the cortex," *Nat. Rev. Neurosci.*, vol. 3, pp. 606–616, aug 2002.

[3] H. Johansen-Berg, T. E. Behrens, M. D. Robson, I. Drobnjak, M. F. S. Rushworth, J. M. Brady, S. M. Smith, D. J. Higham, and P. M. Matthews, "Changes in connectivity profiles define functionally distinct regions in human medial frontal cortex.," *Proc. Natl.*

Acad. Sci. U. S. A., vol. 101, no. 36, pp. 13335–40, 2004.

[4] C. J. Honey, O. Sporns, L. Cammoun, X. Gigandet, J. P. Thiran, R. Meuli, and P. Hagmann, "Predicting human resting-state functional connectivity," *Proc. Natl. Acad. Sci.*, vol. 106, no. 6, pp. 1–6, 2009.

[5] S. B. Eickhoff, S. Jbabdi, S. Caspers, A. R. Laird, P. T. Fox, K. Zilles, and T. E. J. Behrens, "Anatomical and Functional Connectivity of Cytoarchitectonic Areas within the Human Parietal Operculum," *J. Neurosci.*, vol. 30, no. 18, pp. 6409–6421, 2010.

[6] T. Meynert, "Der Bau der Gross-Hirnrinde und seine örtlichen Verschiedenheiten, nebst einem pathologischanatomischen Corollarium," *Neuwied, JH Heuser'sche Ver- lagsbuchhandlung*, pp. 1–68, 1872.

[7] K. Brodmann, *Vergleichende Lokalisationslehre der Großhirnrinde in ihren Prinzipien dargestellt auf Grund des Zellaufbaues*. Leipzig: Barth, 1909.

[8] H. Gray, *Gray's Anatomy of the Human Body*. Lea & Febiger, 1918.

[9] J. D. Schmahmann and D. N. Pandya, *Fiber Pathways of the Brain*, vol. 1. Oxford University Press, apr 2006.

[10] K. E. Stephan, "The history of CoCoMac," *Neuroimage*, vol. 80, pp. 46–52, 2013.

[11] G. Gallardo, W. Wells, R. Deriche, and D. Wassermann, "Groupwise structural parcellation of the whole cortex: A logistic random effects model based approach," *Neuroimage*, pp. 1–14, feb 2017.

[12] G. Gallardo, N. Gayraud, R. Deriche, M. Clerc, S. Deslauriers-Gauthier, and D. Wassermann, "Solving the Cross-Subject Parcel Matching Problem Using Optimal Transport," *Med. Image Comput. Comput. Assist. Interv. – MICCAI 2018. Lect. Notes Comput. Sci.*, no. 11070, 2018.

[13] R. B. Mars, S. N. Sotiropoulos, and R. E. Passingham, "Whole brain comparative anatomy using connectivity blueprints," *bioRxiv*, p. 245209, 2018.

[14] G. Gallardo, B. Sylvain, and D. Wassermann, "Diffusion Driven Label Fusion for White Matter Multi-Atlas Segmentation," *OHBM 2018 - Organ. Hum. Brain Mapp.*, 2018.

[15] L. Xu, A. Krzyżak, and C. Y. Suen, "Methods of Combining Multiple Classifiers and Their Applications to Handwriting Recognition," *IEEE Trans. Syst. Man Cybern.*, vol. 22, no. 3, pp. 418–435, 1992.

Part I

Background

Chapter 1
Introduction to Brain Cytoarchitecture, Neuroanatomy and Brain Function

1.1. Overview

In this chapter we cover the basic aspects of cellular composition, morphology and function of the human brain. We start with a brief introduction to the human nervous system, in order to understand the biological context of the brain. Then, we study the brain from both a microscopic and a macroscopic view. In the microscopic view, we explain the cellular composition of the brain and how it's organized. In the macroscopic view, we zoom out and make a review of the most important divisions and anatomical landmarks of the brain. Finally, we describe the functional role of some of these gross anatomical divisions. This chapter is heavily based on the books: Neuroscience[1] ; Clinical Neuroscience[2] and Atlas of Human Brain Connections[3]. We encourage the reader to further deepen each subject using those books.

1.2. The Human Nervous System

Every organ in our body works as part of a larger system of organs interacting towards a common goal. Our brain, the main actor of this thesis, forms part of the nervous system, the system concerned with concious life. The nervous system is the most complicated and highly organized of the various systems which make up the human body[4]. It is the mechanism concerned with the analysis and integration of internal and external stimuli, and with the reactions and adjustments of the organism in response to them. It is anatomically divided into two parts, central and peripheral 1.1. The central nervous system (CNS) consist of the brain and the spinal cord. The peripheral nervous system (PNS) consists of a series of nerves that link receptors on the body with the central nervous system. These nerves are associated with the functions of the special and general senses and with the voluntary movements of the body. As a system, the PNS transmits stimuli from the environment to circuits within the spinal cord and the brain, which are integrated alongside internal stimuli in order to produce a response. This response travels back trough the PNS and is translated into body movement or the adjustment of internal organs (fig. 1.1).

In this thesis we will focus only on the brain. We start by talking about its cellular composition and internal organization.

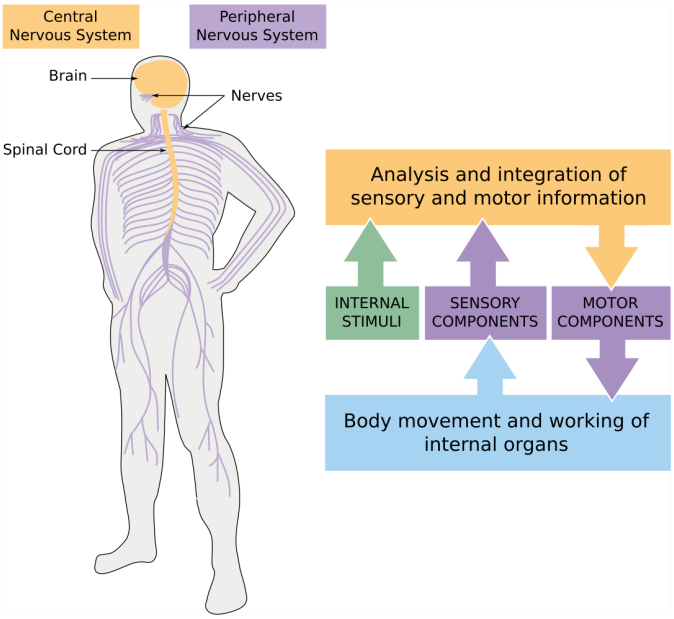

Figure 1.1: The nervous system is anatomically divided in two: The central nervous system (CNS) and the peripheral nervous system (PNS). On the left we show a simplified representation of the CNS and PNS in the human body. On the right we schematize how these systems interact between them: internal and external stimuli gathered by the PNS and sent to process to the CNS, which then decides how to respond. This image was adapted from the book Neuroscience[1].

1.3. A Microscopic View of the Human Brain

At a microscopic level, the human brain is composed by cells that can be divided in two broad categories: nerve cells (or neurons), and supporting cells called neuroglia (or simply glia). Nerve cells (Fig. 1.2 A, B, C) are discrete entities that communicate with one another by means of specialized contacts called "synapses"[1]. Supporting cells (Fig. 1.2 D), in contrast, are not capable of electrical signaling; nevertheless, they have several essential functions in the developing and adult brain such as maintaining the ionic milieu of nerve or modulating the rate of nerve signal propagation. The human brain possesses on average 86.06 +/- 8.12 billion neurons and 84.61 +/- 2.17 billion nonneuronal cells, making it a linearly scaled-up primate brain in its cellular composition[5]. In terms of distribution, 80% of the neurons are present in the cerebellum, and approximately all the rest are in the cortex. Meanwhile, 80% of the nonneuronal cells are

in the cortex, with almost all the rest in the cerebellum.

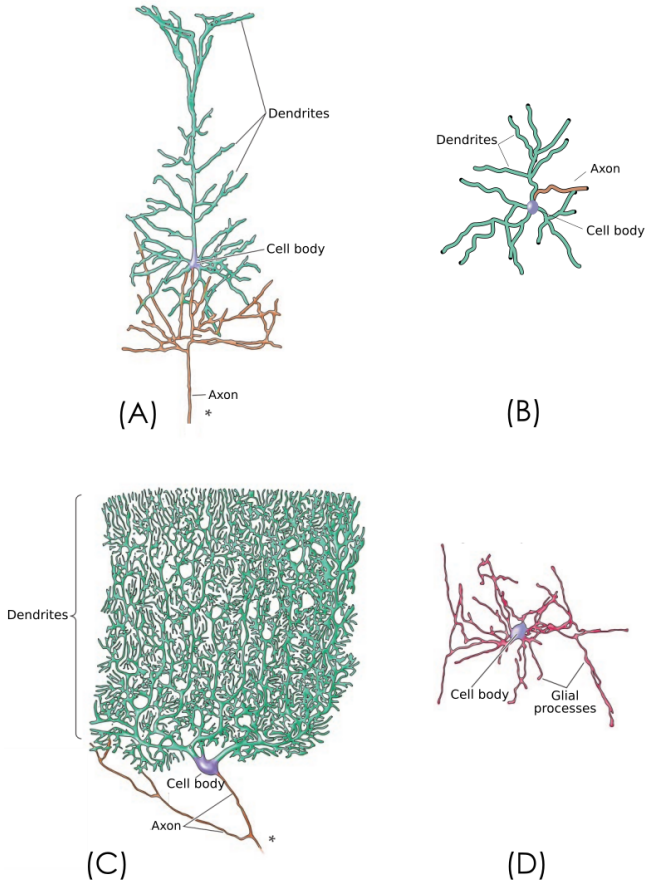

Figure 1.2: Different types of neuronal and nonneuronal cells: (A) pyramidal neuron, (B) granule neuron, (C) neuron with a highly complex arborization, and (D) Neuroglia, or supporting cell. This image was adapted from the book Neuroscience[1].

Neurons

The basic cellular organization of neurons resembles that of other cells; however, they are clearly distinguished by specialization for intercellular communication. This attribute is apparent in their overall morphology, in the specific organization of their membrane components for electrical signaling, and in the structural intricacies of the contacts between neurons. The spectrum of neuronal geometries ranges from a small minority of cells that lack dendrites altogether to neurons with complex dendritic arborizations (i.e. Fig. 1.2 C). The complexity of the dendritic arbor constrains the amount of neurons with who a neuron can communicate, ranging from one or few, to a commensurately larger number of other neurons.

From a functional point of view, we can distinguish two type of neurons: excitatory and inhibitory. Excitatory neurons release the neurotransmitter glutamate to send signals to other cells. Inhibitory neurons release gamma-Aminobutryc acid, in order to reduce neuronal excitability throughout the nervous system[6].

From a morphologic point of view, neurons can be divided in two major types: granule neurons and pyramidal neurons[1]. Granule cells are star-shaped neurons with a typical diameter of less than 20μm. They are multipolar neurons, this is, neurons that posses a single axon and many dendrites. Granule cells are either excitatory or inhibitory, and mostly have purely 'intrinsic' axons, this is, they make only short-range, local connections[1]. On the other hand, pyramidal neurons have large, pyramid-shape bodies that range from 20-120μm. Pyramidal neurons are multipolar and excitatory neurons, and they comprise about two-thirds of all neurons in the mammalian cerebral cortex. On top of their numerical dominance, pyramidal neurons are also "projection neurons", meaning that their axons are often "extrinsic", making long connections[1].

Finally, neurons on a circuit can be classified based on their role in a neuronal circuit. Nerve cells that carry information toward the circuit are called afferent neurons; nerve cells that carry information away from the circuit are called efferent neurons. Interneurons, or local circuit neurons, only participate in the local aspects of a circuit.

Neuroglial

Neuroglial cells are quite different from nerve cells. Glial cells do not participate directly in synaptic interactions and electrical signaling, but instead provide support to define synaptic contacts and maintain the signaling abilities of neurons[1]. The term glia (from the Greek word $\gamma\delta\iota\alpha$ meaning "glue") reflects the nineteenth-century presumption that these cells held the nervous system together in some way. The term has survived despite the lack of evidence that glia actually bind neurons together. Glial roles that are well-established include maintaining the ionic milieu of nerve cells, modulating the rate of nerve signal propagation, modulating synaptic action by controlling the uptake of neurotransmitters at or near the synaptic cleft, providing a scaffold for some aspects of neural development, and aiding in the recovery from neural injury[1].

Neuronal Organization: Cortical Layers

Cortical cells are arranged in horizontal layers, or laminae[7]. More than 90% of the cerebral cortex has a characteristic six-layered composition[8]. Layer I is the molecular layer, which contains very few neurons; layer II the external granular layer; layer III the external pyramidal layer; layer IV the internal granular layer; layer V the internal pyramidal layer; and layer VI the multiform, or fusiform layer. Each cortical layer contains different pre-

dominant neuronal shapes, sizes and density as well as different organizations of nerve fibers[8]. The layer structure varies spatially in regard to cell organization (cytoarchitecture) and myelination (myeloarchitecture), defining distinct cortical areas which are likely to perform different functions[7;9].

Depending on the layers present, the cortex can be divided in agranular, dysgranular and granular regions[10]. The agranular cortex is characterized by not having an internal granule cell layer (layer IV). The granular cortex has two layers of granule cells, an external granular layer (II) and an internal granular layer (IV). Dysgranular cortex has fewer granule cells, which are grouped in a single layer or as distinct clusters.

The fine study of the cortical composition is called Cytoarchitectonics. We discuss the topic of parceling the brain based on cytoarchitecture in chapter 3, for now it is sufficient to say that the cerebral cortex is divided into more than fifty regions based on its cellular composition under the microscope. The most known and frequently cited cytoarchitectural organization is that of Brodmann[11] (Fig. 1.3).

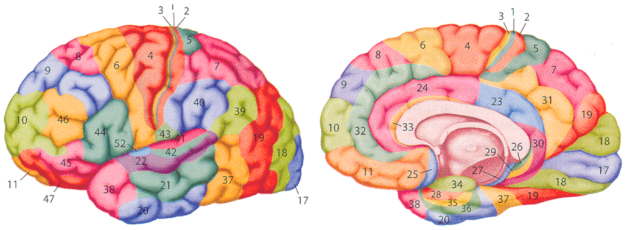

Figure 1.3: The cerebral cortex is divided into more than 50 regions based on its cellular composition. Brodmann's[11] parcellation is the most known and cited one. This image was adapted from the website http://fourier.eng.hmc.edu/e180/lectures/visualcortex/node5.html

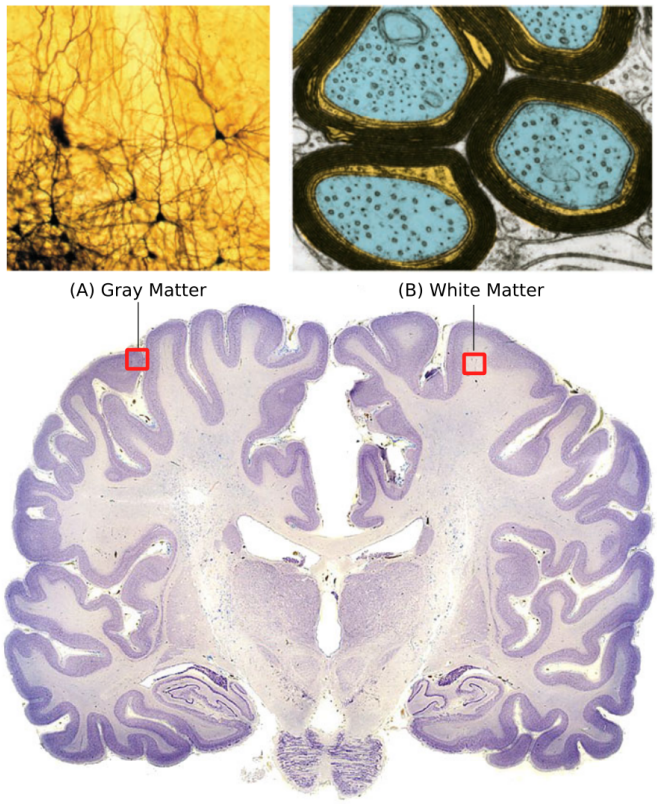

Figure 1.4: Brain tissue can be divided into grey and white matter. (A) Grey matter is composed mainly of cell bodies. (B) White matter is made up mostly of packed axons. This image was adapted from the brain museum (www.brainmuseum.org), and the book Neuroscience[1]

1.4. A Macroscopic View of the Human Brain

In the previous section, we talked about neurons and how they are specialized to transmit information. Indeed, neurons never function in isolation; they are organized into circuits or structures that process specific kinds of information. The brain tissue comprises a diverse collection of these neural structures, each with a distinctive shape and an intricate internal architecture.

Brain tissue can be divided into grey and white matter[2] (Fig. 1.4). Grey matter is composed mainly of neuronal cell bodies, dendrites and synapses. It is sharply demarcated from the adjacent white matter, which is made up mostly of axons travelling from grey matter to grey matter, or to other parts of the nervous system. The pale colour of white matter is due to the lipid-rich myelin sheath that surrounds axons and enhances their conduction velocity[2].

Anatomy of the Grey Matter

The grey matter is composed of: the cerebral cortex; the cerebellum; structures within the white matter, called subcortical structures (e.g. thalamus; hypothalamus; etc), and the grey column, which traverses the spinal cord. In this thesis we will mainly focus on the cerebral cortex.

The cerebral cortex is the most important structure of the gray matter and plays a major role in cognitive functions. It is a layered sheet of tissue, 2–3 millimetres thick, with highly convoluted folds. It's hypothesized that the mechanical tension created by neuronal connections during development is a major driving force of these folds[12]. An advantage of the folding pattern, is that it allows to fit a large surface area within the available cranial volume. In particular, the human cerebral cortex attains a surface area of about 1600 cm^2, nearly three times what it would be in the absence of convolutions[12]. The grooves and ridges created by this folding process are called sulci

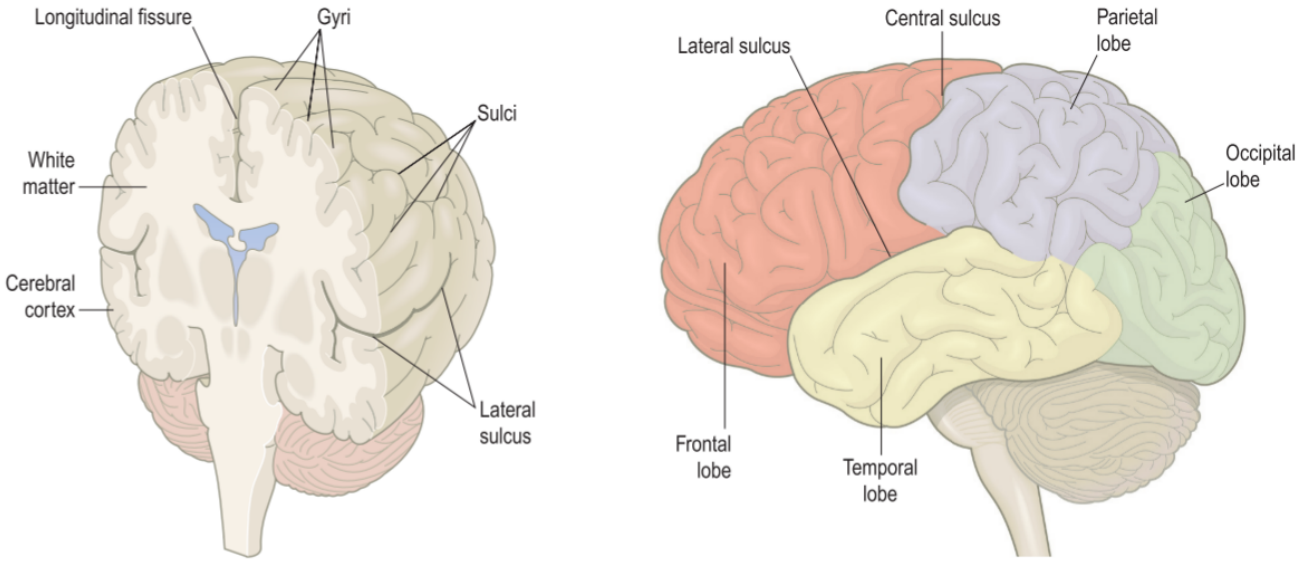

Figure 1.5: The cerebral cortex is characterized by its convoluted folds. Some landmarks are consistent across brains, as the central sulcus; lateral sulcus; parieto-occipital notch and pre-occipital notch. These landmarks help divide the hemispheres into lobes. This image was adapted form the book Clinical Neuroscience [2]

and gyri respectively.

The cerebral cortex is divided in two hemispheres by a prominent central fissure. The hemispheres are characterized by the gyri (singular, gyrus) or crests of folded cortical tissue, and sulci (singular, sulcus) the grooves that divide gyri from one another. Although gyral and sulcal patterns vary from individual to individual, there are some fairly consistent landmarks, particularly the: central sulcus; lateral sulcus; parieto-occipital notch and pre-occipital notch. These landmarks help divide the hemispheres into four lobes: occipital, temporal, parietal, and frontal. Hidden from surface view is the fifth lobe: the insular lobe. Figure 1.5 presents a illustration of this.

Anatomy of the White Matter

Axons in the central nervous system are gathered into bundles of different diameter, and several bundles form larger pathways called fasciculi, or tracts [3]. Most of the cerebral fibers forming the white matter connect distant regions within the cortex. Others, connect cortical region with the peripheral nervous system or subcortical structures. There are some fibers, the less, that connect only subcortical structures.

Some major bundles running along the white matter are well defined in the modern neuronanatomy. Examples of major bundles in the human brain are the Corpus Callosum, the Internal Capsule and the Superior Longitudinal Fasciculus (Fig. 1.6.) The Corpus Callosum is the largest tract of the human brain, composed of some 200 to 300 million myelinated axons it connects both hemispheres, allowing to transfer information from one to another [3]. The internal capsule contains ascending fibres mainly from the thalamus to the cortex, and descending fibres from the cortex to subcortical structures, and the spinal cord [3]. This complex projection system conveys sensorial information to the cortex and controls movement. Our last example, the Inferior Longitudinal Fasciculus, is a tract with long and short fibres connecting the occipital and temporal lobes [3], it is involved in visual and language functions.

Neuroanatomical Naming Conventions

In order to describe the location of structures on the brain, standardized nomenclature is used. Brain's anatomy can be described from its surface, from orthogonal sections that traverse the brain, or from its white matter [3].

The surface of the brain can be viewed from the side (lateral view), the middle (medial view), the front (anterior or frontal view), and the back (posterior or occipital view) (Fig. 1.7 A). Another way to describe relative positions in neuroanatomy is using the terms dorsal and ventral. The dorso-ventral system is defined in general for any animal species, the term dorsal refers to the back and ventral to the front or belly of an organism. Since humans have an upright torso, the dorso-ventral system bends, as shown in figure 1.7 A.

Sectional neuroanatomy describes the relationship between cortical and subcortical structures, most commonly visualized along orthogonal axial, coronal, and sagital

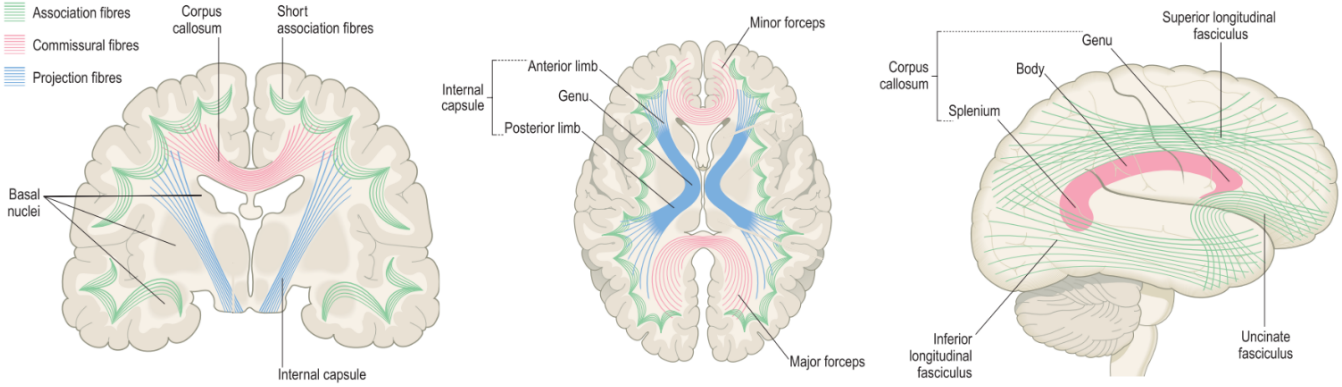

Figure 1.6: Example of major commissural, association, and projection tracts in the white matter. This image was adapted from the book Clinical Neuroscience[2]

planes (Fig. 1.7 B). In radiological convention, the axial slices are viewed from the feet towards the head. The coronal planes are conventionally oriented with the left side of the brain on the right side of the page (frontal view). Finally, the sagittal plane divides the brain into two hemispheres.

White-matter neuroanatomy delineates the origin, course, and termination of connecting pathways (Fig. 1.7 C). The tracts are classified according to their course and terminal projections. Commisural pathways run along a horizontal axis and connect the two hemispheres. The majority of the projection pathways have a perpendicular course along a dorso-ventral (descending) or ventro-dorsal (ascending) axis and connect the cerebral cortex to subcortical nuclei, cerebellum, and the spinal cord. The association tracts connect areas within the same hemisphere, as for example, short U-fibers. Most long association bundles run longitudinal along an antero-posterior axis and connect cortical areas within the same hemisphere.

These gross descriptions of some prominent anatomical landmarks provide a framework for naming, locating and studying different brain structures. Being able to locate brain regions in different subjects is a necessary first step to study the basic of brain function.

1.5. Brain Function

While we know that conciousness emerges from the brain, we still have a long road ahead to unravel how the brain works. So far, and thanks to the study of brain lesions, many motor and cognitive functions have been mapped to coarse brain regions (Fig. 3.5). In this section, we present an overview of the general function attributed to each lobe, while introducing some functional subdivisions used later on this thesis.

Frontal Lobe

The frontal lobe is concerned with motor functions, speech production, planning, personality, insight and foresight.

One of its divisions, the precentral gyrus (Fig. 3.5 A), contains an inverted point-to-point map of the motor functions of the opposite half of the body (Fig. 3.5 B)[2;1;3]. This area is called the primary motor cortex, and corresponds to Brodmann's region 4. It was mapped by Penfield et al.[13] trough experimenting with electrical stimulation. A remarkable fact is that the area allocated for each body part is proportional to the precision of movement control[2]. In particular, the areas for the hands, face and tongue are disproportionately large (Fig. 3.5 B).

The region in front of the primary motor cortex is the lateral premotor area (Fig. 3.5 A). Defined as the Brodmann Area 6, it does not correspond to any particular gyral or sulcal boundaries[2;1]. The premotor cortex also contains an inverted body map and is concerned with preparation and execution of movement sequences in response to external stimuli (as catching a ball, rather than throwing one)[2].

The large portion of the frontal lobe anterior to the motor and premotor areas is the prefrontal cortex (Fig. 3.5 A) and is involved in personality, behaviour, language and intellect[2]. It is mainly concerned with organizing and planning behaviour in pursuit of short-, medium- and long-term goals. It also has a cognitive inhibitory role, preventing inappropriate behaviour[14].

Finally, the opercular and triangular parts of the inferior frontal gyrus (Brodmann Areas 44 and 45) correspond to Broca's area (Fig. 3.5 A). This area is involved in the expressive aspects of spoken and written language (production of sentences constrained by the rules of grammar and syntax)[2]. The area was named after Pierre Paul Broca, who reported speach production impairments in two patients. This area tends to be lateralized to the hemisphere in charge of the dominant hand.

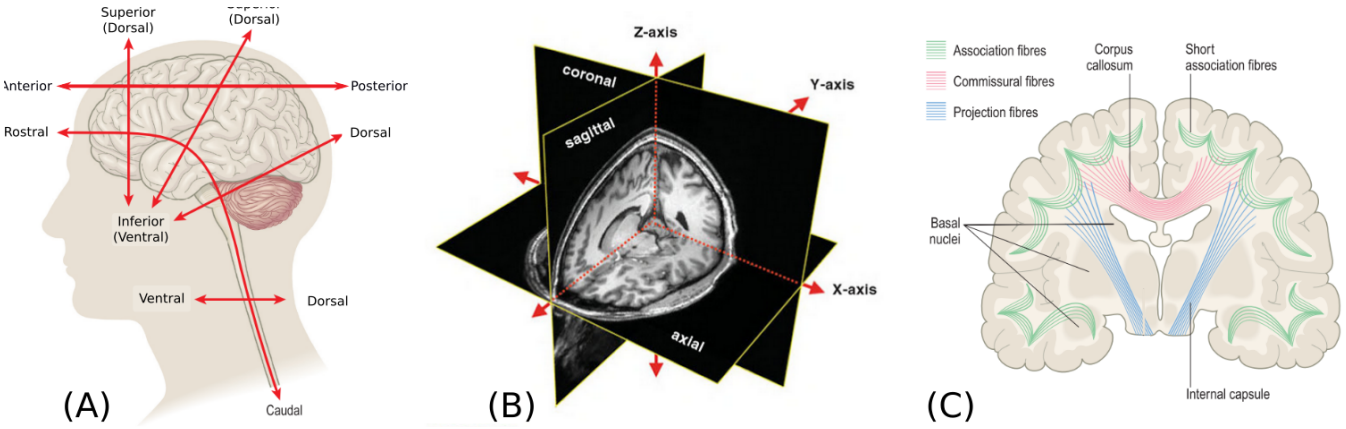

Figure 1.7: In order to describe the location of structures on the brain, standardized nomenclature is used. Brain's anatomy can be described: (A) from its surface, (B) from orthogonal sections that traverse the brain. (C) White matter tracts are categorized based on their trajectory, and starting and ending points. This image was adapted form the book Clinical Neuroscience[2], and the book Atlas of Human Brain Connections[3]

Parietal Lobe

The parietal lobe is concerned with language comprehension, spatial orientation and perception, and somatic senses, such as touch and temperature.

Located on the parietal lobe, immediately posterior to the centrar sulcus, and parallel to the precentral gyrus, there is the postcentral gyrus. It corresponds to the primary somatosensory cortex (Fig. 3.5 A). The sensory cortex contains an inverted map of the contraleteral side of the body that mirrors that of the motor cortex, but the relative proportions of the body parts reflect the degree of tactile sensitivity[2].

Occipital Lobe

The occipital lobe is concerned with visual processing and association. It contains the Brodmann Area 17, which correspondes to the primary visual cortex (Fig. 3.5 A). The primary visual cortex is highly specialized for processing visual information, and possess a point-to-point (retinotopic) representation of the visual field[2]. The visual system continues in the visual association cortex (BA 18 and 19), which helps in the detection of complex patterns and are believed to contribute in detecting global motion[2;1].

Temporal Lobe

The temporal lobe is involved in hearing, speech comprehension and visual recognition.

It contains the auditory cortex (Fig. 1.5 A), which has a tonotopic map representing the audible frequency spectrum (low frequencies laterally, high frequencies medially)[2]. More ventral is the fusiform gyrus, which is involved in the recognition of complex visual patterns, as tools or human faces[15]. Another region, Wernicke's area, corresponds to the posterior third of the superior temporal gyrus (Fig. 3.5 A) and it is involved in language comprehension[2].

Insula

The insular cortex is hidden in the depths of the lateral sulcus (Fig. 1.5). The insula is involved in attention, and in the integration of sensory, affective, and cognitive cues[16;2].

1.6. Systems Neuroscience

So far in this introduction to neuroanatomy, we have presented brain function as studied by the modular paradigm. In this paradigm, a discrete and continuous piece of cortical tissue is specialized to serve one cognitive function or to represent one essential aspect of the information processed by it[17]. The interaction between many of such modules would lead to complex cognitive function. However, accumulating evidence shows that the paradigm has serious limitations. For example, lesions in the brain almost never derive in the loss or degradation of only one cognitive function[17]. Furthermore, even the functions of primary sensory areas, long standing thought as modular, appear to be part of a network that integrates multisensory stimuli[18].

A new paradigm is emerging in neuroscience, that moves beyond the simplistic one to one mapping between cognitive functions and brain regions, and instead maps cognitive functions to large-scale networks in the brain. So far, at least 8 major core functional networks have been defined[16]: (i) a spatial attention network anchored in posterior parietal cortex and frontal eye fields; (ii) a language

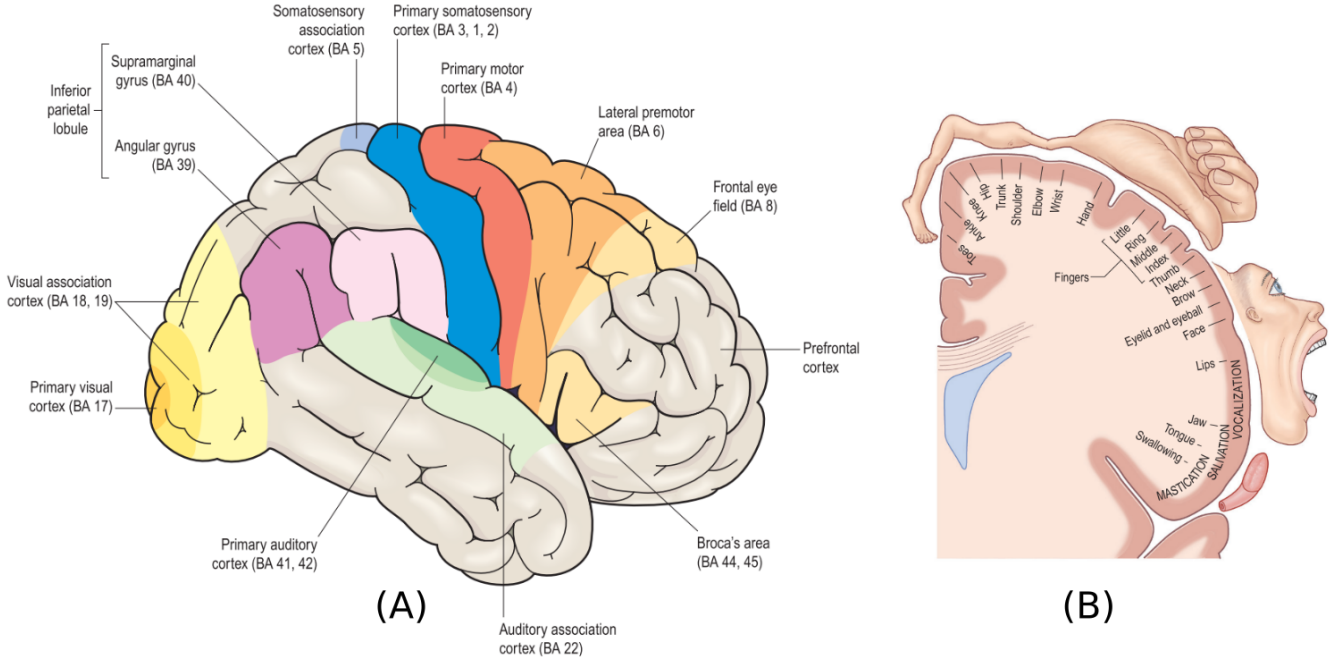

Figure 1.8: According to the modular paradigm, the brain can be divided in regions that are functionally specialized. (A) Illustration of different cytoarchitectonic regions of the brain, and their functional specialization. (B) The motor strip contains an orderly somatotopic (point-to-point) representation of the contralateral half of the body. The size of the cortical representation for each body part reflects the precision of motor control. This image was adapted form the book Clinical Neuroscience[2]

network anchored in Wernicke's and Broca's areas; (iii) an explicit memory network anchored in the hippocampal–entorhinal complex and inferior parietal cortex; (iv) a face-object recognition network anchored in midtemporal and temporopolar cortices; (v) a working memory-executive function network anchored in prefrontal and inferior parietal cortices; (vi) central-executive network anchored in dorsolateral prefrontal cortex and posterior parietal cortex; (vii) a salience network anchored in anterior insula and anterior cingulate cortex; and (viii) a default mode network, a set of functional networks that emerge while a person is resting.

Thinking the brain as a set of interacting networks, instead of single anatomical regions, creates a sound base to study cognition[16]. However, if a single network can be said to support a specific cognitive function is still an open question in neuroscience. Answering it will depend on the developing of new techniques to study not only brain function, but also brain connectivity.

1.7. Conclusions

This chapter introduced the basic knowledge in neuroanatomy necessary to understand the rest of the thesis. Moreover, it highlighted how the interaction between neurons by means of connectivity drives not only the brain morphology but also its function. It also presented how neuroscience is moving from viewing the brain as a mosaic of functionally specialized regions, to an interactive network from which cognition arises. This view of the brain as a network is a key aspect that drives some contributions of this thesis.

Most of the knowledge of this chapter comes from studies done on postmortem primate brains, or from results obtained with highly invasive techniques. As with the modular paradigm, neuroscience is also moving forward towards the use of non-invasive techniques. In the next chapter, we explain how advances in quantum physics helped to develop Magnetic Resonance Imaging (MRI), which translated in a new era of non-invasive brain imaging.

Bibliography

[1] D. Purves, G. J. Augustine, D. Fitzpatrick, W. C. Hall, A.-S. Lamantia, J. O. Mcnamara, and S. M. Willians, *Neuroscience*, vol. 3. 2004.

[2] P. Johns, *Clinical Neuroscience*.

[3] M. Catani and M. Thiebaut de Schotten, *Atlas of Human Brain Connections*. Oxford University Press, mar 2012.

[4] H. Gray, *Gray's Anatomy of the Human Body*. Lea & Febiger, 1918.

[5] F. A. Azevedo, L. R. Carvalho, L. T. Grinberg, J. M. Farfel, R. E. Ferretti, R. E. Leite, W. J. Filho, R. Lent, and S. Herculano-Houzel, "Equal numbers of neuronal and nonneuronal cells make the human brain an isometrically scaled-up primate brain," *J. Comp. Neurol.*, vol. 513, no. 5, pp. 532–541, 2009.

[6] J. M. Bekkers, "Pyramidal neurons," *Curr. Biol.*, vol. 21, no. 24, p. R975, 2011.

[7] M. D. Waehnert, J. Dinse, M. Weiss, M. N. Streicher, P. Waehnert, S. Geyer, R. Turner, and P. L. Bazin, "Anatomically motivated modeling of cortical laminae," *Neuroimage*, vol. 93, pp. 210–220, 2014.

[8] P. Rand S. Swenson, M.D., "Review of Clinical and Functional Neuroscience," 2006.

[9] S. T. Bok, "Der Einfluß der in den Furchen und Windungen auftretenden Krümmungen der Großhirnrinde auf die Rindenarchitektur.," *Z. Gesamte Neurol. Psychiatr.*, vol. 121, no. 1, pp. 682–750, 1929.

[10] M. Mesulam and E. J. Mufson, "Insula of the Old World Monkey . I : Architectonics in the Insuloorbito- temporal Component of the," *J. Comp. Neurol.*, vol. 22, pp. 1–22, 1982.

[11] K. Brodmann, *Vergleichende Lokalisationslehre der Großhirnrinde in ihren Prinzipien dargestellt auf Grund des Zellaufbaues*. Leipzig: Barth, 1909.

[12] D. C. Van Essen, "A tension-based theory of morphogenesis and compact wiring in the central nervous system," 1997.

[13] W. Penfield and H. Jasper, *Epilepsy and the Functional Anatomy of the Human Brain*. 1954.

[14] M. Sigman, *The Secret Life of the Mind: How Our Brain Thinks, Feels, and Decides*. William Collins, 2017.

[15] Z. M. Saygin, D. E. Osher, K. Koldewyn, G. Reynolds, J. D. E. Gabrieli, and R. R. Saxe, "Anatomical connectivity patterns predict face selectivity in the fusiform gyrus," *Nat. Neurosci.*, vol. 15, pp. 321–327, dec 2011.

[16] S. L. Bressler and V. Menon, "Large-scale brain networks in cognition: emerging methods and principles," *Trends Cogn. Sci.*, vol. 14, no. 6, pp. 277–290, 2010.

[17] J. M. Fuster, "The Module: Crisis of a Paradigm," *Neuron*, vol. 26, pp. 51–53, 2000.

[18] A. A. Ghazanfar and C. E. Schroeder, "Is neocortex essentially multisensory?," *Trends Cogn. Sci.*, vol. 10, no. 6, pp. 278–285, 2006.

Chapter 2
Introduction to Non-invasive Imaging Techniques

2.1. Overview

In order to infer connections running through the white-matter, or functional specialization in the grey-matter, neuroscientist have long relayed in postmortem studies or invasive techniques. The advent of Magnetic Resonance Imaging (MRI) allowed for the first time to non-invasively study brain structure in vivo. Further developments opened the possibility to quantify which regions activate during a certain task (or in the absence of), and to estimate gross axonal connectivity. In this chapter, we start by introducing some concepts in nuclear physics and explain how they are applied in MRI to study the human brain. Then, we explain how modifying the acquisition sequences allows to study the physical process of diffusion, enabling to estimate the location of tracts in the white-matter. Finally, we make a brief introduction to how to detect brain activation in response to functional or cognitive tasks in the brain using Functional MRI. This chapter is strongly based on the book Diffusion MRI[1], the lessons of Dr. Michael L. Lipton[2] available online, and the review paper in fMRI of Gary Glover[3]. We refer the read to them in order to deepen on the subjects.

2.2. A Brief History on Brain Imaging

Magnetic Resonance Imaging (MRI) and its derivates are among the biggest advances, if not the biggest, in medicine of the last 50 years. They allow to study not only the brain, but also other internal organs, with an unprecedented level of resolution, and in vivo.

MRI has its origins in 1946, when Felix Bloch[4] and Edward M. Purcell[5] simultaneously formalize Nuclear Magnetic Resonance (NMR), work for which they would later receive the Nobel Prize in Physics. Shortly after, in 1950, Hahn[6] observes that the physical process of diffusion influences the signals measured using NMR. To quantify this influence, during 1965 Stejskal and Tanner[7] invent the Pulse Gradient Spin Echo sequence that allows to measure the amount of diffusion in a specific direction. A couple of years later, NMR use in medicine becomes promising after Raymond Damadian shows in 1971 that NMR could be used to differentiate healthy tissue from tumors[8]. Soon after, in 1973, Paul Lauterbur proposes a method based on gradient magnetic fields to reconstruct two dimensional MR images[9], which with improvements of Peter Mansfield[10] lead to the development of modern MRI. In 1990, Ogawa et al.[11], inspired by Pauling and Coryell's work[12], shows that MRI can be modified to be sensitive to blood flow, and therefore, brain activity in rats. Three years later, Ogawa et al.[13] present similar results in the human brain, producing the first fMRI acquisition. In 1994 Basser et al.[14] invent Diffusion Tensor Imaging (DTI), an efficient way to model diffusion in the brain, allowing to start tracking brain pathways. In 2003, Lauterbur and Mansfield jointly receive the Nobel Prize in Physiology and Medicine for their contributions in MRI.

In the following sections we will review on a deeper way all the non-invasive techniques used in this thesis. We will put special emphasis in dMRI, since our main interest is brain connectivity. However, in order to explain diffusion MRI is necessary to explain MRI and the physics behind it: Nuclear Magnetism.

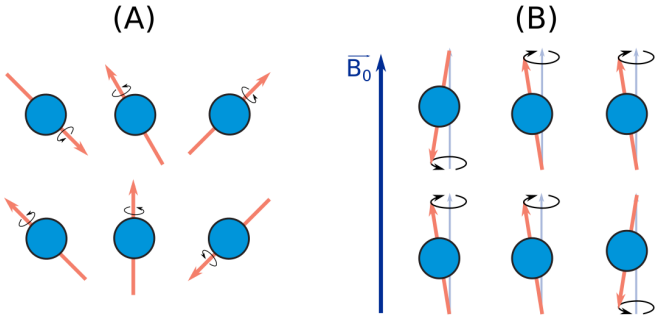

Figure 2.1: (A) When atomic nuclei rest under no constraints, they spin along random directions. (B) However, when putted under the effect of a magnetic field, the spin of the nuclei will align to the magnetic field's direction and start to precess around it.

2.3. Physics Background

Nuclear Magnetism

Atomic nuclei with a different number of neutrons and protons are said to possess a non-zero spin, which is an intrinsic form of angular momentum. While there is not an actual movement, the nucleus spin can be interpreted as the particle spinning around its own axis[15], since it possess all the same physical properties. This "movement" of charges in the nucleus, induces what is known as a nuclear magnetic moment (Fig. 2.1 A).

When atomic nuclei are placed inside of an external magnetic field, their spin will align with the field's direction and start to precess around it (Fig. 2.1) B). While the spins could align either parallel or anti-parallel to the gra-

dient, the laws of thermodynamics ensure that a bigger number of spins will do it in the parallel direction.

The frequency with which the spin precess around the magnetic field is known as the Larmor frequency [16], and is expressed as:

$$\omega = \vec{\mu} \times \vec{B} = \gamma \vec{J} \times \vec{B}, \tag{2.1}$$

where $\vec{\mu}$ is the magnetic moment of the nucleus; $\vec{B}$ is the magnetic field; γ is the gyromagnetic ratio of the atom, an intrinsic physical property of each atom; and $\vec{J}$ is the angular momentum of the nucleus.

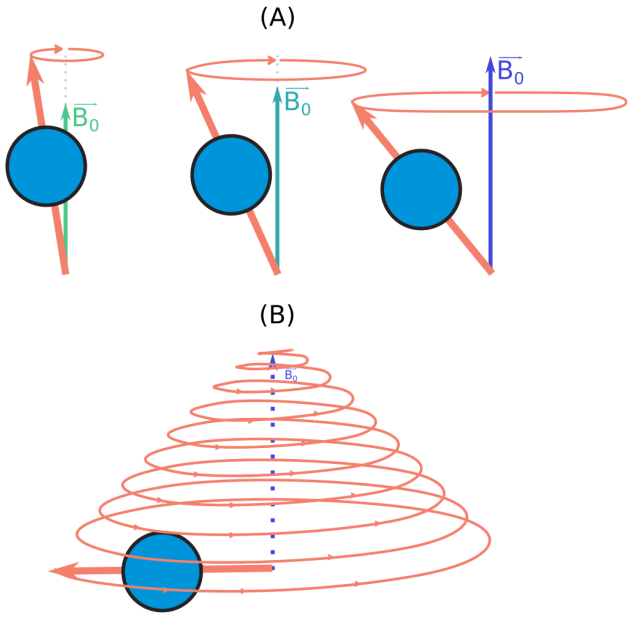

Figure 2.2: (A) The higher the strength of the magnetic field, the bigger the angle between the nucleus spin and the magnetic field will be. (B) If the magnetic field ceases, the spin will return to its initial angle of precession.

The angle formed between the precessing spin and the magnetic field is driven by the strength of the magnetic field. The angle between the spin and the magnetic field increases as the strength of the magnetic field does (Fig. 2.2 A). In fact, by increasing the energy of the magnetic field enough, it is possible to 'excite' the nucleus, moving the precessing towards the plane transversal to the magnetic field. However, if the external magnetic field goes off, the nucleus will start to 'relax' (Fig. 2.2 B), and the precessing will begin to move once again towards the direction of the magnetic field. An important remark is that the precessing angle does not decrease linearly during the relaxation. This is because the relaxation process represents a redistribution of the energy within the system. The energy that the system won during excitation, has to go somewhere else in order for the spin to go back to its initial state. In particular, spins lose energy by giving it to other non excited spin of the same kind (spin-spin interaction), or by giving it to surrounding elements (spin-lattice interaction). This means that how the relaxation happens is governed by the composition of the nucleus itself, and the chemical composition of its environment. This process was mathematically formalized by Bloch in what is known as the Bloch Equations [4].

Nuclear Magnetic Resonance

The organs in the human body are composed by different types of tissue, each with its own chemical composition. If we subject a human body to the effects of excitation and relaxation by means of a magnetic field, and place a coil in the transversal plane, we should be able to measure different relaxation signals for different types of tissue. The problem is, that the amount of energy necessary to create a detectable precession would surely kill a human. Another way to increment the energy of the system is needed, and for this is that the concept of Resonance is used.

Resonance is a physical phenomenon in which a system or external force drives another system to oscillate with greater amplitude at specific frequencies. In our case, we are interested in introducing more energy into the human body. Knowing that hydrogen atoms (^1H) are widely present in the body, we can compute their Larmor frequency (Eq. 2.1), and produce energy at that frequency. By resonance, the produced energy will be injected into the tissue.

2.4. Nuclear Magnetic Resonance Imaging

Having covered the necessary physical notions, we are now ready to introduce MRI. A MR scanner is a machine able to create strong magnetic fields and radio frequency pulses in different frequencies. Particularly, while functioning a MR scanner is constantly emitting a homogeneous magnetic field referred as $\vec{B}_0$ (Fig. 2.3 A). If we place a coil in the plane transversal to $\vec{B}$, and emit a radio frequency pulse at the frequency of hydrogen, we will be able to measure a signal coming from the body. This measure will represent the mixture of all the signals generated by different tissues. What we are interested in, is to separate the signal coming from different places on the body, in order to compare them after. A necessary first step to disentangle the different contributions of each tissue is to do slice selection.

Slice selection makes use of a gradient magnetic field. A gradient is a magnetic field which strength varies linearly along a specific direction. Following the Larmor equation (eq. 2.1) we can predict that, nucleus along the gradient will change their spin frequency in a predictable way. Particularly, applying a gradient $B(z)\hat{z}$ in a specific di-

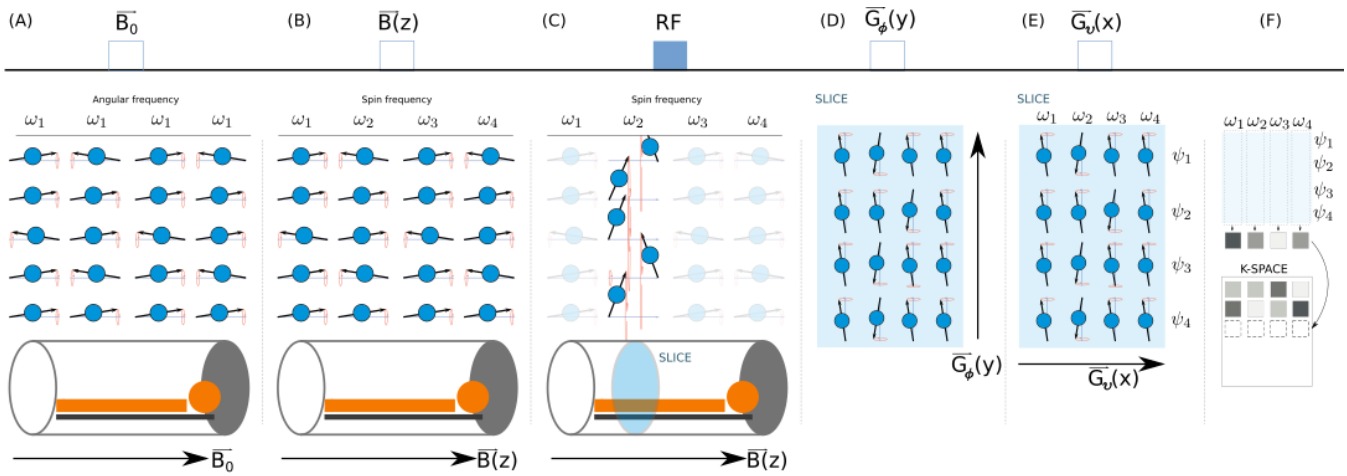

Figure 2.3: Simplified scheme of a MRI acquisition. (A) A MRI scanner is constantly emitting a homogeneous magnetic field $\vec{B}_0$ an atomic nucleus are precessing around it. (B) A gradient magnetic field is emitted in order to change in a predictable way the frequency of the nuclei. (C) A radio frequency pulse is generated, making certain nuclei to resonate and moving their precession to the transversal plane. (D) Now the slice is selected, a frequency encoding gradient is briefly applied to put out of phase nuclei in different vertical positions. (E) A phase encoding gradient is then turned on, to change in a predictable way the frequency in every horizontal position. (F) An acquisition is done and written down in the k-space.

rection (Fig. 2.3 B), will induce a frequency to the nuclei with magnetic momentum $\vec{\mu}$ of:

$$\omega(z) = \vec{\mu} \times B_z(z)\hat{z}. \tag{2.2}$$

Then if a radio frequency (RF) pulse with a frequency of $w(z_0)$ is generated, only the spins in the position $z_0\hat{z}$ will start to resonate. Therefore, the signal obtained by the transversal coil will only correspond to the spins in the slice at position $z_0\hat{z}$ (Fig. 2.3 C). It is important to state that, because of hardware limitations, it's impossible to generate a RF pulse in an exact frequency. What actually happens is that the pulse is generated for a small slice of frequencies, meaning that the spins in a small band around z_0 will also resonate.

So far, all the spins inside of the slice are precessing in the same way. We can think of the slice as a two dimensional matrix, with two coordinates: $\hat{x}$ being the rows and $\hat{y}$ being the columns (Fig. 2.3 B). In order to retrieve the signal generated at each position, two more gradients are needed, a frequency encoding gradient ($\vec{G}_\nu$) and a phase encoding gradient ($\vec{G}_\phi$).

First, $\vec{G}_\phi$ is applied for a short period of time in one of the directions, lets say $\hat{y}$. Following the Larmor equation (eq. 2.1), all the spins along $\hat{y}$ start to precess at a frequency that depends on their position (Eq. 2.2). After the gradient is shut down, the spins will return to precess all at the same velocity, but off phase, since they were separated by the previous gradient. This is, the spins of each row will have the same angular velocity, but a different phase (Fig. 2.3 D).

Then, $\vec{G}_\nu$ is applied in the orthogonal direction ($\hat{y}$). Now it will happen that: the spins of each row will be oscillating in a different phase, because of $\vec{G}_\phi$ and the spins of each row will be oscillating at a different velocity, following the new gradient $\vec{G}_\nu$ (Fig. 2.3 E).

If we sample the signal using a coil over the direction $\hat{x}$, we will obtain as many data points as columns. All data points will have a mixture of all the signals the rows (Fig. 2.3 F). However, each data point will comprise the difference in phase and the difference in frequency that we applied to the matrix. By iteratively measuring these data points, changing only the phase encoding gradient, we sample what is known as the k-space[17]. A space where the signal generated by our sample is encoded by phase in the rows, and by frequency in the columns. As shown by Likes et al.[17], taking the 2D Fourier transform of the k-space, decodes the image of the tissue being sampled.

2.5. Diffusion MRI

While NMRI allows to visualize the different tissue composition of the brain, diffusion MRI aims to quantify how the water molecules diffuse in the brain. This is of great importance because in fibrous structure such as white matter, water molecules tend to diffusion along fibers. Therefore, characterizing diffusion can help to describe the underlying structure of the white matter. Now, we start by explaining the phenomenon of diffusion and its implications in MRI.

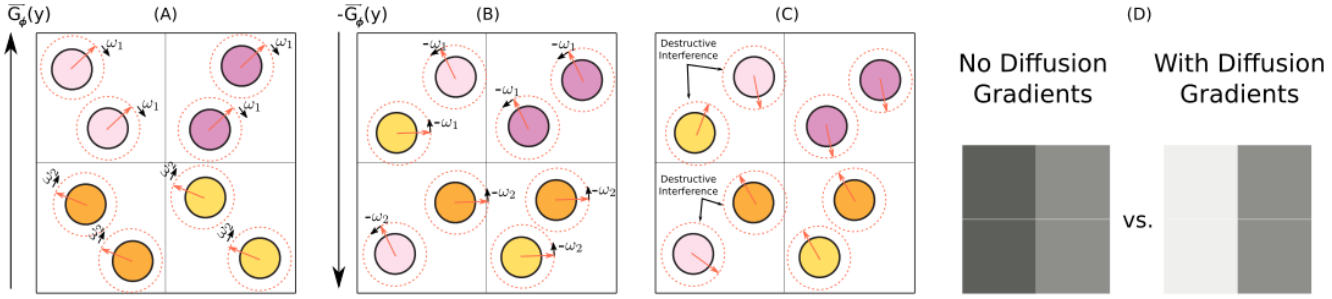

Figure 2.4: Simplified scheme of how diffusion is measured. We illustrated in the same plane as the gradient's direction so simplify the figure. (A) A first gradient field is applied, and the nuclei in the same rows start to precess in phase. (B) After some time, a gradient with the same strength is applied in the opposite direction. This gradient should cancel the phase shift induced by the first one. However, the particles undergoing diffusion would have change place. (C) Nuclei precessing at different phases will cause a destructive interference between them. (D) The off phase precessing is translated into lesser signal respect to the image acquired with no diffusion gradients.

Brownian Motion and MRI

The molecules inside a fluid in equilibrium are not still, on the contrary, they move randomly. This physical phenomena is known as Brownian motion [18] or diffusion. In 1950, Hahn [6] observes that the signal measured during the relaxation period in MRI can be affected by the process of diffusion.

In order to characterize the effects of diffusion in nucleus relaxation, a new experiment is devised. Imagine that after applying the RF pulse to do slice selection, we apply two gradient fields (called diffusion gradients), one after the other, with the same strength but in opposite directions (Fig. 2.4 A). As explained in section 2.3.1, this will induce two phase shifts to the nuclei. The first gradient will make them go off phase, while the second one should cancel the first, and put them back in phase. However, the particles undergoing diffusion would have changed place, and therefore, change their phase differently (Fig. 2.4 B). Nuclei precessing at different phase on a same sections of the sample will cause a destructive interference between them, resulting in a lower signal. The ratio between the signal obtained with diffusion gradients and the one without them quantifies the amount of ongoing diffusion (Fig. 2.4 C).

In 1956, H.C. Torrey [19] extends the Bloch Equations [4] in order to quantify the effects of diffusion in nucleus relaxation when multiple diffusion gradients are used. The new equations, known as Bloch-Torrey equation cannot be solved analytically. It's not until 1965 that Stejskal and Tanner [7] invent the Pulsed Gradient Spin Echo (PGSE) sequence to measure diffusion in a specific direction. In their sequence, two opposite diffusion gradients are applied for δms, with a separation of Δms between them. If we assume δ to be infinitely narrow (i.e. the diffusion during that time is negligible), then, the Bloch-Torrey equations can be solved, and the signal attenuation at time $2\tau = 2(\delta + \Delta)$ can be expressed as:

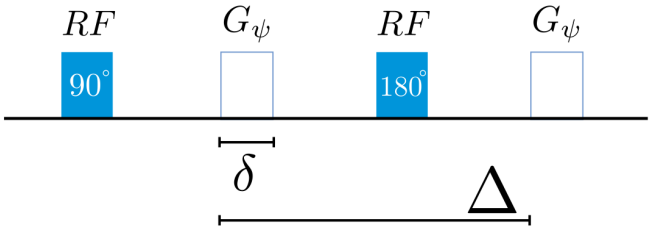

Figure 2.5: Pulsed Gradient Spin Echo sequence.

$$E(2\tau) = \frac{S(2\tau)}{S_0} = e^{-\gamma^2 g^2 \delta^2 (\Delta - \frac{\delta}{3}) D}, \tag{2.3}$$

where g is the strength of the diffusion gradient, S_0 the image acquired without diffusion gradients, and D the diffusion coefficient.

In 1985 Le Bihan [20] proposed to gather all the parameters in a single one:

$$b = \gamma^2 g^2 \delta^2 \left(\Delta - \frac{\delta}{3} \right)$$

,

simplifying the equation 2.3 to:

$$E(2\tau) = e^{-bD}$$

where b has a physical meaning, it represents the reciprocal of the diffusion intensity [20].

In 1991 Callaghan et al. [21] developed the q-space analysis. Based on the work of Stejskal and Tanner, Callaghan shows that it's possible to express the signal attenuation as:

$$E(q,\tau) = \frac{S(q,\tau)}{S_0} = \int_{R^2} P(r;\tau) e^{-2\pi i q r} dr, \tag{2.4}$$

with $q = \gamma\delta g/2\pi$, and $P(r|r_0, \tau)$ a probability density function (diffusion propagator) modeling the probability that a molecule had a relative displacement of r in time τ. One of the main advantages of q-space is that it does not assume any a prior model, allowing to define different strategies for $p(r; t)$. More importantly, equation 2.4 shows that the signal attenuation is the 3D Fourier transform $\mathcal{F}$ of the average propagator P.

$$E(q, \tau) = \frac{S(q, \tau)}{S_0} = \mathcal{F}[P(r|r_0, \tau)]. \tag{2.5}$$

In particular, if the diffusion propagator is assumed to be Gaussian, then the Fourier integral can be solved analytically, and the solution is the same as the one obtained by Stejskal and Tanner (Eq. 2.3)

Diffusion Tensor Imaging (DTI)

In 1994 Basser et al.[14] propose to measure the signal attenuation in different directions, and to model the diffusion coefficient in the Stejskal and Tanner equation (eq. 2.3) with a second order tensor. This sets the bases of what is known as Diffusion Tensor Imaging. DTI represents the diffusion as a 3-dimensional (3D) ellipsoid, which can be coded in a symmetric matrix:

$$D = \begin{pmatrix} D_{xx} & D_{xy} & D_{xz} \\ D_{xy} & D_{yy} & D_{yz} \\ D_{xz} & D_{yz} & D_{zz} \end{pmatrix}.$$

Since the matrix has 6 unknown variables, at least 6 acquisitions in different directions have to be done. DTI is until today, one of the most used techniques to model the diffusion signal. Its main drawback is that it does not allow to correctly characterize the crossing of fibers. Both the isotropic diffusion and the crossing of fibers get modeled as spheres.

High Angular Resolution Diffusion Imaging

Two factors drive newer imaging techniques: Callaghan's relationship[21] between the signal attenuation and the diffusion propagator (Eq. 2.5), and the ability to acquire data across many angles with different b-values. Either using one b-value (single shell) or multiple b-values (multi shell), HARDI techniques rely on taking acquisitions across many angles, in order to reconstruct the true diffusion propagator. Notable examples of High Angular Resolution Diffusion Imaging (HARDI) are Diffusion Spectrum Imaging (DSI)[23], Q-space Imaging (QSI)[21], Q-Ball Imaging[24], Composite hindered and restricted model of diffusion (CHARMED)[25], Mean Apparent Propagator (MAP)-MRI[26], Constrained Spherical Deconvolution[27], and Neurite Orientation Dispersion and Density Imaging (NODDI)[28]. While each technique relies in different assumptions about the diffusion propagator, they all try to capture multiple fiber directions within the same imaging voxel. HARDI acquisitions are currently being improved every day with better material and better reconstruction algorithms.

Estimating Axonal Connectivity

So far, we discussed about imaging techniques to measure diffusion. Now is time to present how to use such techniques in order to study the structure of white matter.

Water particles in the white matter diffuse constrained by the axonal bundles. The nuclei present at any point of the white matter will be able to diffuse only inside a tract and along its path. If dMRI had enough resolution, we could trace each brain connection by simply looking at the diffusion signal. However, this is not the case, dMRI resolution is several orders of magnitude coarser than axonal diameters (millimeters vs micrometers)[29]. What is done in practice, is to fit one of the models named in previous sections (sec. 2.5.2, 2.5.3), and use them to derive a probabilistic map of transition from each voxel to their neighbors. The resulting network can be used on a Monte Carlo procedure where, starting from a voxel, at each step we randomly select to which neighboring voxel to move, following the probabilistic map. This process of simulating the random walk of a water particles through the white matter is known as Tractography[30].

The field of tractography is not exempt of problems, most state state-of-the-art algorithms create about four time more false-positive tracts than true-positive ones[31]. Also, most of them suffer from gyral bias, in which tractography bundles are biased towards finishing in gyral crowns rather than sulcal banks[29]. However, tractography has shown to be able to recover some major bundles in humans[32]. Also, it has been validated using high-resolution postmortem diffusion imaging and tractography in Old World monkeys. Particularly, Donahue et al.[33] found a correlation coefficient of 0.58 between tractography-based and tracer-based estimates of connectivity; the correlation is highest for strong, short-distance pathways but is informative even for weak connections and widely separated areas. This results, encourage to use tractography, despite of its flaws.

2.6. Brief Introduction to Functional MRI

Built on the contributions of Pauling and Coryell[12], and Ogawa[13;11] among others, functional MRI (fMRI) characterizes blood flow in the brain. Since blood flow is directly related with brain activity, fMRI gives us a way to study brain function. While not central to our thesis, we do believe that at least a brief description of how

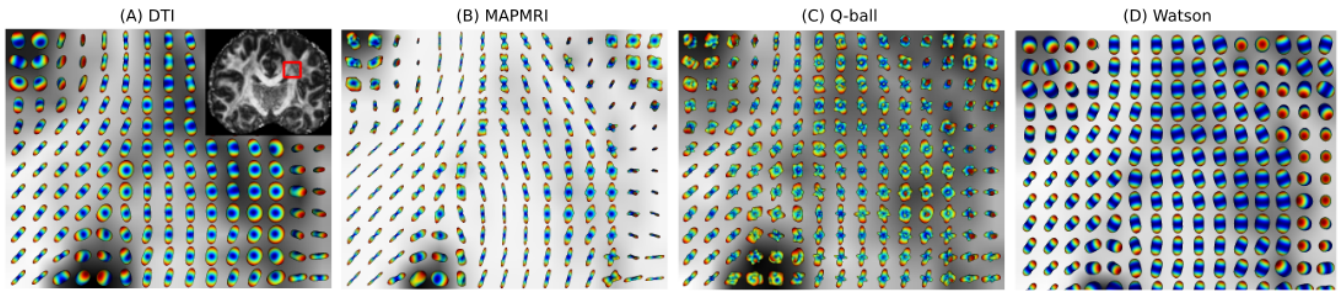

Figure 2.6: Comparison of different models in the reconstruction of diffusion signal: (A) Diffusion Tensor Imaging, (B) Mean Apparent Propagator (MAP)-MRI, (C) Q-Ball Imaging, and (D) Watson distributions of NODDI. It can be seen that DTI finds an average orientation, where Q-Ball, MAPMRI and SMT find crossing structures. This image was adapted from Fick[22] (2017).

functional MRI (fMRI) works should be given.

When a region of the brain is activated by a cognitive task, the local firing of neurons generates a higher energy requirement[3]. The brain responds by adjusting its blood supply to the region in a process known as the haemodynamic response. This increase in blood flow produces an increase in the ratio of oxygenated hemoglobin relative to deoxygenated hemoglobin in that specific area (BOLD contrast). Oxygenated hemoglobin is magnetically indistinguishable from brain tissue. On the contrary, deoxygenated hemoglobin has 4 unpaired electrons and is highly paramagnetic[3]. This results in local gradients that put out of phase the surrounding nuclei, causing destructive interference in the observed MR signal. Using a special type of pulse sequence called gradient refocused echo[34] it is possible to make MR scanners sensible to this effect.

After obtaining the fMRI signal, it is possible to estimate which brain regions are being more active during the desired cognitive task by means of statistics. In particular, it is expected to see a high activation of the area being used for a task while the subject is doing such task. For example, in order to obtain the area to finger movement, we could ask a subject to start and stop moving the finger at regular intervals. The area responsible for moving the finger should show a regular activation pattern, correlated with the moments in which the finger was moving. We can compute such area by selecting the voxels in which the fMRI signal correlates the most with the square signal of finger movement (1 when the finger was moving, 0 when not).

2.7. Conclusion

This chapter introduced the imaging techniques of MRI, Diffusion MRI and Functional MRI. These three methods provide means to study the brain anatomy, its axonal organization and function in a non-invasive way. Even when each technique has its own limitations, either in spatial or temporal resolution, they all allowed to highly advance the state-of-the-art in neuroscience. In the next chapter we will see how these advances in imaging allowed to parcellate the brain, making it easier to study brain function.

Bibliography

[1] P. J. Basser and E. Özarslan, "Introduction to Diffusion MR," in *Diffus. MRI* (H. Johansen-Berg and T. E. J. Behrens, eds.), ch. 1, pp. 2–10, Academic Press, Inc., 2009.

[2] M. L. Lipton, "Introducing MRI," 2014.

[3] G. H. Glover, "Overview of functional magnetic resonance imaging," *Neurosurg Clin N Am*, vol. 22, no. 2, pp. 133–139, 2011.

[4] F. Bloch, "Nuclear Induction," *Phys. Rev.*, vol. 70, pp. 460–474, oct 1946.

[5] E. Purcell, H. Torrey, and R. Pound, "Resonance Absorption by Nuclear Magnetic Moments in a Solid," *Phys. Rev.*, vol. 69, no. 1-2, pp. 37–38, 1946.

[6] E. L. Hahn, "Spin echoes," *Phys. Rev.*, vol. 80, pp. 580–594, 1950.

[7] E. O. Stejskal and J. E. Tanner, "Spin Diffusion Measurements: Spin Echoes in the Presence of a Time-Dependent Field Gradient," *J. Chem. Phys.*, vol. 42, no. 1, p. 288, 1965.

[8] Damadian R, "Tumor detection by nuclear magnetic resonance," *Science (80-.).*, vol. 171 (3976), no. March, pp. 1151–1153, 1971.

[9] P. C. Lauterbur, "Image formation by induced local interactions. Examples employing nuclear magnetic resonance," *Nat. (London, United Kingdom)*, vol. 242, pp. 190–191, 1973.

[10] P.˜Mansfield, "Multi-planar image formation using {NMR} spin echoes," *J. Phys. C*, vol. 10, no. 3, pp. 580–594, 1977.

[11] S. Ogawa, R. S. Menon, D. W. Tank, S. G. Kim, H. Merkle, J. M. Ellermann, K. Ugurbil, K. Ugurbilt, and K. Ugurbil, "Functional brain mapping by blood oxygenation level-dependent contrast magnetic resonance imaging. A comparison of signal characteristics with a biophysical model.," *Biophys. J.*, vol. 64, no. 3, pp. 803–812, 1993.

[12] L. Pauling and C. D. Coryell, "The Magnetic Properties and Structure of Hemoglobin, Oxyhemoglobin and Carbonmonoxyhemoglobin," *Proc. Natl. Acad. Sci.*, vol. 22, no. 4, pp. 210–216, 1936.

[13] S. Ogawa, T. M. Lee, A. S. Nayak, and P. Glynn, "Oxygenation-sensitive contrast in magnetic resonance image of rodent brain at high magnetic fields.," *Magn. Reson. Med.*, vol. 14, no. 1, pp. 68–78, 1990.

[14] P. J. Basser, J. Mattiello, and D. Lebihan, "Estimation of the Effective Self-Diffusion Tensor from the NMR Spin Echo," *J. Magn. Reson. Ser. B*, vol. 103, pp. 247–254, mar 1994.

[15] M. SEGALA, "ABRAHAM PAIS, Niels Bohr's Times, in physics, philosophy, and polity, Oxford, Clarendon Press, 1991, XVII + 565 pp. ill. (ISBN 0 19 852049 2).," *Nuncius*, vol. 8, pp. 364–367, jan 1993.

[16] J. Larmor, "LXIII. On the theory of the magnetic influence on spectra; and on the radiation from moving ions," *Philos. Mag. Ser. 5*, vol. 44, no. 271, pp. 503–512, 1897.

[17] R. Likes, "Moving gradient zeugmatography," 1981.

[18] R. Brown, "XXVII. A brief account of microscopical observations made in the months of June, July and August 1827, on the particles contained in the pollen of plants; and on the general existence of active molecules in organic and inorganic bodies," *Philos. Mag. Ser. 2*, vol. 4, no. 21, pp. 161–173, 1828.

[19] H. C. Torrey, "Bloch Equations with Diffusion Terms," *Phys. Rev.*, vol. 104, pp. 563–565, nov 1956.

[20] D. Le Bihan and E. Breton, "Imagerie de diffusion in vivo par résonance magnétique nucléaire," *Comptes rendus l'Académie des Sci. Série 2, Mécanique, Phys. Chim. Sci. l'univers, Sci. la Terre*, vol. 301, no. 15, pp. 1109–1112, 1985.

[21] P. T. Callaghan, A. Coy, D. MacGowan, K. J. Packer, and F. O. Zelaya, "Diffraction-like effects in NMR diffusion studies of fluids in porous solids," *Nature*, vol. 351, pp. 467–469, jun 1991.

[22] R. Fick and R. Fick, "Advanced dMRI signal modeling for tissue microstructure characterization To cite this version : PhD THESIS prepared at Specialized in Control , Signal and Image Processing Advanced dMRI Signal Modeling for Tissue Microstructure Characterization," 2017.

[23] V. J. Wedeen, R. P. Wang, J. D. Schmahmann, T. Benner, W. Y. Tseng, G. Dai, D. N. Pandya, P. Hagmann, H. D'Arceuil, and A. J. de Crespigny, "Diffusion spectrum magnetic resonance imaging (DSI) tractography of crossing fibers," *Neuroimage*, vol. 41, no. 4, pp. 1267–1277, 2008.

[24] D. S. Tuch, "Q-ball imaging," *Magn. Reson. Med.*, vol. 52, pp. 1358–1372, dec 2004.

[25] Y. Assaf and P. J. Basser, "Composite hindered and restricted model of diffusion (CHARMED) MR imaging of the human brain," *Neuroimage*, vol. 27, no. 1, pp. 48–58, 2005.

[26] E. Özarslan, C. Guan, T. M. Shepherd, M. E. Komlosh, M. O. Irfanoglu, C. Pierpaoli, and P. J. Basser, "NeuroImage Mean apparent propagator (MAP)-MRI : A novel diffusion imaging method for mapping tissue microstructure," *Neuroimage*, vol. 78, pp. 16–32, 2013.

[27] J.-D. Tournier, F. Calamante, D. G. Gadian, and A. Connelly, "Direct estimation of the fiber orientation density function from diffusion-weighted MRI data using spherical deconvolution," *Neuroimage*, vol. 23, pp. 1176–1185, nov 2004.

[28] H. Zhang, T. Schneider, C. A. Wheeler-kingshott, and D. C. Alexander, "NeuroImage NODDI : Practical in vivo neurite orientation dispersion and density imaging of the human brain," *Neuroimage*, vol. 61, no. 4, pp. 1000–1016, 2012.

[29] D. C. Van Essen, S. Jbabdi, S. N. Sotiropoulos, C. Chen, K. Dikranian, T. Coalson, J. Harwell, T. E. Behrens, and M. F. Glasser, "Mapping Connections in Humans and Non-Human Primates," in *Diffus. MRI*, no. January 2014, pp. 337–358, Elsevier, 2014.

[30] T. E. Behrens, M. Woolrich, M. Jenkinson, H. Johansen-Berg, R. Nunes, S. Clare, P. Matthews, J. Brady, and S. Smith, "Characterization and propagation of uncertainty in diffusion-weighted MR imaging," *Magn. Reson. Med.*, vol. 50, pp. 1077–1088, nov 2003.

[31] K. H. Maier-Hein, P. F. Neher, J.-C. Houde, M.-A. Côté, E. Garyfallidis, J. Zhong, M. Chamberland, F.-C. Yeh, Y.-C. Lin, Q. Ji, W. E. Reddick, J. O. Glass, D. Q. Chen, Y. Feng, C. Gao,

Y. Wu, J. Ma, H. Renjie, Q. Li, C.-F. Westin, S. Deslauriers-Gauthier, J. O. O. González, M. Paquette, S. St-Jean, G. Girard, F. Rheault, J. Sidhu, C. M. W. Tax, F. Guo, H. Y. Mesri, S. Dávid, M. Froeling, A. M. Heemskerk, A. Leemans, A. Boré, B. Pinsard, C. Bedetti, M. Desrosiers, S. Brambati, J. Doyon, A. Sarica, R. Vasta, A. Cerasa, A. Quattrone, J. Yeatman, A. R. Khan, W. Hodges, S. Alexander, D. Romascano, M. Barakovic, A. Auría, O. Esteban, A. Lemkaddem, J.-P. Thiran, H. E. Cetingul, B. L. Odry, B. Mailhe, M. S. Nadar, F. Pizzagalli, G. Prasad, J. E. Villalon-Reina, J. Galvis, P. M. Thompson, F. D. S. Requejo, P. L. Laguna, L. M. Lacerda, R. Barrett, F. Dell'Acqua, M. Catani, L. Petit, E. Caruyer, A. Daducci, T. B. Dyrby, T. Holland-Letz, C. C. Hilgetag, B. Stieltjes, and M. Descoteaux, "The challenge of mapping the human connectome based on diffusion tractography," *Nat. Commun.*, vol. 8, p. 1349, dec 2017.

[32] M. Catani and M. Thiebaut de Schotten, "A diffusion tensor imaging tractography atlas for virtual in vivo dissections," *Cortex*, vol. 44, no. 8, pp. 1105–1132, 2008.

[33] C. J. Donahue, S. N. Sotiropoulos, S. Jbabdi, M. Hernandez-Fernandez, T. E. Behrens, T. B. Dyrby, T. Coalson, H. Kennedy, K. Knoblauch, D. C. Van Essen, and M. F. Glasser, "Using Diffusion Tractography to Predict Cortical Connection Strength and Distance: A Quantitative Comparison with Tracers in the Monkey," *J. Neurosci.*, vol. 36, no. 25, pp. 6758–6770, 2016.

[34] A. D. Elster, "Gradient-echo MR imaging: techniques and acronyms.," *Radiology*, vol. 186, no. 1, pp. 1–8, 1993.

Chapter 3
Mapping the Brain: A review of brain parcellations

3.1. Overview

Neuroscientists have long thought of the brain as a mosaic of spatially contiguous regions. How to define such regions is a hot topic in modern neuroscience. Different brain parcellations exist based on criteria such as anatomy, cytoarchitecture or functional specialization [1;2;3]. In this chapter, we introduce the main topic of our thesis: brain parcellation. We review the main criteria used to divide the brain, the methodology used to create brain parcellations under each criteria, and some widely used brain parcellations.

3.2. Introduction

Composed of billions of interconnected neurons, the brain is a highly complex biological machine. Untangling this network is the main goal of neuroscience, a task that has proven to be arduous. The problem is two fold. First, it is not feasible to characterize cellular function or axonal connectivity at the scale of the brain with current approaches. Second, even if we could characterize the neural network at a cellular level, studying it is unrealistic given the huge amount of neurons in the brain [4]. These current technical limitations highlight the need to abstract the complexity of the brain's neuronal network before studying it.

Studies in cytoarchitecture [5;1;6], brain function [7;8], and connectivity using tracers [9;10] show that neurons tend to organize and activate in spatially coherent groups. This provides us with a biological basis for dividing the brain as a set of spatially coherent regions. This process, known as parcellation, reduces the dimensionality of the neuronal network from billions of neurons to a tractable number of regions. Furthermore, if a parcellation is consistent and reproducible across subjects, we can then infer properties about the human brain in general. As of today, there is no unique parcellation of the human brain. Many brain parcellations coexist, each one based on different criteria such as: brain anatomy, function, cytoarchitecture, and structure.

In recent years we have witnessed a rapid growth in the field of brain mapping, driven by advances in Magnetic Resonance Imaging (MRI) and computational power. In this chapter, we review the state-of-the-art in brain parcellation. We focus on four different types: anatomical, functional, cytoarchitectonic and structural parcellations. For each modality we explain the criteria behind them, and the most notorious parcellations created based on them. We limit ourselves to present parcellations without benchmarking them, for more information on benchmarking please refer to the works of Thirion et al. [14], and Arslan et al. [15]. This review is by no means extensive,

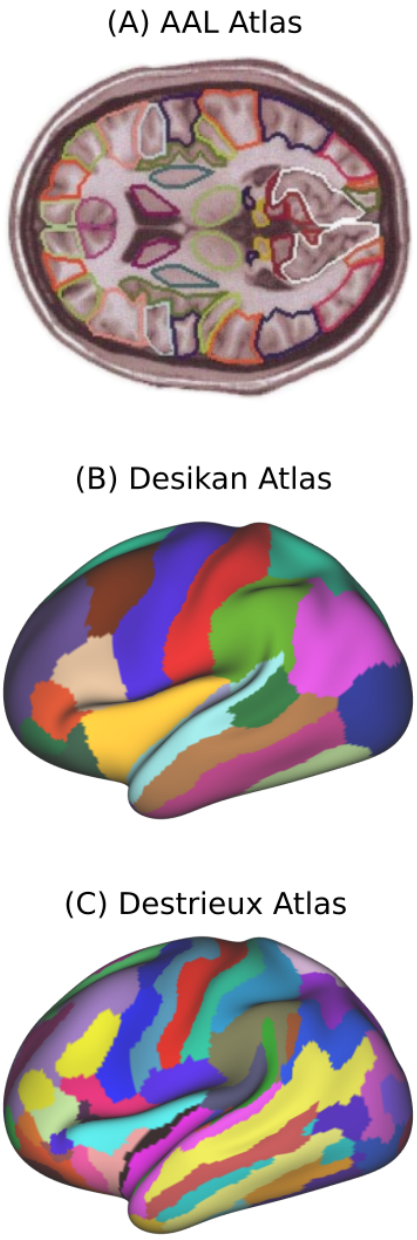

Figure 3.1: Examples of anatomical parcellations: (A) The AAL atlas [11], (B) Desikan Atlas [12], and (C) Destrieux Atlas [13]. The image of the AAL atlas was adapted from Landeau et al. [11].

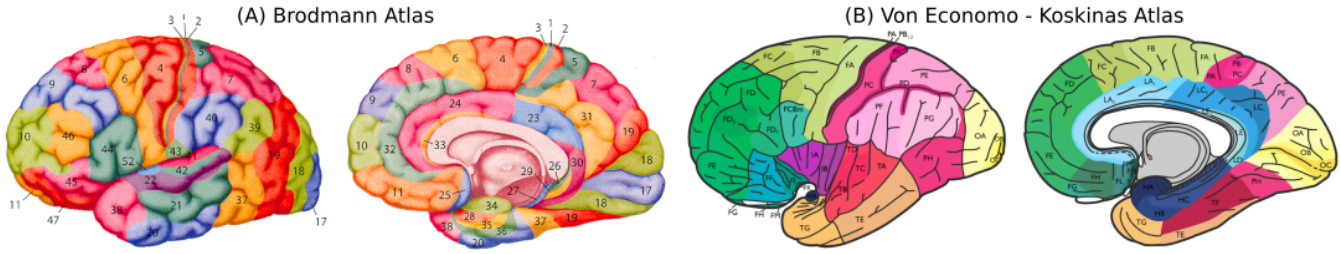

Figure 3.2: Two cytoarchitectonic parcellations: (A) The Brodmann atlas[1], and the von Economo and Koskinas atlas[6].

and more information can be found in Amunts et al.[16], Triarhou[17] Jbabdi et al.[18], Arslan et al.[15], de Reus et al.[19], and Eichhoff et al.[20;21].

3.3. Anatomical Parcellations

In Anatomical parcellations, a region is characterized by its shape or relative position in the brain. For example, in the Desikan atlas, the pars opercularis region is defined as "the first gyrus from the precentral gyrus"[12]. Anatomical parcellations were most probably the first way to subdivide the brain, since references to anatomical landmarks can already be found in ancient texts[24;25].

Early anatomical atlases where solely based on the study of post-mortem brains, being the most notable example being that of Talairach[26]. This atlas is based on the dissection of one human brain, and defines a standardized coordinate system for neurosurgery. In moderns times, the advent of MRI allowed to acquire massive amount of brain images and create brain templates. A brain template is an image which is a representative of the different brains on a population[27]. Two examples of this are the Colin27 atlas[2], based on the average of 27 scans of a healthy subject, and the Montreal Neurological Institute (MNI) brain[28], which latest version (ICBM152) is based on the average of 152 healthy subjects images. The parcellation of a brain template is, by definition, anatomically consistent across subjects, and therefore is considered an atlas. This is the case for example of the AAL atlas. The AAL atlas[11], is based on the manual parcellation of the MNI brain atlas. The MNI single-subject main sulci were first delineated and further used as landmarks for the 3D definition of 45 anatomical volumes of interest (AVOI) in each hemisphere.

When working only on the cortical surface, a well known anatomical atlas is that of Desikan et al.[12]. The Desikan et al. atlas is based on the segmentation of a surface template, generated from the average cortical folding of 40 healthy subjects projected on a sphere. The template was manually segmented into 34 coarse structures per hemisphere. In order to label a new subject, the subject's cortical folding is projected into the sphere and aligned to the template, then the labels are mapped from the atlas to their cortical surface. The automatic labeling method developed by Desikan et al. shows a great accuracy when labeling new subjects[12]. Another parcellation, made by Destrieux et al.[13], presents a finer division of the cortex in 74 parcels per hemisphere. In the case of Destrieux et al., not only the cortical folding is taken into account in order to label a region. Their underlying probabilistic model takes into account information as: the curvature and average convexity of the cortical surface, prior labeling probability for that vertex, and as the labels of vertices in its local neighborhood. Finally, the MarsAtlas[29] by Auzias et al., uses the superior temporal and inferior frontal sulcus as orthogonal axis to defines a grid over the cortex. The rest of the sulci in the brain are aligned to this grid, and used to divide the cortical surface in 41 regions. As shown in their paper, the resulting parcels have good correspondence with some specific functional activations[29].

3.4. Cytoarchitectonic Parcellations

Cytoarchitectonic divisions of the brain are based solely in the cellular composition of the cortex. In these atlases, a region is characterized by its thickness and cellular organization. For example, Brodmann Area 4 has "an unusually thick cortex; possess giant pyramidal cells, and lacks both its internal and external granular layer"[1].

Campbell[30] is considered the first neuroanatomist to create a cytoarchitectonic parcellation of the brain, composed of 14 regions with different cellular composition. Shortly after Campbell, Elliot Smith[31] divided the cortex in 50 cytoarchitectonic areas. Two years after, Broadmann published his cytoarchitectonic map of the brain[1]. Broadmann defines 52 cortical regions, based on the inspection trough microscope of cortical sections of post-mortem brains of different species. In 1925 von Economo and Koskinas published their Atlas of Cytoarchitectonics of the Adult Human Cerebral Cortex[6]. Von Economo and Koskinas' atlas recognized 54 fundamental cytoarchitectonic areas with 76 variants and 107 modifications[17]. Their atlas is based on the examination of mentally healthy subjects in the range of 30 to 40 years of age through improved dissection and acquisition methodologies. The

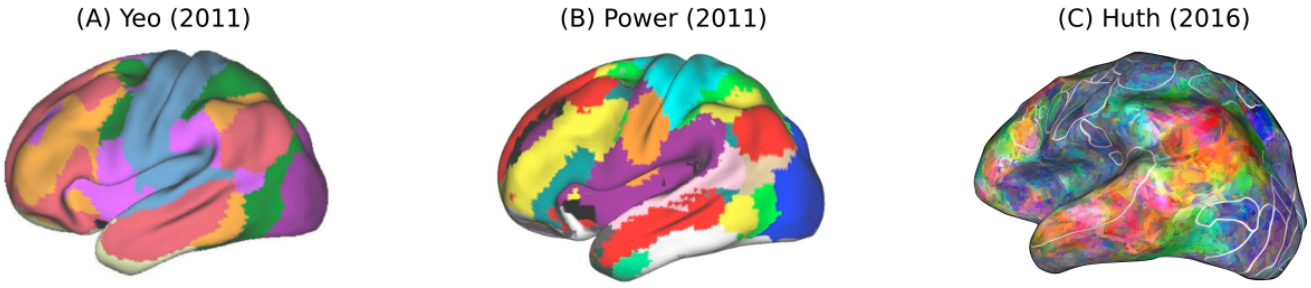

Figure 3.3: Three functional parcellations of the brain: (A) A parcellation from the resting state fMRI of 1000 subjects by Yeo et al.[3], (B) Functional networks defined by Power et al.[22], and (C) a semantic map generated by Huth et al.[23].

von Economo and Koskinas atlas is considered one of the most detailed and reproducible cytoarchitectonic atlas available[32].

More recently, Schleicher and Zilles[33] introduced a microstructural metric, the gray level index, to create observer-independent parcellation methods. Also, new cytoarchitectonic subdivisions of anatomical regions have been defined, as the one by Eickhoff et al.[34], who studied neurotransmitter receptors to map divisions in the visual cortex, or the atlas of the human ventral visual stream obtained by Rosenke et al.[35] based on the analysis of 11 post-mortem brains. Finally, new atlases have been created, such as the Jubrain[36], a cytoarchitectonic probabilistic map base of the histological sections of ten post-mortem human brains; or the one by Ding et al.[37], based on the manual dissection and parcellation of a 34 years old brain.

3.5. Functional Parcellations

Functional parcellations map cognitive functions to brain regions in the brain. In this type of parcellation, each parcel is said to be specialized to serve one cognitive function or to represent one essential aspect of the information processed by it[38].

The first functional maps were derived from lesions. The language regions for example, are named after Broca and Wernicke, who in the late 1800 reported lesions in that region for aphasic patients[39]. Another example is that of the human homunculus, a representation of motor and sensory functions, which Penfied[33] mapped through experimenting with electrical stimulation of different brain areas of patients undergoing open brain surgery.

The advent of functional MRI (fMRI) allowed to measure the blood-oxygen level dependant signal. Knowing that the level of oxygen in blood increases when neurons activate, fMRI can help to characterize which region of the brain active during specific cognitive tasks, or during rest (resting state fMRI, rs-fmri). Many functional parceling techniques rely on what is known as a functional connectivity matrix, a two dimensional matrix that quantifies the correlation between the fMRI time series of a set of brain regions. Such regions can be as big as pre-defined anatomical region or as small as a single voxel. The simplest way to quantify connection between two regions is by means of the Pearson's correlation between the fMRI time series at each region.

Most parceling techniques work by applying clustering algorithms to the functional connectivity matrix. The most popular techniques use mixture models[40;41]; ward clustering[42]; k-means clustering[3;43;44]; hierarchical clustering[45;46]; spectral clustering[47;48;49], and boundary detection[50;51;49].

Some widely used whole-brain atlases are those of Yeo et al.[3], Power et al.[22], Craddock[48]. Yeo et al.[3] propose to use k-means clustering on the average rs-fmri connectivity from 1000 subjects. The results yield two parcellations, with 7 parcels and 17 parcels respectively, that show to be reproducible across groups of subjects. Power et al.[22] use graph analysis and subgraph detection techniques in order to characterize functional subnetworks in the connectivity graph. Finally, Craddock et al.[48] use spectral clustering on rs-fmri connectivity to create fine-grained parcellations ranging form 200 to 1000 parcellations.

Other papers worth mentioning are those of Deen et al.[52] and Hurt et al.[23]. Deen et al. present a functional division of the insula, that has been proved to be highly reproducible across subjects and studies. Meanwhile, Huth et al. present an innovative atlas which maps semantic domains (e.g. violent, temporal, professional) across the cortex[23]. They use voxel-wise modelling of functional MRI (fMRI) data collected while subjects listened to hours of narrative stories.

3.6. Structural Parcellations

Structural parcellations are based on estimations of axonal connectivity. On a structural parcellations, each parcels presents a distinct pattern of connectivity with

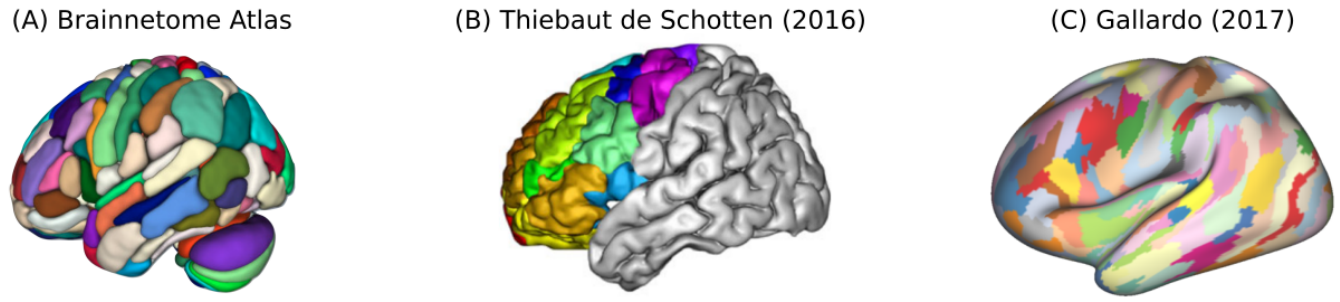

Figure 3.4: Examples of structural parcellations of the brain: (A) The Brainnetome Atlas by Fan et al.[53], (B) A parcellation of the frontal lobe by Thiebaut de Schotten et al.[54] and (C) a groupwise parcellation from Gallardo et al.[55].

respect to a predefined set of regions of interest. For example, area MFG-5 of the Brainnetome atlas has "connections with the major frontal subregions, the limbic area, the parietal subregions and the subcortical connections with the thalamus and basal ganglia subregions"[53].

The first structural atlases were defined on macaque by means of chemical tracing[10]. Advances in Diffusion MRI (dMRI) and tractography algorithms enabled the in vivo exploration of axonal connectivity on the human brain. This allowed to non-invasively estimate connectivity between different brain regions. As with functional data, the most common way to generate a parcellation is by first computing a connectivity matrix between regions (in this case, a structural connectivity matrix), and then parcellate it using some clustering technique.

The most popular techniques to parcellate the structural connectivity matrix are thresholding[56]; mixture models[57;58;59]; k-means[60]; Principal Component Analysis[61;54]; Independent Component Analysis[62]; spectral reordering[63]; spectral clustering[53]; watershed based dimension reduction[64;65]; and hierarchical clustering[66;55].

Notables work are those of Behrens et al.[56], Anwander et al.[60], Thiebaut et al.[54], Moreno-Dominguez et al.[66], Bajada et al[63] and Fan et al.[53]. Behrens et al.[56] define a structural parcellation of the thalamus. Using tractography, they compute how a set of seed voxels in the thalamus are connected to anatomically defined cortical regions. Then, they assign to each seed-voxels the label of the cortical region with which it connects the most. Anwander et al.[60] uses k-means clustering over the connectivity matrix of Broca's area, obtaining a division in 3 regions, consistent with cytoarchitectonic divisions. Thiebaut de Schotten et al.[54] parcellate the frontal lobe in 12 regions by means of principal component analysis, and shows its reproducibility across subjects and datasets. Moreno-Dominguez creates a hierarchical parcellation of the brain by using ward clustering[66], allowing to obtain a parcellation of the brain with different granularities. Fan et al.[53] use spectral clustering over connectivity data to subdivide regions of the Desikan atlas[12], obtaining a parcellation with 210 cortical areas and 36 subcortical regions. Finally, Bajada et al.[63] take a different approach and use spectral reordering to create a soft parcellation over the temporal lobe. This allows to have parcels that diffuse into each other, instead of sharp boundaries dividing them.

3.7. Multi-modal

Multi-modal parcellations are relatively new in the field of brain mapping. By combining information from different neuroimaging methodologies, multi-modal techniques create regions which boundaries are consistent with multiple independent neurobiological properties.

Examples of multi-modal parcellations are those of Diez et al.[68], Parisot et al.[69], and the Glasser-van Essen atlas[67]. Diez et al.[68] merges structural connectivity and functional connectivity in order to compute common structure-function modules (SFMs). Their methodology defines a cross-modularity index, that indicates how modular a parcellation is with respect to both matrices, and how similar is the internal connectivity in both modalities. By searching for the parcellation that maximizes this index, they obtain a cortical parcellation with 20 structure-function modules. Parisot et al.[69] starts by computing a set of parcellations from fMRI, rs-fMRI, estimations of myelin maps, and tractography. These parcellations are then fused based on their local reliabilities by means of mixture models. The fused parcellation is iteratively refined, forcing the parcellations to converge towards a set of mutually informed modality specific parcellations. Finally, Glasser et al.[67] divide the cortex in 180 regions which borders are consistent with: myelin content maps, cortical thickness maps, and task-fMRI activations. Their approach combines a semi-automated prior segmentation with a machine learning algorithm to optimize the border placement.

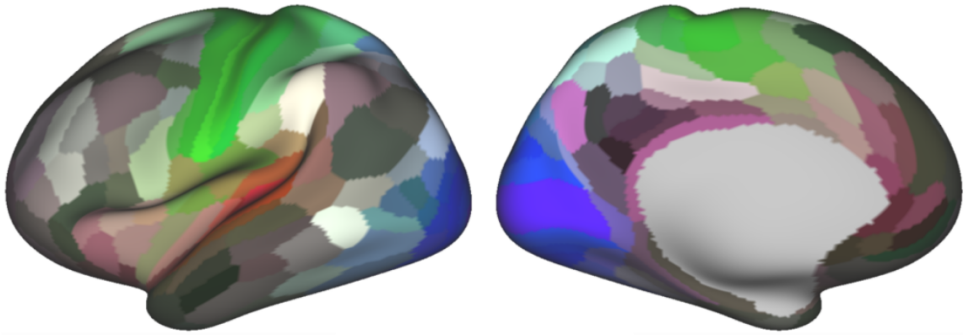

Figure 3.5: The atlas of Glasser et al.[67] is a well-known multi-modal parcellation of the brain.

3.8. Discussion

The brain is a highly complex cellular network, in order to study it, some way of dimensionality reduction is needed. Given that neurons tend to organize and activate in a spatially coherent way, it is possible to model the brain as a mosaic of regions. As seen in sections 3.3-3.7, the brain is divided on criteria such as anatomy, function, cytoarchitecture or extrinsic connectivity. Each criterion sees the brain in a different way, and relies on different acquisition methods.

Cytoarchitectonic parcellations denote the cellular composition of the brain, therefore, they are the perfect candidate to abstract populations of neurons. Also, the close relationship between cytoarchitecture and brain function[16] makes them useful as functional parcellations. However, when using these parcellations is important to acknowledge their limitations. First, existent cytoarchitectonic maps do not cover the whole brain, in fact, only approximately 40% of the cortical surface has been mapped[16]. Second, all cytoarchitectonic atlases are based on just a few post-mortem brains, making them hard to represent a population. This is product of the complex process of dissecting a brain, delimiting its regions, and registering the results to a common space. The whole process requires in most cases one person year of work per region. Finally, and most importantly, given the amount of variability[70] in different subjects, registering a cytoarchitectonic atlas to a new brain based on anatomical features does not guarantee the correct localization of the areas. Until now, post-mortem dissection remains as the only way to correctly locate cytoarchitectonic areas.

Anatomical parcellations are based on fairly common brain landmarks, making them highly reproducible across subjects, but incurring in the trade-off of having coarse brain regions. Nowadays, the general function of most anatomical parcels is known, making them useful to use as a gross first delimitation of the brain when studying particular brain functions. When using anatomical atlases, it is important to remind that only the borders of a few architectonically defined areas show a sufficiently precise association with sulci[16]. Hence, anatomical atlases are not good candidates to abstract populations of neurons in the brain.

Functional parcellations map cognitive functions to brain locations, and are a key element to understand how the brain works. Many functions have been shown to be consistent across subjects[39;7;3], and the close relationship with cytoarchitecture makes them good candidate to abstract population of neurons. However, functional parcellations are based on the modular paradigm, which states that one brain region is specialized on one cognitive function. New evidence suggests that the modular paradigm has serious limitations and might in fact be misleading[71].

Structural parcellations define regions with homogeneous axonal connectivity. Axonal connectivity plays a fundamental role in the interaction between brain regions[9]. Moreover, long-range axonal connections are strongly related to brain function[72], and cytoarchitecture[62]. The downside is that tractography, the underlying technique to estimate axonal connectivity, is still not mature enough. In fact, recent studies show that state-of-the-art tractography algorithms create four times more false positives than true positives[73].

Multi-modal parcellations combine information from different neuroimaging methodologies, in order to create regions consistent with multiple neurobiological properties. Their main limitation is that sometimes, regions tend to over represent one modality. A clear example is the subdivision of the precentral and poscentral gyrus in the atlas of Glasser et al.[67]. Even when motor tasks are used during the construction of the atlas, the resulting subdivisions of both motor and sensory cortex appear to be driven by myelination. This result is inconsistent with the well known functional subdivision of both motor and sensory cortex.

We finish this review by highlighting that, if a universal parcellation of the brain exists, it has not been found yet. Meanwhile, different atlases and techniques to divide the

brain coexist. As discussed above, parcellations based on different criteria have different advantages and disadvantages. At the end, which parcellation to use in practice will heavily depend on the hypothesis and the goal of the study to be done.

3.9. Conclusion

In this chapter we presented parcellations based on different criteria and discussed their advantages. In the following chapter we will introduce the first contribution of this thesis: a parsimonious model for the long-range connectivity and a whole-brain structural parceling technique. We will show that our technique creates parcels in agreement with anatomical, structural and functional parcellations existent in the literature.

Bibliography

[1] K. Brodmann, *Vergleichende Lokalisationslehre der Großhirnrinde in ihren Prinzipien dargestellt auf Grund des Zellaufbaues*. Leipzig: Barth, 1909.

[2] D. L. Collins, A. P. Zijdenbos, V. Kollokian, J. G. Sied, N. J. Kabani, C. J. Holmes, and A. C. Evans, "Design and construction of a realistic digital brain phantom," *IEEE Trans. Med. Imaging*, vol. 17, no. 3, pp. 463–468, 1998.

[3] B. T. Yeo, F. M. Krienen, J. Sepulcre, M. R. Sabuncu, D. Lashkari, M. Hollinshead, J. L. Roffman, J. W. Smoller, L. Zollei, J. R. Polimeni, B. Fischl, H. Liu, and R. L. Buckner, "The organization of the human cerebral cortex estimated by intrinsic functional connectivity," *J. Neurophysiol.*, vol. 106, pp. 1125–1165, 2011.

[4] G. Gong, Y. He, L. Concha, C. Lebel, D. W. Gross, A. C. Evans, and C. Beaulieu, "Mapping anatomical connectivity patterns of human cerebral cortex using in vivo diffusion tensor imaging tractography," *Cereb. Cortex*, vol. 19, no. 3, pp. 524–536, 2009.

[5] T. Meynert, "Der Bau der Gross-Hirnrinde und seine örtlichen Verschiedenheiten, nebst einem pathologischanatomischen Corollarium," *Neuwied, JH Heuser'sche Ver- lagsbuchhandlung*, pp. 1–68, 1872.

[6] C. von Economo and G. N. Koskinas, *Die Cytoarchitektonik der Hirnrinde des erwachsenen Menschen. Textband und Atlas*. Wien: Springer, 1925.

[7] W. Penfield and H. Jasper, *Epilepsy and the Functional Anatomy of the Human Brain*. 1954.

[8] C. von der Malsburg, "The Correlation Theory of Brain Function," in *Model. Neural Networks SE - 2* (E. Domany, J. van Hemmen, and K. Schulten, eds.), Physics of Neural Networks, pp. 95–119, Springer New York, 1994.

[9] J. D. Schmahmann and D. N. Pandya, *Fiber Pathways of the Brain*, vol. 1. Oxford University Press, apr 2006.

[10] K. E. Stephan, "The history of CoCoMac," *Neuroimage*, vol. 80, pp. 46–52, 2013.

[11] N. Tzourio-Mazoyer, B. Landeau, D. Papathanassiou, F. Crivello, O. Etard, N. Delcroix, B. Mazoyer, and M. Joliot, "Automated anatomical labeling of activations in SPM using a macroscopic anatomical parcellation of the MNI MRI single-subject brain," *Neuroimage*, vol. 15, no. 1, pp. 273–289, 2002.

[12] R. S. Desikan, F. Ségonne, B. Fischl, B. T. Quinn, B. C. Dickerson, D. Blacker, R. L. Buckner, A. M. Dale, R. P. Maguire, B. T. Hyman, M. S. Albert, and R. J. Killiany, "An automated labeling system for subdividing the human cerebral cortex on MRI scans into gyral based regions of interest," *Neuroimage*, vol. 31, pp. 968–980, jul 2006.

[13] C. Destrieux, B. Fischl, A. Dale, and E. Halgren, "Automatic parcellation of human cortical gyri and sulci using standard anatomical nomenclature," *Neuroimage*, vol. 53, no. 1, pp. 1–15, 2010.

[14] B. Thirion, G. Varoquaux, E. Dohmatob, and J. B. Poline, "Which fMRI clustering gives good brain parcellations?," *Front. Neurosci.*, vol. 8, no. 8 JUL, pp. 1–13, 2014.

[15] S. Arslan, S. I. Ktena, A. Makropoulos, E. C. Robinson, D. Rueckert, and S. Parisot, "Human brain mapping: A systematic comparison of parcellation methods for the human cerebral cortex," 2018.

[16] K. Amunts, A. Schleicher, and K. Zilles, "Cytoarchitecture of the cerebral cortex - More than localization," *Neuroimage*, vol. 37, no. 4, pp. 1061–1065, 2007.

[17] L. C. Triarhou, "The Economo-Koskinas atlas revisited: Cytoarchitectonics and functional context," 2007.

[18] S. Jbabdi and T. E. Behrens, "Long-range connectomics," *Ann. N. Y. Acad. Sci.*, vol. 1305, pp. 83–93, dec 2013.

[19] M. A. de Reus and M. P. van den Heuvel, "The parcellation-based connectome: Limitations and extensions," *Neuroimage*, vol. 80, pp. 397–404, 2013.

[20] S. B. Eickhoff, B. Thirion, G. Varoquaux, and D. Bzdok, "Connectivity-based parcellation: Critique and implications," *Hum. Brain Mapp.*, vol. 36, no. 12, pp. 4771–4792, 2015.

[21] S. B. Eickhoff, B. T. T. Yeo, and S. Genon, "Imaging-based parcellations of the human brain," *Nat. Rev. Neurosci.*, 2018.

[22] J. D. Power, A. L. Cohen, S. S. M. Nelson, G. S. Wig, K. A. Barnes, J. A. Church, A. C. Vogel, T. O. Laumann, F. M. Miezin, B. L. Schlaggar, and S. E. Petersen, "Functional network organization of the human brain," *Neuron*, vol. 72, no. 4, pp. 665–678, 2011.

[23] A. G. Huth, W. A. De Heer, T. L. Griffiths, F. E. Theunissen, and J. L. Gallant, "Natural speech reveals the semantic maps that tile human cerebral cortex," *Nature*, vol. 532, no. 7600, pp. 453–458, 2016.

[24] C. A. Elsberg, "The anatomy and surgery of the Edwin Smith surgical papyrus," *. J. Mt. Sinai Hoop*, vol. 12, pp. 141–151, 1945.

[25] M. Collice, R. Collice, and A. Riva, "Who discovered the Sylvian fissure?," 2008.

[26] J. Talairach and P. Tournoux, *Co-Planar Stereotaxic Atlas of the Human Brain*. New York: Thieme Medical Publishers, Inc, 1988.

[27] A. C. Evans, A. L. Janke, D. L. Collins, and S. Baillet, "NeuroImage Brain templates and atlases," *Neuroimage*, vol. 62, no. 2, pp. 911–922, 2012.

[28] C. J. Holmes, R. Hoge, L. Collins, and A. C. Evans, "Enhancement of T1 MR images using registration for signal averaging," in *NeuroImage, 2sd Int. Conf. Funct. Mapp. Hum. Brain, Boston, USA*, vol. 3, No. 3,, p. S28, 1996.

[29] G. Auzias, O. Coulon, and A. Brovelli, "MarsAtlas: A cortical parcellation atlas for functional mapping," *Hum. Brain Mapp.*, vol. 37, no. 4, pp. 1573–1592, 2016.

[30] A. W. Campbell, *Histological Studies on the Localization of Cerebral Function*. Cambridge: University Press, 1905.

[31] E. G. Smith, "A new topographical survey of the human cerebral cortex, being an account of the distribution of the anatomically distinct cortical areas and their relationship to the cerebral sulci," *J Anat Physiol*, vol. 41, pp. 237–254, 1907.

[32] J. K. Peden and G. V. Bonin, "The Neocortex of Hapale," *J. Comp. Neurol.*, vol. 86, pp. 37–63, 1947.

[33] A. Schleicher and K. Zilles, "A quantitative approach to cytoarchitectonics: Analysis of structural inhomogeneities in nervous tissue using an image analyser," *J. Microsc.*, vol. 157, no. 3, pp. 367–381, 1990.

[34] S. B. Eickhoff, C. Rottschy, M. Kujovic, N. Palomero-Gallagher, and K. Zilles, "Organizational principles of human visual cortex revealed by receptor mapping," *Cereb. Cortex*, vol. 18, no. 11, pp. 2637–2645, 2008.

[35] M. Rosenke, K. S. Weiner, M. A. Barnett, K. Zilles, K. Amunts, R. Goebel, and K. Grill-Spector, "A cross-validated cytoarchitectonic atlas of the human ventral visual stream," *Neuroimage*, vol. 170, no. February 2017, pp. 257–270, 2018.

[36] H. Mohlberg, S. B. Eickhoff, A. Schleicher, K. Zilles, and A. K., "A new processing pipeline and release of cytoarchitectonic probabilistic maps – JuBrain," *OHBM 2012*, 2012.

[37] S. L. Ding, J. J. Royall, S. M. Sunkin, L. Ng, B. A. Facer, P. Lesnar, A. Guillozet-Bongaarts, B. McMurray, A. Szafer, T. A. Dolbeare, A. Stevens, L. Tirrell, T. Benner, S. Caldejon, R. A. Dalley, N. Dee, C. Lau, J. Nyhus, M. Reding, Z. L. Riley, D. Sandman, E. Shen, A. van der Kouwe, A. Varjabedian, M. Write, L. Zollei, C. Dang, J. A. Knowles, C. Koch, J. W. Phillips, N. Sestan, P. Wohnoutka, H. R. Zielke, J. G. Hohmann, A. R. Jones, A. Bernard, M. J. Hawrylycz, P. R. Hof, B. Fischl, and E. S. Lein, "Comprehensive cellular-resolution atlas of the adult human brain," *J. Comp. Neurol.*, vol. 524, no. 16, pp. 3127–3481, 2016.

[38] J. M. Fuster, "The Module: Crisis of a Paradigm," *Neuron*, vol. 26, pp. 51–53, 2000.

[39] P. Johns, *Clinical Neuroscience*.

[40] D. Lashkari, E. Vul, N. Kanwisher, and P. Golland, "Discovering structure in the space of fMRI selectivity profiles," *Neuroimage*, vol. 50, no. 3, pp. 1085–1098, 2010.

[41] S. Ryali, T. Chen, K. Supekar, and V. Menon, "A parcellation scheme based on von Mises-Fisher distributions and Markov random fields for segmenting brain regions using resting-state fMRI," *Neuroimage*, vol. 65, pp. 83–96, 2013.

[42] T. Blumensath, S. Jbabdi, M. F. Glasser, D. C. Van Essen, K. Ugurbil, T. E. Behrens, and S. M. Smith, "Spatially constrained hierarchical parcellation of the brain with resting-state fMRI," *Neuroimage*, vol. 76, pp. 313–324, 2013.

[43] X. Shen, F. Tokoglu, X. Papademetris, and R. T. Constable, "Groupwise whole-brain parcellation from resting-state fMRI data for network node identification," *Neuroimage*, vol. 82, pp. 403–415, 2013.

[44] T. Kahnt, L. J. Chang, S. Q. Park, J. Heinzle, and J.-D. Haynes, "Connectivity-based parcellation of the human orbitofrontal cortex," *J. Neurosci.*, no. 32, pp. 6240–6250, 2012.

[45] S. B. Eickhoff, D. Bzdok, A. R. Laird, C. Roski, S. Caspers, K. Zilles, and P. T.Foxd, "Co-activation patterns distinguish cortical modules, their connectivity and functional differentiation," *Neuroimage*, vol. 57, no. 938, 2011.

[46] E. Eger, C. Keribin, V. Michel, A. Gramfort, and B. Thirion, "A supervised clustering approach for fMRI -based inference of brain states," *Pattern Recognit.*, vol. 45, pp. 2041–2049, 2012.

[47] B. Thirion, G. Flandin, P. Pinel, A. Roche, P. Ciuciu, and J. B. Poline, "Dealing with the shortcomings of spatial normalization: multi-subject parcellation of fmri datasets," *Hum. Brain Mapp.*, vol. 27, pp. 678–693, 2006.

[48] R. C. Craddock, G. A. James, P. E. Holtzheimer, X. P. Hu, and H. S. Mayberg, "A whole brain fMRI atlas generated via spatially constrained spectral clustering," *Hum. Brain Mapp.*, vol. 33, no. 8, pp. 1914–1928, 2012.

[49] A. Schaefer, R. Kong, E. M. Gordon, T. O. Laumann, X.-n. Zuo, A. J. Holmes, S. B. Eickhoff, and B. T. Yeo, "Local-Global Parcellation of the Human Cerebral Cortex from Intrinsic Functional Connectivity MRI," *Cereb. Cortex*, pp. 1–20, 2017.

[50] E. M. Gordon, T. O. Laumann, B. Adeyemo, J. F. Huckins, W. M. Kelley, and S. E. Petersen, "Generation and Evaluation of a Cortical Area Parcellation from Resting-State Correlations," *Cereb. Cortex*, vol. 26, no. 1, pp. 288–303, 2016.

[51] G. S. Wig, T. O. Laumann, A. L. Cohen, J. D. Power, S. M. Nelson, M. F. Glasser, F. M. Miezin, A. Z. Snyder, B. L. Schlaggar, and S. E. Petersen, "Parcellating an individual subject's cortical and subcortical brain structures using snowball sampling of resting-state correlations," *Cereb. Cortex*, vol. 24, no. 8, pp. 2036–2054, 2014.

[52] B. Deen, N. B. Pitskel, and K. A. Pelphrey, "Three systems of insular functional connectivity identified with cluster analysis," *Cereb. Cortex*, vol. 21, no. 7, pp. 1498–1506, 2011.

[53] L. Fan, H. Li, J. Zhuo, Y. Zhang, J. Wang, L. Chen, Z. Yang, C. Chu, S. Xie, A. R. Laird, P. T. Fox, S. B. Eickhoff, C. Yu, and T. Jiang, "The Human Brainnetome Atlas: A New Brain Atlas Based on Connectional Architecture," *Cereb. Cortex*, vol. 26, no. 8, pp. 3508–3526, 2016.

[54] M. Thiebaut de Schotten, M. Urbanski, B. Batrancourt, R. Levy, B. Dubois, L. Cerliani, and E. Volle, "Rostro-caudal Architecture of the Frontal Lobes in Humans," *Cereb. Cortex*, pp. 1–15, 2016.

[55] G. Gallardo, W. Wells, R. Deriche, and D. Wassermann, "Groupwise structural parcellation of the whole cortex: A logistic random effects model based approach," *Neuroimage*, pp. 1–14, feb 2017.

[56] T. E. Behrens, H. Johansen-Berg, M. W. Woolrich, S. M. Smith, C. A. M. Wheeler-Kingshott, P. A. Boulby, G. J. Barker, E. L. Sillery, K. Sheehan, O. Ciccarelli, A. J. Thompson, J. M. Brady, and P. M. Matthews, "Non-invasive mapping of connections between human thalamus and cortex using diffusion imaging," *Nat. Neurosci.*, vol. 6, pp. 750–757, jul 2003.

[57] S. Jbabdi, M. W. Woolrich, and T. E. Behrens, "Multiple-subjects connectivity-based parcellation using hierarchical Dirichlet process mixture models," *Neuroimage*, vol. 44, no. 2, pp. 373–384, 2009.

[58] M. J. Clarkson, I. B. Malone, M. Modat, K. K. Leung, N. Ryan, D. C. Alexander, N. C. Fox, and S. Ourselin, *A Framework For Using Diffusion Weighted Imaging To Improve Cortical Parcellation*, vol. 6362 of *Lecture Notes in Computer Science*. Berlin, Heidelberg: Springer Berlin Heidelberg, 2010.

[59] S. Parisot, S. Arslan, J. Passerat-Palmbach, W. M. Wells, and D. Rueckert, "Tractography-Driven Groupwise Multi-scale Parcellation of the Cortex.," *Inf. Process. Med. Imaging*, vol. 24, pp. 600–12, 2015.

[60] A. Anwander, M. Tittgemeyer, D. von Cramon, A. Friederici, and T. Knosche, "Connectivity-Based Parcellation of Broca's Area," *Cereb. Cortex*, vol. 17, pp. 816–825, may 2006.

[61] M. Thiebaut de Schotten, M. Urbanski, R. Valabregue, D. J. Bayle, and E. Volle, "Subdivision of the occipital lobes: An anatomical and functional MRI connectivity study," *Cortex*, vol. 56, pp. 121–137, 2014.

[62] J. O'Muircheartaigh and S. Jbabdi, "Concurrent white matter bundles and grey matter networks using independent component analysis," 2018.

[63] C. J. Bajada, R. L. Jackson, H. A. Haroon, H. Azadbakht, G. J. Parker, M. A. Lambon Ralph, and L. L. Cloutman, "A graded tractographic parcellation of the temporal lobe," *Neuroimage*, vol. 155, no. April, pp. 503–512, 2017.

[64] P. Roca, D. Rivière, P. Guevara, C. Poupon, and J. F. Mangin, "Tractography-based parcellation of the cortex using a spatially-informed dimension reduction of the connectivity matrix," *Lect. Notes Comput. Sci. (including Subser. Lect. Notes Artif. Intell. Lect. Notes Bioinformatics)*, vol. 5761 LNCS, no. PART 1, pp. 935–942, 2009.

[65] S. Lefranc, P. Roca, M. Perrot, C. Poupon, D. Le Bihan, J.-F. Mangin, and D. Rivière, "Groupwise connectivity-based parcellation of the whole human cortical surface using watershed-driven dimension reduction," *Med. Image Anal.*, vol. 30, pp. 11–29, may 2016.

[66] D. Moreno-Dominguez, A. Anwander, and T. R. Knösche, "A hierarchical method for whole-brain connectivity-based parcellation," *Hum. Brain Mapp.*, vol. 35, pp. 5000–5025, oct 2014.

[67] M. F. Glasser, T. S. Coalson, E. C. Robinson, C. D. Hacker, J. Harwell, E. Yacoub, K. Ugurbil, J. Andersson, C. F. Beckmann, M. Jenkinson, S. M. Smith, and D. C. Van Essen, "A multi-modal parcellation of human cerebral cortex.," *Nature*, vol. 536, no. 7615, pp. 171–8, 2016.

[68] I. Diez, P. Bonifazi, I. Escudero, B. Mateos, M. A. Muñoz, S. Stramaglia, and J. M. Cortes, "A novel brain partition highlights the modular skeleton shared by structure and function," *Sci. Rep.*, vol. 5, pp. 1–13, 2015.

[69] S. Parisot, B. Glocker, S. I. Ktena, S. Arslan, M. D. Schirmer, and D. Rueckert, "A flexible graphical model for multi-modal parcellation of the cortex," *Neuroimage*, vol. 162, no. September, pp. 226–248, 2017.

[70] K. Zilles and K. Amunts, "Individual variability is not noise," *Trends Cogn. Sci.*, vol. 17, pp. 153–155, apr 2013.

[71] S. L. Bressler and V. Menon, "Large-scale brain networks in cognition: emerging methods and principles," *Trends Cogn. Sci.*, vol. 14, no. 6, pp. 277–290, 2010.

[72] R. E. Passingham, K. E. Stephan, and R. Kötter, "The anatomical basis of functional localization in the cortex," *Nat. Rev. Neurosci.*, vol. 3, pp. 606–616, aug 2002.

[73] K. H. Maier-hein, P. Neher, J. Christophe, and M. Alexandre, "Tractography - based connectomes are dominated by false - positive connections," *bioRxiv*, pp. 1–23, 2016.

Part II

Methods

Chapter 4
Groupwise Structural Parcellation of the Whole Cortex: A Logistic Random Effects Model Based Approach

4.1. Overview

So far in this thesis we have introduced the necessary concepts in neuroanatomy; non-invasive imaging techniques to study the brain, and brain parcellation. In the first chapter we explained the importance of brain connectivity and its relation to brain function. On the second chapter, we explained how to estimate brain connectivity and brain function in a non-invasive way. The third chapter showed the ongoing effort to find new and relevant ways to divide the brain, in order to improve the way to study it. In particular, all of the parcellations based on structural connectivity are computationally expensive; need tuning of several parameters or rely on ad-hoc constraints. Furthermore, none of these methods present a model for the cortical extrinsic connectivity of the cortex. In this chapter, we propose a parsimonious model for the extrinsic connectivity and an efficient parceling technique based on clustering of tractograms. Our technique allows the creation of single subject and groupwise parcellations of the whole cortex. We show that our technique creates parcellations in agreement with anatomical, structural and functional parcellations extant in the literature.

This work has been published in the journal Neuroimage [1]

4.2. Introduction

The human brain is arranged in areas based on criteria such as cytoarchitecture, functional specialization or axonal connectivity [2;3;4]. Parceling the cortex into such areas and characterizing their interaction is key to understanding how the brain works. Nowadays it is accepted that axonal connectivity plays a fundamental role in the interaction between brain regions [5]. Moreover, current theories hold that long-range physical connections trough axonal bundles, namely *extrinsic connectivity*, are strongly related to brain function, for example, this has been shown in macaques [6]. Therefore, understanding how the cortex is arranged based on its extrinsic connectivity can provide key information in unraveling the internal organization of the brain.

Diffusion MRI (dMRI) enables the in vivo exploration of extrinsic connectivity and other aspects of white matter anatomy on the brain. However, in using diffusion MRI to infer long-distance connectivity, several challenges arise. A primary issue is the spatial resolution of diffusion imaging: it is several orders of magnitude coarser than axonal diameters (millimeters vs. micrometers) [7], making hard to infer some brain pathways. In addition, there is as yet no quantitative measure of the strength of connections from diffusion [8]. Given these general limitations, obtaining a cortical parcellation based on extrinsic connectivity remains challenging [7;8]. Moreover, most current parceling techniques compute either single-subject or groupwise parcellations. Single-subject techniques work by refining other parcellations [9], which introduces a bias in the resulting parcellation; parceling only part of the cortex [10;11;12;4] or using ad-hoc metrics to compare extrinsic connectivity [13]. Meanwhile, existing groupwise methods rely on average connectivity profiles [9;14], which prevents obtaining single subject parcellations; seek a matching across subjects after independent parcellations [13], relying on possible noisy results, or need fine tuning of parameters, as the expected number of clusters to find [15].

In this work, we present a parsimonious model for the cortical connectivity alongside an efficient parceling technique based on it. We summarize both contributions in Fig. 4.1. Our model assumes that the cortex is divided in patches of homogeneous extrinsic connectivity. That is, nearby neurons in the cortex share approximately the same long-range physical connections, we call this the *local coherence criterion*. Our assumption is based on histological results in the macaque brain [5]. Inspired by statistical models for clustered data [16], our model accounts for the variability in the axonal connections of neurons within a patch and for variability in patch boundaries across subjects. Our parceling technique allows us to create single subject and groupwise parcellations of the whole cortex in agreement with extant parcellations.

We validate our technique by taking advantage of data available from the Human Connectome Project (HCP). Using our technique, we compute single subject and a groupwise parcellations. In this work we will focus on the groupwise case. For results of our method on the single-subject case please refer to Gallardo et al. [1] Here, we first assess the consistency of our groupwise parceling technique by comparing the groupwise parcellations of three disjoint groups of 46 subjects from the HCP. We also show that our technique computes a similar parcellation to the one obtained by Thiebaut de Schotten et al. [4] when parceling only the frontal cortex. Later, to test the

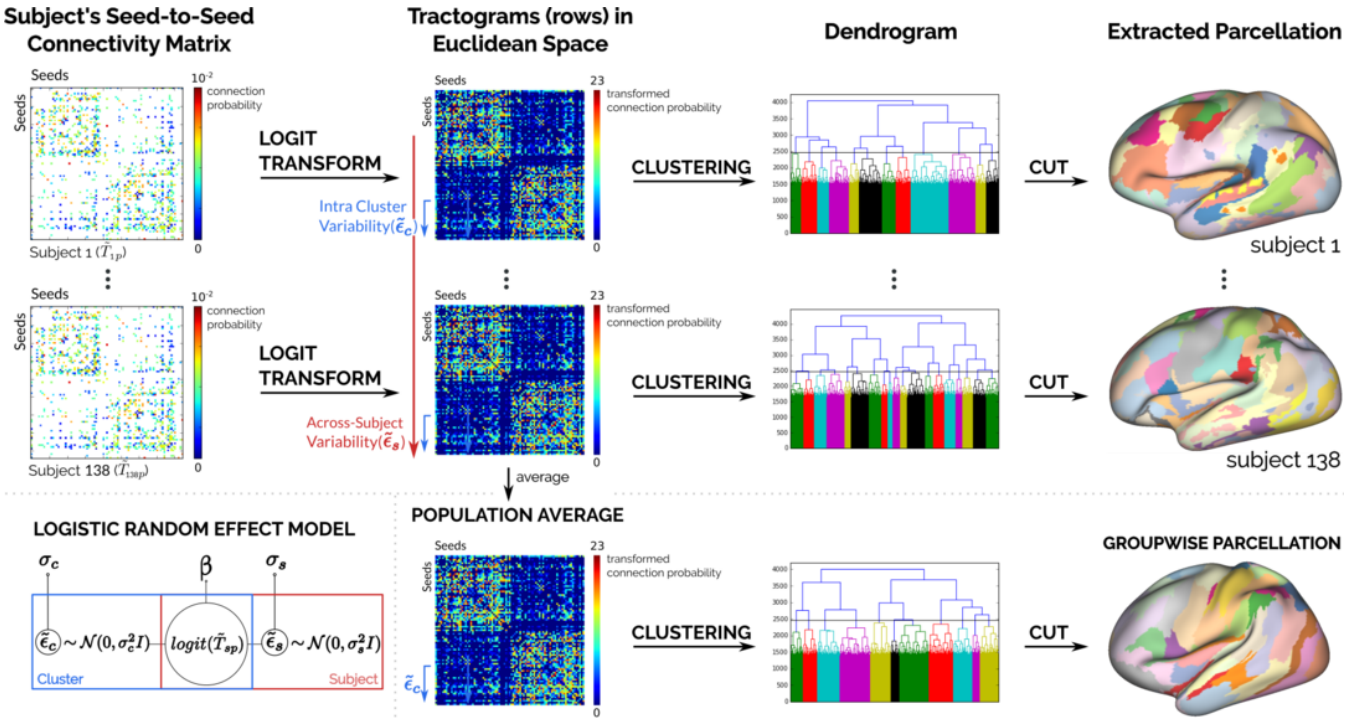

Figure 4.1: Lower left corner: graphical model of the linear relationship between the tractogram of a subject s for a seed p ($\tilde{T}_{sp}$); and the intra-cluster ($\tilde{\epsilon}_c$) and across-subject ($\tilde{\epsilon}_s$) variability of the seed's patch. We transform the tractograms into a Euclidean space while explicitly accounting for the variability. This allows us to use well known clustering techniques and compress different levels of granularities for a same parcellation in a dendrogram.

functional specialization of our frontal lobe parcels, we use a data-base of meta-analysis of fMRI studies[17], as in Thiebaut de Schotten et al. citeThiebautdeSchotten2016. After, we show that our groupwise parcels subdivide some well-known anatomical structures by comparing our results against Desikan's atlas[18]. Also, we show the functional specialization of some of our parcels by comparing against results from Glasser et al.[19]. Finally, we compare our groupwise parcellation of 138 subjects against the multi-modal parcellation of Glasser et al.[20]. We show that, while the parcellations boundaries differ, our parcels show similar or better functional specialization, specially for motor related tasks.

This work is organized as follows: In the Methods section we present our model for cortical connectivity and frame tractography within our model. Also, we present both our single-subject and groupwise case methodologies to parcellate the cortex. In the Experiments and Results section we present our results on HCP data. We then discuss our results and position ourselves with respect to the state of the art in the Discussion section. Finally, in the last section we provide our conclusions.

4.3. Methods

Cortical Connectivity Model and Tractography

Our model assumes that the cortex is divided in clusters of homogeneous extrinsic connectivity. That is, nearby neurons in the cortex share approximately the same long-ranged physical connections, we call this the *local coherence criterion*. Our assumption is based on histological results in the macaque brain[5]. As in clustered data models in statistics[16], we allow intra-cluster and across-subject variability in the connectivity. We formalize this concept as:

$$K = \bigcup_{i=1}^{k} K_i \tag{4.1}$$

$$\forall_{1 \leq i,j \leq k}, i \neq j \rightarrow K_i \cap K_j = \emptyset \wedge \text{conn}(K_i) \neq \text{conn}(K_j)$$

where the set of points on the cortex K is the disjoint union of each cluster K_i and conn$(\cdot)$ is the extrinsic connectivity fingerprint of a cluster. We will make the notion of variability explicit in eq. 4.3. In this work, the connectivity fingerprint of a seed-point in the brain is a binary vector denoting to which other seed-points it is connected through axonal bundles. That is, the physical connections of a point $p \in K_i$ in the brain are represented by its connectivity fingerprint conn(p) = conn(K_i).

Currently, the most common tool for estimating the extrinsic connectivity fingerprint of a point in vivo is probabilistic tractography[8]. Given a seed-point in the brain,

probabilistic tractography creates a *tractogram*: an image where each voxel is valued with its probability of being connected to the seed through axonal bundles. One way of calculating these probabilities is with a Monte Carlo procedure, simulating the random walk of water particles through the white matter [21]. Each one of these paths is known as a streamline. If we model these streamlines as Bernoulli trials, where we get a value for the connection from our seed with other points (1 if they connected by the streamline, 0 if not) [21], then, we can model the tractogram of the subject s in the seed-point p as:

$$\begin{aligned} T_{sp} &= [P(\tilde{C}_{spi} = 1)]_{1\leq i\leq n} \\ &= [\theta_{spi}]_{1\leq i\leq n}, \quad \tilde{C}_{spi} \sim \text{Bernoulli}(\theta_{spi}), \end{aligned} \tag{4.2}$$

where $\tilde{C}_{spi}$ is a Bernoulli random variable[1] representing "the point p of the subject s is connected to the voxel i". Each Bernoulli's parameter (θ_{spi}) represents the probability of being connected, and is estimated as the proportion of success in the Bernoulli trials of each seed.

To formulate the tractogram in accordance to our hypothesis of cortical connectivity, we model it as a vector of random variables. In our model, each element in a tractogram comes from a random variable depending on the point's cluster along with its intra-cluster and across-subject variability:

$$p \in K_c \rightarrow \tilde{T}_{sp} = [P(\tilde{C}_{spi} = 1 | \operatorname{conn}(K_c),\ \tilde{\epsilon}_{ci},\ \tilde{\epsilon}_{si})]_{1\leq i\leq n} \tag{4.3}$$

in this case, the point p belongs to the cluster c; $\tilde{\epsilon}_{ci}$ represents the intra-cluster variability and $\tilde{\epsilon}_{si}$ represents the across-subject variability for the connectivity to voxel i in the cluster c.

Since each $\tilde{C}_{spi}$ follows a Bernoulli distribution (Eq. 4.2) it is difficult to find an explicit formulation for $P(\tilde{C}_{spi} = 1 | \operatorname{conn}(K_c),\ \tilde{\epsilon}_{ci},\ \tilde{\epsilon}_{si})$ accounting for the variabilities. For this, we use the generalized linear model (GLM) theory. In this theory, the data is assumed to follow a linear form after being transformed with an appropriate link function [22]. Using the following notation abuse:

$$\operatorname{logit}(\tilde{T}_{sp}) \triangleq [\operatorname{logit}(P(\tilde{C}_{spi} = 1 | \operatorname{conn}(K_c),\ \tilde{\epsilon}_{ci},\ \tilde{\epsilon}_{si})]_{1\leq i\leq n}, \tag{4.4}$$

we derive from GLM a logistic random-effects model [16] for each point p:

$$\operatorname{logit}(\tilde{T}_{sp}) = \beta_c + \tilde{\epsilon}_c + \tilde{\epsilon}_s \in \mathbb{R}^n, \tag{4.5}$$

$$\tilde{\epsilon}_c \sim \mathcal{N}(\vec{0}, \sigma_c^2 Id),\ \tilde{\epsilon}_s \sim \mathcal{N}(\vec{0}, \sigma_s^2 Id),$$

where ϵ_c and ϵ_s represent the intra-cluster and across-subject variability respectively. According to GLM theory $\beta_c \in \mathbb{R}^n$ is the extrinsic connectivity fingerprint of cluster K_c transformed:

$$\operatorname{logit}^{-1}(\beta_c) = E(\tilde{T}_{sp}) = \operatorname{conn}(K_c)\ . \tag{4.6}$$

The choice of logit as link function is based on the work of Pohl et al. [23]. In their work, Pohl et al. [23] show that logit function's codomain is a Euclidean space, which allows us to transform and manipulate the tractograms in a well-known space.

Single Subject and Groupwise Parceling Methodologies

In the previous section, we hypothesized that the cortex is divided in clusters with homogeneous extrinsic connectivity, alongside intra-cluster and across-subject variability. In using the previous hypothesis, it is important to remark that we don't have a priori knowledge of the cluster's location or their variability. But, thanks to the proposed logistic random effects model, we formulated the problem of finding these clusters as a well-known clustering problem. This is because, after transforming the tractograms with the logit function as in eq. 4.4 they will be in a Euclidean space [23]. Even more, eq. 4.5 states that the transformed tractograms come from a mixture of Gaussian distributions, e.g. it is a Gaussian mixture model.

To solve the Gaussian mixture model and find the clusters, we use a modified Agglomerative Hierarchical Clustering (AHC) algorithm. This was inspired by the method of Moreno-Dominguez et al. [13]. To enforce the local coherence criterion we also modify the algorithm to accept one parameter: the minimum size of the resulting clusters. Clusters smaller than this size are merged with neighbors, i.e. physically close clusters in the cortex. As we are working in a Euclidean space, we use Ward's Hierarchical Clustering method [24]. This method creates clusters with minimum within-cluster variance. The method's result is a dendrogram: a structure that comprises different levels of granularity for the same parcellation. This allows us to explore different parcellation granularities by choosing cutting criteria, without the need of recomputing each time.

The main advantage of the model we proposed in this work is that it allows us to create a groupwise parcellation using linear operations. Assuming direct seed correspondence across subjects, as in the HCP data set, our model lets us remove the subject variability of each seed's tractogram by calculating the expected value across subjects:

$$\begin{aligned} E_s(g(\tilde{T}_{sp})) &= E_s(\beta_c + \tilde{\epsilon}_c + \tilde{\epsilon}_s), \\ &= \beta_c + \tilde{\epsilon}_c + E_s(\tilde{\epsilon}_s) = \beta_c + \tilde{\epsilon}_c. \end{aligned} \tag{4.7}$$

where the last equality is due to $E_s(\tilde{\epsilon}_s) = 0$ (Eq. 4.5). Since in our model the variabilities are normally dis-

[1] For the sake of clarity we denote all random variables with a tilde, e.g. $\tilde{C}$.

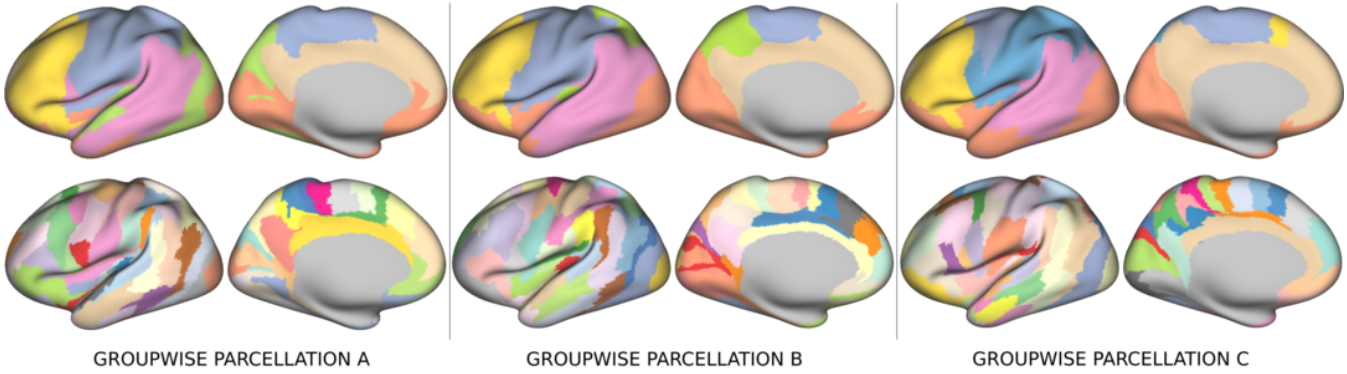

Figure 4.2: Groupwise parcellations of 3 disjoint groups of 46 people each. We show results from the same dendrogram cut to get 6 parcels (upper) and 55 parcels (lower). Labels with best overlap in upper figures share the same color. Notice that there are two different shades of blue for the group C.

tributed (Eq. 4.5), we can estimate the expected value across subjects by averaging a seed's tractograms across subjects. This allows us to create population-representative tractograms for each seed free of across-subject variability, which then can be clustered to create a groupwise parcellation.

4.4. Experiments and Results

In the previous section we presented a model for the cortical extrinsic connectivity and a clustering technique to parcellate the whole brain. Our technique allows us to create single subject and groupwise parcellations, encoded with different levels of granularity in a dendrogram. Now, we show the results of applying our technique over the HCP dataset. First, we explain how the preprocessing step of tractography was made. Then, we elaborate in detail how we applied our technique. Later, we show that our groupwise technique creates results consistent when parceling different groups. Also, we show that our techniques creates parcels in accordance with those by Thiebaut de Schotten[4] when parceling only the frontal lobe. Then, we present a proof-of-principle that our parcels are related to brain anatomy and functional specialization. Most of the results in this section are focused in the groupwise case, for further information on the single-subject technique please refer to Gallardo et al.[1]. Finally, we study the (dis)similarity between our groupwise parcellation and that of Glasser et al.[20].

Data and Preprocessing

Human Connectome Project Dataset A total of 138 subjects (65 males and 73 females, ages 31-35) were randomly selected from the group S500 of the Human Connectome Project (HCP). For information on the acquisition protocols please refer to Van Essen et al.[25]. Every subject has been already preprocessed with the HCP minimum pipeline[19]. Also, each subject's cortical surface is coregistered and represented as a triangular mesh of approximately 32000 vertices per hemisphere[19]. For each vertex, the corresponding label from Desikan's Atlas is known[18]. Finally, the group S500 contains tfMRI information representing the average response to functional stimuli in 100 unrelated subjects (U100)[26].

Probabilistic Tractography To create the tractograms of each subject, we performed Constrained Spherical Deconvolution (CSD) based tractography[27] from a dense set of points in the cortex. Specifically, since each subject has a mesh representing their gray-matter/white-matter interface[19], we used their vertices as seeds to create tractograms. Vertices corresponding to the medial wall were excluded. To avoid superficial cortico-cortical fibers[28], we shrank each of the 138 surfaces $2mm$ into the white matter. For each subject, we fitted a CSD model[27] to their diffusion data using Dipy (version 0.11)[29] and created 5000 streamlines per seed-voxel using the implementation of probabilistic tractography in Dipy. Later, we created a tractogram as in (Eq. 4.2) by calculating for each seed the fraction of they particles that visited other seed-voxel.

Parceling Subjects From the Human Connectome Project

After performing tractography, we applied our parceling technique over each subject in our HCP sample. Specifically, we first transformed each tractogram with the logit function as in eq. 4.4. Then, we clustered the tractograms of each subject using the modified AHC algorithm while imposing a minimum cluster size of $3mm^2$ in the finest granularity. To retrieve parcellations from the resulting dendrogram we use the horizontal cut method[30;13;1]. Two examples of obtained single-subject parcellations at a granularity of 55 parcels are shown in fig. 4.3. To cre-

ate the groupwise parcellation, we took advantage of the vertex correspondence across subjects in the HCP data set[19]. After transforming the tractograms with the logit transform, we computed the average connectivity of each seed by averaging its tractograms across-subject. Then, we computed the groupwise parcellation by clustering the averaged tractograms with our proposed technique (sec. 4.3.2). The obtained groupwise parcellation at a granularity of 55 parcels is shown in fig. 4.3.

Groupwise Parcellation Technique Consistency

To study the consistency of our technique, we randomly divided our HCP subject sample in 3 disjoint groups, trying to maintain the same proportion of males and females on each. The resulting groups had: 24 females, 22 males (group A); 23 females, 23 males (group B) and 28 females, 18 males (group C). For each group we computed their groupwise parcellation. The resulting parcellations at two different levels of granularity are shown in fig. 4.2. To study the similarity between the obtained groupwise parcellations, we compared them at different levels of granularity using the adjusted Rand index[31]. To have a baseline for the comparisons, we generated random parcellations of the cortex and computed the similarity between them. We computed two types of random parcellations: The first one is an homogeneous random parcellation with n parcels, inspired in a method used by Parisot et al.[15]. To compute it, we start by choosing n starting points in the cortex, then, we randomly expand each parcel on the cortex. By comparing these random parcellations between them we compute the minimum obtainable Rand index by mere chance at each level of granularity. In the second type of random parcellation, we simulate the behavior of our technique. For this, we create a parcellation with 300 parcels and then, we iteratively merge two parcels chosen at random until all the parcels are merged in one. By comparing these random parcellations between them we obtain the minimum obtainable Rand index by a random Hierarchical Clustering Algorithm. Examples of these random parcellations can be seen in Fig 4.4. The baselines presented in fig. 4.5 (yellow and violet lines) were computed by comparing 1000 of these random parcels at different levels of granularity. The result of comparing the groupwise parcellations of each group appear in fig. 4.5. The figure shows that the similarity between our groupwise parcellations (lines red, green and blue) are significantly higher than the baselines (violet and yellow). That is, the similarity between our parcellations differs (for most cases) more than 3 standard deviations from the baselines' mean. Moreover, the similarity between our results differs more than 4 standard deviations from the comparison between synthetic hierarchical parcels. This results show that our groupwise parceling technique creates consistent parcellations.

Relationship with a Frontal Lobe Parcellation

Here we assess the agreement of our technique with an state-of-the-art extrinsic connectivity parceling technique. We do so by using our technique to parcellate the frontal lobe and compare our result against that of Thiebaut de Schotten et al.[4]. In their work, Thiebaut de Schotten et al.[4] use a principal component analysis (PCA) statistical framework to parcellate the frontal lobe. They obtain a parcellation with 12 parcels. Then, they show that each one of these parcels possess a functional specialization by using the Decode tool[2] from Neurosynth[17]. Thiebaut's parcellation is currently available in Neurovault[32] as an annotated volume[3], registered on the Collin27 template[33]. We downloaded this parcellation and projected its parcels into a dense mesh representing the cortex of the Collin27 template. The dense mesh had the same amount of vertices as our chosen HCP subjects, and such vertices were coregistered with the HCP subjects' cortical surfaces ones.

From the Desikan Atlas[18] of each of our HCP subjects, we derived a groupwise mask for the frontal lobe. Then, we computed a groupwise parcellation with our technique, using only the tractograms in the mask. Figure 4.6 shows both the parcellation downloaded from Neurovault and our groupwise parcellation projected in the Collins template cortical surface. The figure shows our parcellation with 10 parcels since this level of granularity showed the best Rand index against the Thiebaut's parcellation. The colors of each parcel in our groupwise parcellation were picked in base to the position and amount of overlapping with the Thiebaut's parcels on the surface. While the similarity according to the Rand index is not significantly high (0.4), some visual similarity can be observed on the obtained parcellation, particularly in the blue, yellow, orange and green parcels. Moreover, as shown in table 1, our parcels show the same or even a higher level of functional specialization when processed with Neurosynth.

To study the consistency of our result we computed the frontal lobe groupwise parcellation in each of the 3 disjoint groups from the previous experiment. Figure 4.7 shows the three obtained parcellation alongside the Thiebaut's one. The obtained parcels show consistency, obtaining an adjusted Rand index score of 0.61±0.05 between them. Finally, we studied if the masking affected the clustering of the frontal lobe. To do so, we applied the frontal lobe mask over a groupwise whole-brain parcellation of the 138 subjects. The resulting frontal lobe parcellation contained 12 parcels. This parcellation showed consistency with the one obtained by clustering only the tractograms in the frontal lobe. More specifically, the adjusted Rand

[2] http://www.neurosynth.org/decode/
[3] http://neurovault.org/collections/1597/

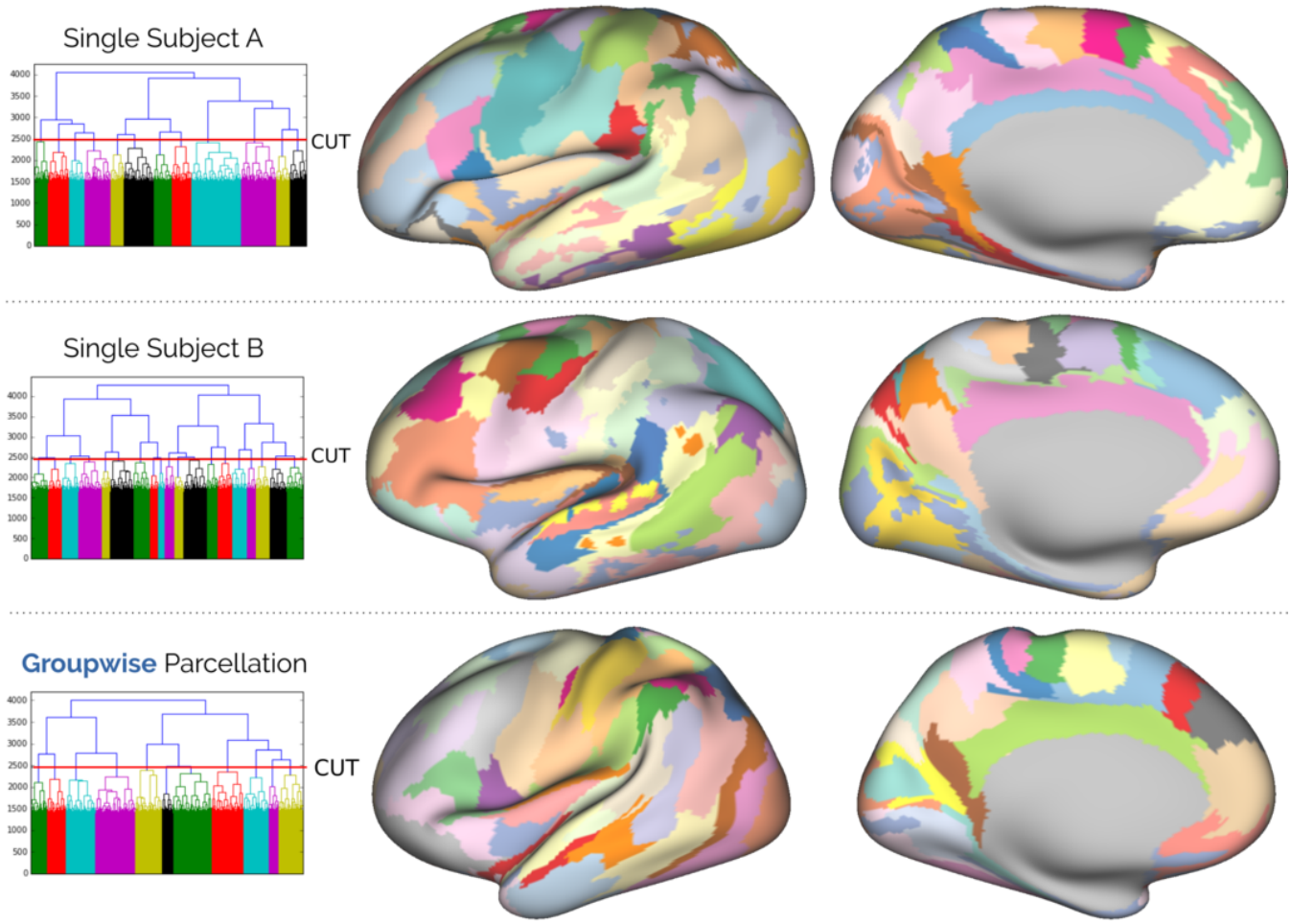

Figure 4.3: Examples of two single-subject parcellations and the groupwise parcellations computed with our technique. All the parcellations shown have 55 parcels. The corresponding dendrogram for each case, along with the chosen cut height (red line) are shown. The groupwise parcellation is based on 138 subjects from the Human Connectome Project.

index score between them was 0.65. We repeated this procedure for the 3 disjoints groups from the previous experiment. In each group, both frontal lobe parcellations showed to be consistent, achieving an adjusted Rand index of 0.57±0.04.

Anatomical Relationship and Functional Specialization of Our Parcels

Here we present a proof of concept that our technique creates parcels within anatomical boundaries and with functional meaning. To do so, first, we extracted a parcellation with 55 parcels from the groupwise parcellation computed from the 138 subjects. This was made to get a parcellation with coarse granularity while having at least the amount of parcels in the anatomical atlas of Desikan[18] (36 parcels). We compare this extracted parcellation against the Desikan Atlas and a functional study made to every subject in the HCP[19].

Relationship with Anatomical Boundaries To assess if some anatomical structures were present in the dendrogram and if our resulting parcels were subdividing them, we compared our extracted parcellation with the Desikan atlas[18]. To do so, we projected the Desikan regions over our parcels and then calculated: how many of our parcels were contained by a anatomical region in more than a 90%, and which anatomical regions were contained inside of one of our parcels. Using this criterion, the Insula; Cingulate; Lateral-Occipital; Fusiform; Superior Frontal; Lingual; Sensory and Motor Cortex appear to be found as shown in Fig. 4.8.

Functional Specialization. To study the relationship between our parcels and brain function, we projected our parcels over z-score maps representing responses to functional stimuli[26]. These maps are available as part of the HCP data, and represent the average activation of 100 subjects. In particular, we used the maps related to the

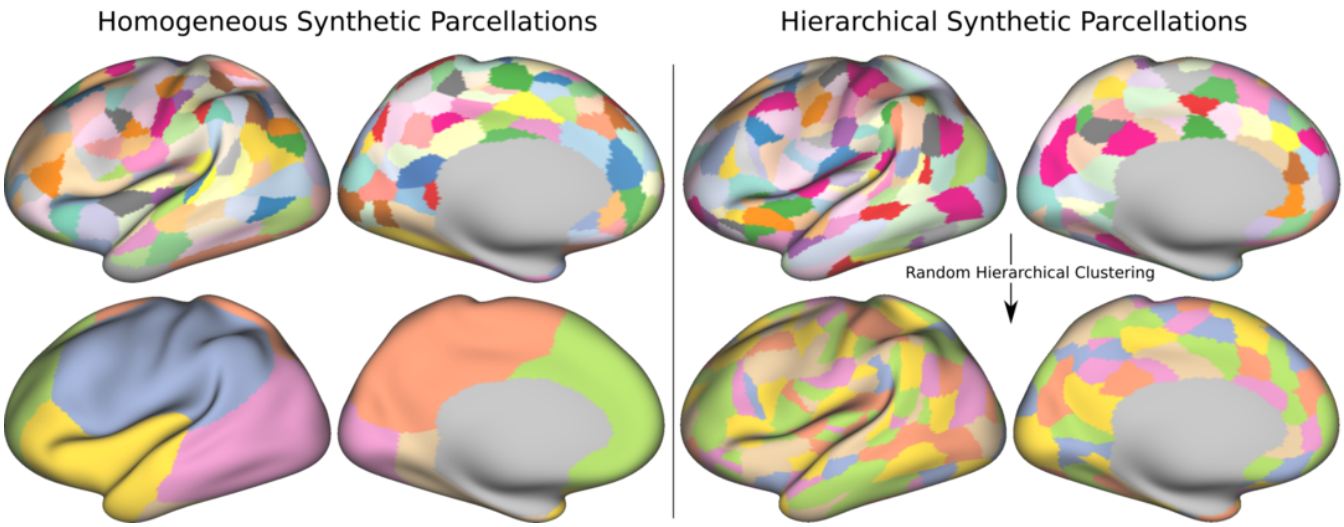

Figure 4.4: Examples of synthetic parcellations created to compute a baseline adjusted rand index. Parcellations on the left were created by dividing the brain in a homogeneous way, inspired by the random parcellation presented in Parisot et al.[15]. Parcellations on the right were created by randomly merging parcels of a coarse parcellation.

Table 1. Correlation value reported (Neurosynth)

Parcel	Term	r (Thiebaut et al.)	r (Ours)
1	foot	0.267	**0.319**
2	motor	0.129	**0.208**
3	eye field	0.081	0.048
4	speech production	0.077	**0.138**
5	pre sma	0.245	0.234
6	phonological	0.206	0.019
7	-	-	-
8	executive control	0.049	0.042
9	-	-	-
10	semantic	0.178	**0.226**
11	social	0.137	0.110
12	semantic	0.139	0.086

Table 1. Spatial correlation value reported by Neurosynth for specific terms in each parcel of Thiebaut de Schotten et al.[4] and for our parcels. Enumeration comes from figure 4.6.

following tasks: right hand, foot and tongue movement; face, shape recognition and story categorization. For information on the functional tasks, acquisition and processing of this data please refer to Barch et al.[26]. Figure 4.9 shows our parcels projected over contrasts in motor tasks. In particular, our parcels are projected over the following contrasts: tongue-average; hand movement-average and foot movement-average. Figure 4.10 shows our parcels projected over contrasts in cognitive tasks: face-shape recognition; shape-face recognition and short-story categorization. The figures show a good overlap between our parcels and the regions with maximum activation of each task. In both figures the distribution of z-scores inside of specific regions are shown as histograms. Further information about the z-score is present in tables 2 and 3. These tables show that our parcels contain zero or few negatives values; that the mean of their contained z-score is always positive and also, that many of those parcels enclose the maximum achievable z-score.

Relationship with a Multi-Modal Parcellation of the Cortex

Finally, we study the (dis)similarities between our groupwise parcellation and that of Glasser et al.[20]. In their work, Glasser et al.[20] compute a parcellation of the whole cortex using information from different MRI modalities. In particular, they use information from task functional MRI; resting state functional MRI; myelin maps computed from T1 and T2 images and cortical thickness. It is important to remark that dMRI data, in which our work is solely based, was not used to construct their parcellation.

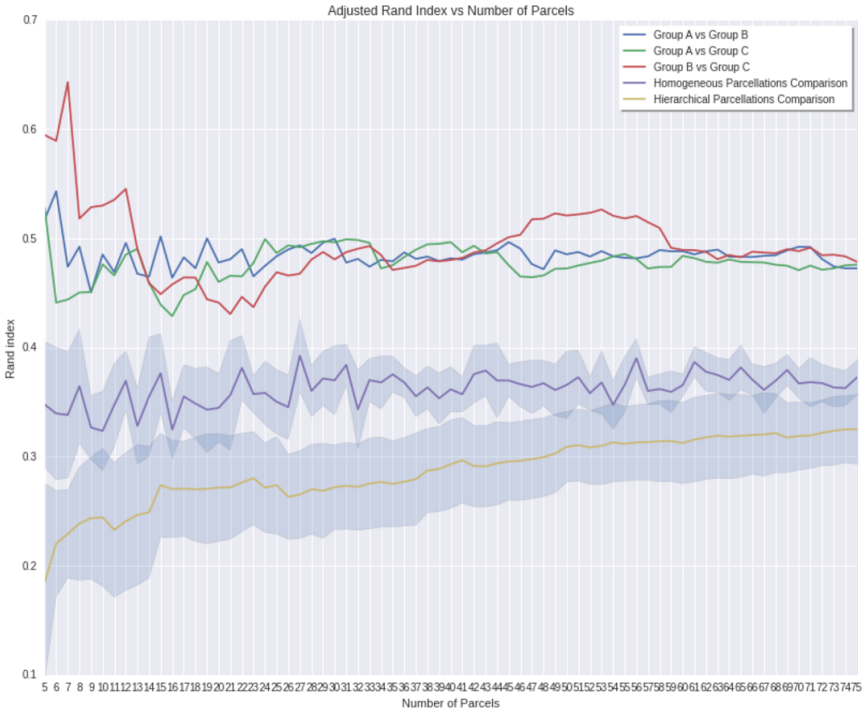

Figure 4.5: Adjusted Rand Index obtained when comparing: (red) Group A vs Group B; (blue) Group A vs Group C; (green) Group B vs Group C; (purple) Synthetic Homogeneous Parcels and (yellow) Synthetic hierarchical Parcels.

To compare our results against Glasser's atlas, we first extracted a parcellation of 180 parcels from the groupwise dendrogram of our 138 HCP subjects. That is, we extracted a parcellation with the same number of parcels as Glasser's one. Figure 4.11 show both parcellations side by side. We compared both parcellations using the adjusted Rand Index, obtaining a score of 0.28. Such low score indicates that there's almost no similarity between our result and that of Glasser et al.[20]. Also, there's no relationship with our groupwise parcellation with 55 parcels used in the previous section since Glasser's parcels (finest) do not subdivide ours (coarsest). Since Glasser's parcellation comes from functional information in the HCP, we studied the functional specialization of its parcels in the same manner as previous section. Figure 4.12 shows the histogram of z-score contained for some parcels when using the same maps as in section Functional Activations. It's important to remark that the z-score maps used come from responses to functional stimuli of HCP subjects[19]. In particular, histograms a; b and c in fig. 4.12 show that their subdivisions of the sensori-motor cortex contain a wide range of z-scores, centered in zero.

4.5. Discussion

In this work we presented a parsimonious statistical model for long-ranged axonal connectivity. Our model (section 4.3.1), assumes that the cortex is divided in patches of homogeneous extrinsic connectivity, as histological results showed in the macaque brain[5]. By borrowing ideas from statistical clustered data models[16], our model accounts for the variability in the axonal connections of a patch's neurons and for variability in patch boundaries across subjects.

Taking advantage of our proposed model, in Section 4.3.2 we presented an efficient technique to parcellate the cortex based on its extrinsic connectivity. Our technique uses only dMRI information, without the need of relying on initial parcellations[9]. Also, our technique allows parcellation of the whole cortex, overcoming the problem of working with only part of it[10;11;12;4]. Additionally, our technique allows creation of both single subject and groupwise parcellations. Our groupwise parcellation technique relies on anatomical seed-correspondence across subjects. In our experiments, this is achieved as each HCP subject possess a coregistered dense mesh representing they cortical surface[19]. Given the anatomical differences across-subjects, this purely anatomical matching of seeds is probably sub-optimal. However, it allows us to compute single and groupwise parcellations independently. By doing this, we avoid the need to impose constraints between our single and group parcellations[9;14;15].

Inspired by Moreno-Dominguez et al.[13], our technique uses Hierarchical Clustering to comprise multiple granularities of the same parcellation in a dendrogram. This

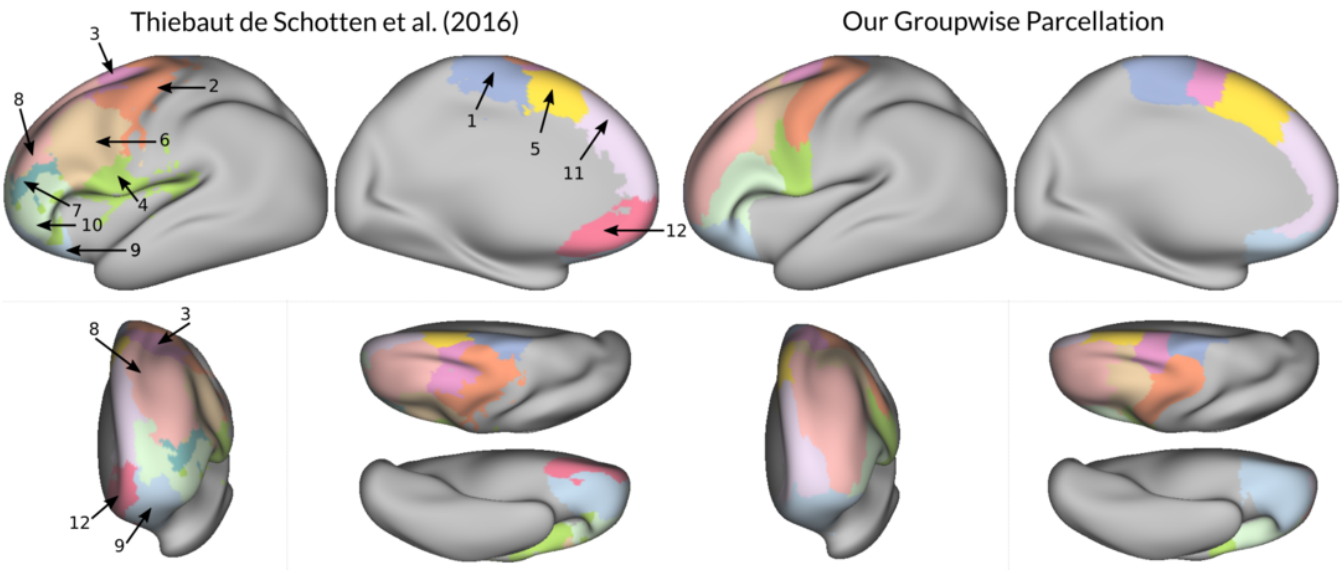

Figure 4.6: Thiebaut de Schotten et al.[4] parcellation (left) and our groupwise parcellation using only tractograms from the frontal lobe (right). Our parcels are colored after the parcel from Thiebaut de Schotten et al.[4] with which they best overlap.

Table 2. Statistics on z-score distribution in parcels from figure 4.9

Contrast	Parcel	Min.	Max.	Mean ± Std. Dev.	Max. Score in Map
T-Avg	**1**	-3.62	15.03	5.67±4.91	15.03
T-Avg	**2**	4.11	14.88	10.30 ± 2.56	15.03
RH-Avg	**3**	-7.02	14.50	5.05 ± 4.95	14.50
RH-Avg	**4**	-11.25	14.07	6.35 ± 6.25	14.50
RF-Avg	**5**	-7.10	9.57	2.99 ± 3.84	14.56
RF-Avg	**6**	1.04	14.01	7.13 ± 3.20	14.56
RF-Avg	**7**	-0.83	13.98	9.23 ± 3.32	14.56
RF-Avg	**8**	-0.46	14.56	8.73 ± 3.81	14.56

Table 2. Minimum; maximum and mean z-score contained by each of the parcels enumerated in figure 4.9. The highest z-score of each map is reported to facilitate comparison. T-Avg: Tongue movement versus average; RH-Avg: Right Hand Movement versus average; RF-Avg: Right Foot Movement versus average.

allows us to overcome the need of other techniques[15] to specify an expected number of clusters. Hence, we don't need to recompute the whole pipeline each time a new parcellation is required. As in Moreno-Dominguez et al.[13], we also create the dendrogram using only one comprehensive parameter: the minimum size of each cluster. This parameter imposes the local coherence criterion. Our fundamental difference with Moreno-Dominguez' technique is how we compare and merge tractograms during the clustering process. Moreno-Dominguez et al.[13] use Centroid Clustering[34] with the cosine distance. This can lead to an erroneous parcellation since the centroid criterion doesn't minimize the cosine distance between points. Also, their method creates dendrograms with inversions[34], which are then removed heuristically. In our case, using a Logistic Random Effect model (eq. 4.5) allowed us to transform the tractograms into a Euclidean space (sec. 4.3.2) and compare them using the Euclidean distance. In doing this, it is important to remark that we are making a trade off. Since we are comparing high-dimensional vectors with the Euclidean distance, we are probably affected by the dimensionality curse[35]. However, working in an Euclidean space possess many advantages. The first advantage is that we can compute clusters with minimum intra-cluster variance by using Ward's Hierarchical method. We can use this algorithm since its only hypothesis is that the features to cluster are in a Euclidean space. Also, since we work with the Euclidean distance, we can apply the Lance and Williams[36] formula during clustering. This formula gives us the dissimilarity between the new centroid created at each step and the rest of the existing tractograms in constant time. As far as we know there's no Lance and Williams formula when using the cosine distance with the centroid linkage. This allows us to lower the time complexity of our algorithm with respect to Moreno-Dominguez. Since we use Ward's clustering, our resulting dendrograms do not have inversions, which means that we don't need to post-process

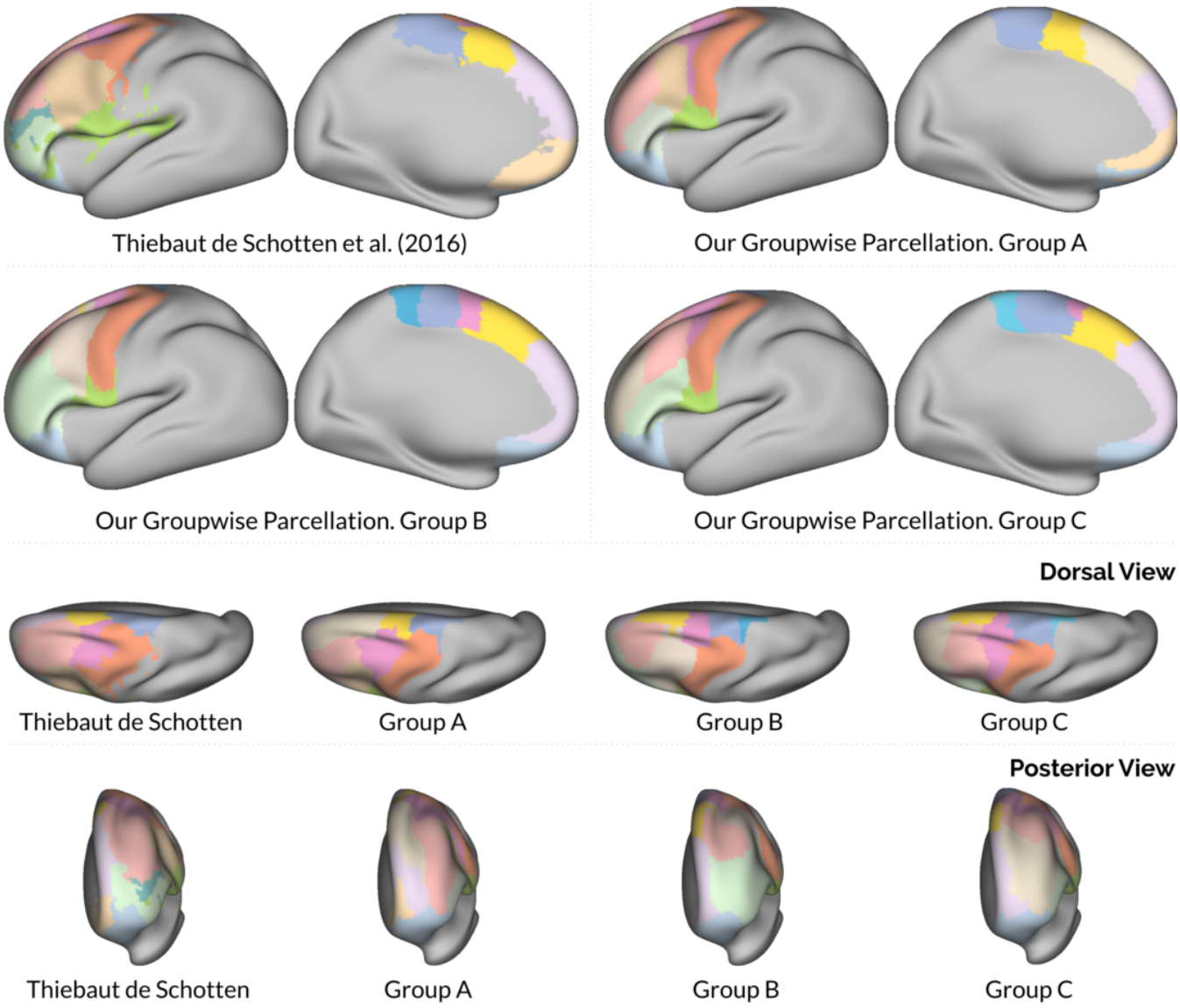

Figure 4.7: Thiebaut de Schotten et al.[4] parcellation (top-left) and our frontal lobe groupwise parcellations computed over 3 disjoint groups of subjects. Our parcels are colored after the parcel from Thiebaut de Schotten et al.[4] with which they best overlap.

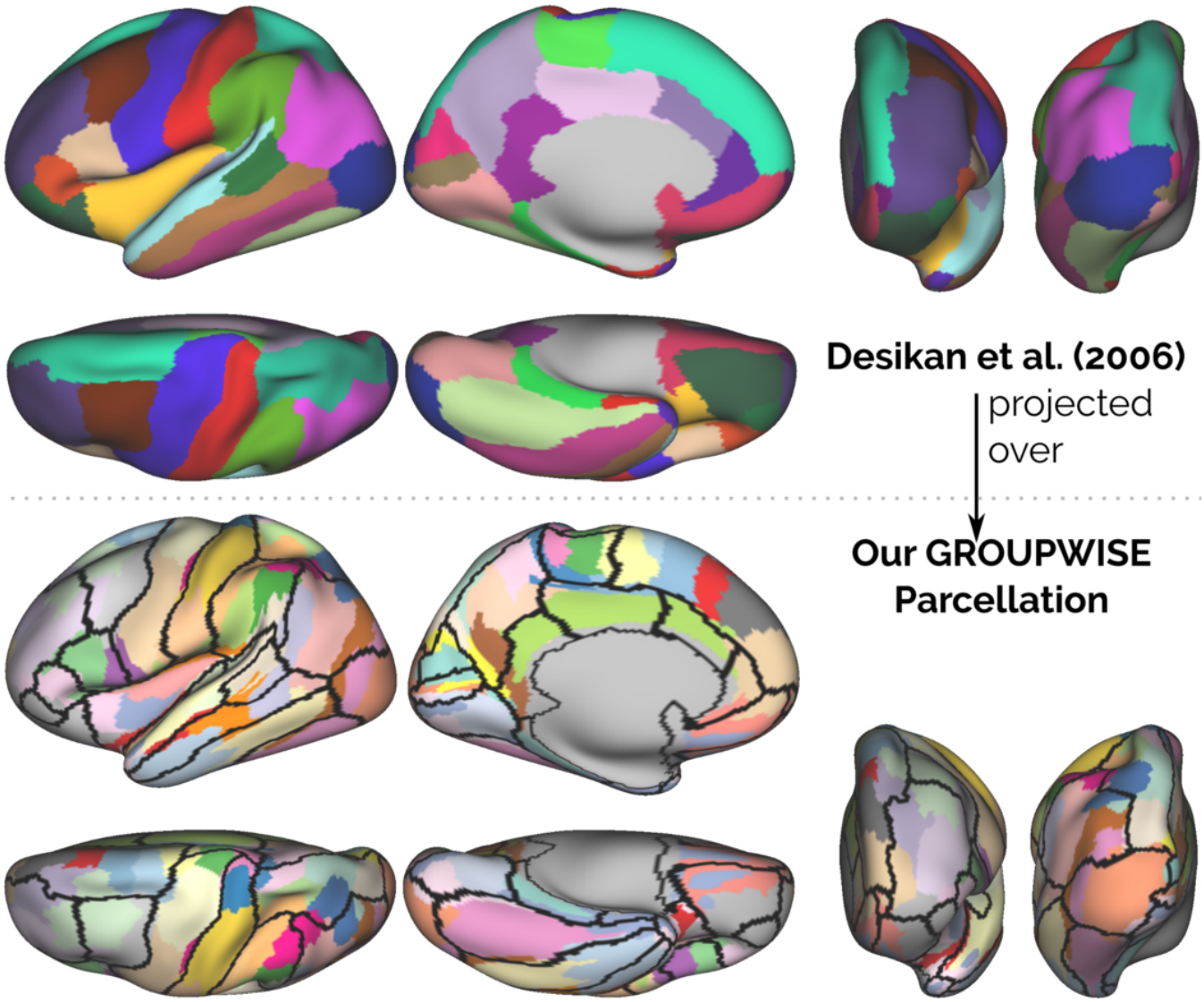

Figure 4.8: Relation between our pure extrinsic parcellation and the anatomical atlas of Desikan[18]. Desikan atlas projected over the groupwise parcellation with 55 parcels. Insula; Cingulate; Lateral-Occipital; Fusiform; Superior Frontal; Lingual; Sensory and Motor Cortex appear to be found.

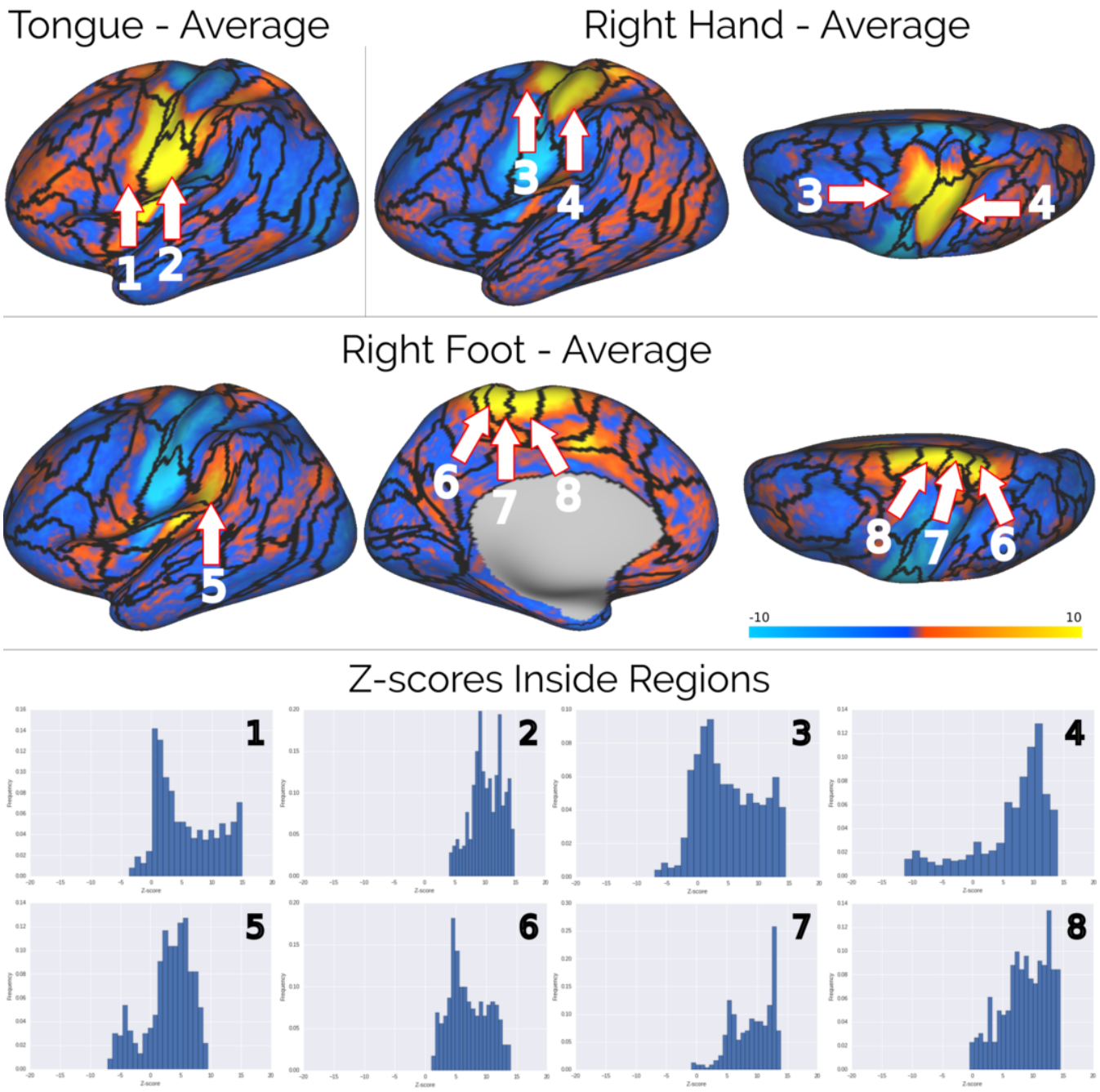

Figure 4.9: Our groupwise parcellation with 55 parcels projected over z-scores representing responses to motor tasks. Each histogram shows the distribution of z-score inside our parcels. The null or small fraction of negative values shows the functional specialization of our parcels

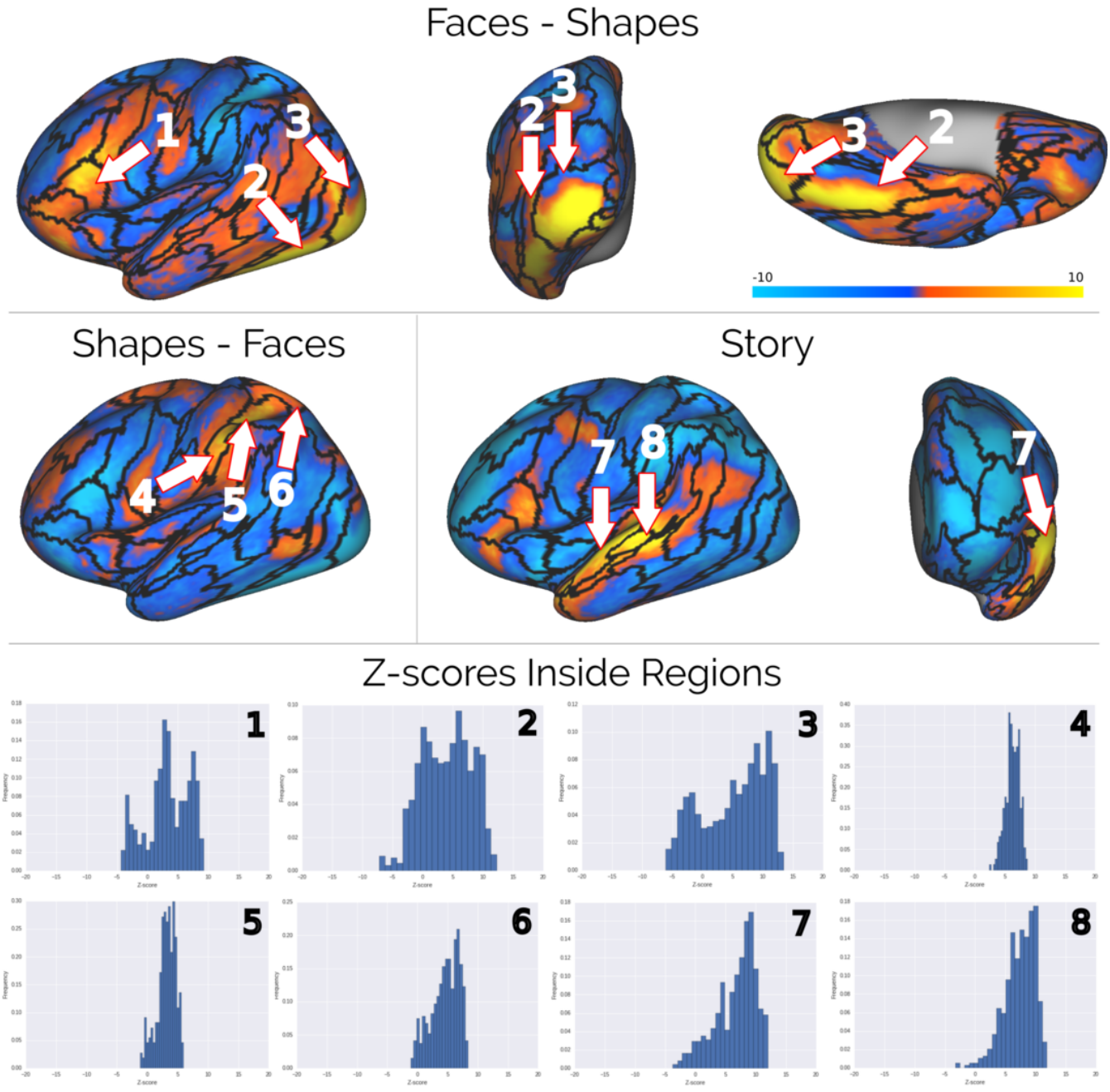

Figure 4.10: Our groupwise parcellation with 55 parcels projected over z-scores representing responses to cognitive tasks. Each histogram shows the distribution of z-score inside our parcels. The null or small fraction of negative values shows the functional specialization of our parcels

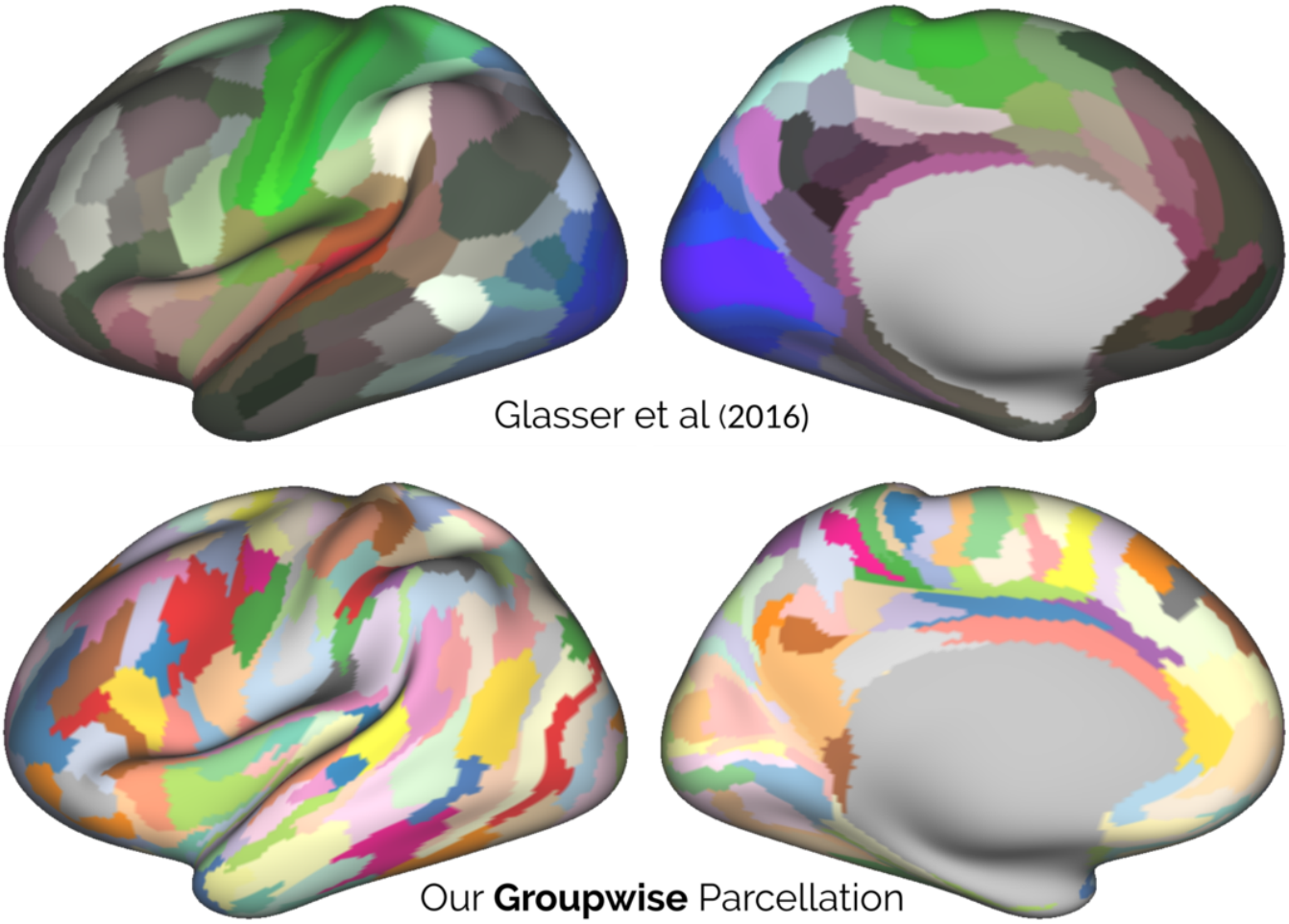

Figure 4.11: Glasser et al.[20] parcellation (upper) and our groupwise parcellations computed from 138 HCP subjects. Both parcellations contain 180 parcels. There's almost no overlap according to the adjusted Rand index between them (0.28).

Table 3. Statistics on z-score distribution in parcels from figure 4.10

Contrast	Parcel	Min.	Max.	Mean ± Std. Dev.	Max. Score in map
Faces-Shapes	**1**	-4.33	9.28	3.35 ± 3.51	13.45
Faces-Shapes	**2**	-7.16	12.36	4.01 ± 4.09	13.45
Faces-Shapes	**3**	-6.07	13.45	5.16 ± 5.25	13.45
Shapes-Faces	**4**	-5.73	5.37	0.93 ± 1.78	8.79
Shapes-Faces	**5**	-4.11	7.67	1.11 ± 2.11	8.79
Shapes-Faces	**6**	-1.13	5.94	3.17 ± 1.49	8.79
Story	**7**	-3.72	12.02	6.72 ± 3.35	12.02
Story	**8**	-3.24	11.92	7.41 ± 2.50	12.02

Table 3. Minimum; maximum and mean z-score contained by each of the parcels enumerated in figure 4.10. The highest z-score of each map is reported to facilitate comparison. Faces-Shapes: Face recognition versus shape recognition contrast; Shapes-Faces: Shape recognition versus face recognition; Story: Short story categorization.

them. Another advantage is that we can retrieve a parcellation from the dendrogram using a simple technique: horizontal cut[30]. While other methods to cut the dendrogram exist[30], horizontal cut is sufficient to solve our Gaussian Mixture Model (eq. 4.5) as shown in Gallardo et al.[1]. Finally, even if our algorithm is probably affected by the dimensionality curse, our parcellations showed to be consistent across-groups and in agreement with extant parcellations in the literature.

Our Groupwise Parcellations are Consistent Across Similar Groups:

We assessed the consistency of our groupwise parcellation by quantifying the consistency across 3 disjoint groups of 46 subjects each. The consistency is shown by the adjusted Rand index in Fig. 4.5, which quantifies consistency across parcellations[31]. As seen in Fig. 4.5 whole-cortex parcellations obtained with our method are consistent across groups, and the Adjusted Rand Index is significantly higher, i.e. more than 3 standard deviations, for all granularities when compared with the null case of randomly-generated parcellations.

Our whole-cortex groupwise parcellation reaches a maximum consistency score when the cortex is divided in 6 regions, see Fig. 4.5. As seen in Fig. 4.2, these parcellations are consistent with specific anatomo/functional networks: the frontal lobe section anterior to the prefrontal cortex is shown in yellow; the sensorimotor area is shown in cyan, the cingulate area is shown in beige; the fronto-occipital connection in orange, and the temporo-parietal system in pink.

Our Method Creates Parcels in Agreement With a Single-Lobe Parceling Technique Extant in the Literature.

We showed that our technique obtains results similar to another method extant in the literature. We did so by parceling only the frontal and showing the visual similarity between our resulting parcels and those obtained by Thiebaut de Schotten et al.[4]. Moreover, the blue, pink and green parcels in fig. 4.6 share not only similar boundaries and location, but also functional specialization (Table 1). In some cases our parcels possess even higher spatial-correlation with functional task according to Neurosynth's[17] Decode tool[4]. We assessed the consistency of our obtained groupwise parcellation by computing the groupwise frontal lobe parcellation of three disjoints groups of 46 subjects and comparing them using the adjusted Rand index. The obtained value of 0.61 shows that our parcellation of the frontal lobe is consistent across groups.

Our Method Creates Several Parcels in Agreement with Brain Anatomy.

We showed that many of our parcels are in agreement with brain anatomy. In particular, we showed that in our groupwise parcellation, with 55 parcels, the following anatomical structures appeared to be found: Cingulate; Insula; Lateral-Occipital; Fusiform; Superior Frontal; Lingual; Motor and Sensory cortex. Here we discuss why some of these parcels were found and how are their conectivity fingerprints. In the case of the Cingulate, its fingerprint, shown in fig. 4.13, is strongly related with the Cingulate Fascicle (CF) pathway. This is consistent with the fact that the seeds located in the Cingulate will end up into the CF after being pushed in the white-matter. In the case of the Insula, each subdivision showed a specific pattern of connectivity as shown in fig. 4.13. These parcels show a gradient of connections from the occipital lobe to the frontal lobe consistent with that of Ghaziri et al.[37]. In the Lateral-Occipital region, we see a specific pattern of local connectivity which cannot be attributed to gyral bias since the Lateral-Occipital covers many sulci and gyrus. In the case of the fusiform, it is almost completely contained in one of our parcellations, which goes from the Fusiform up to the Lateral-Occipital

[4]http://neurosynth.org/decode/

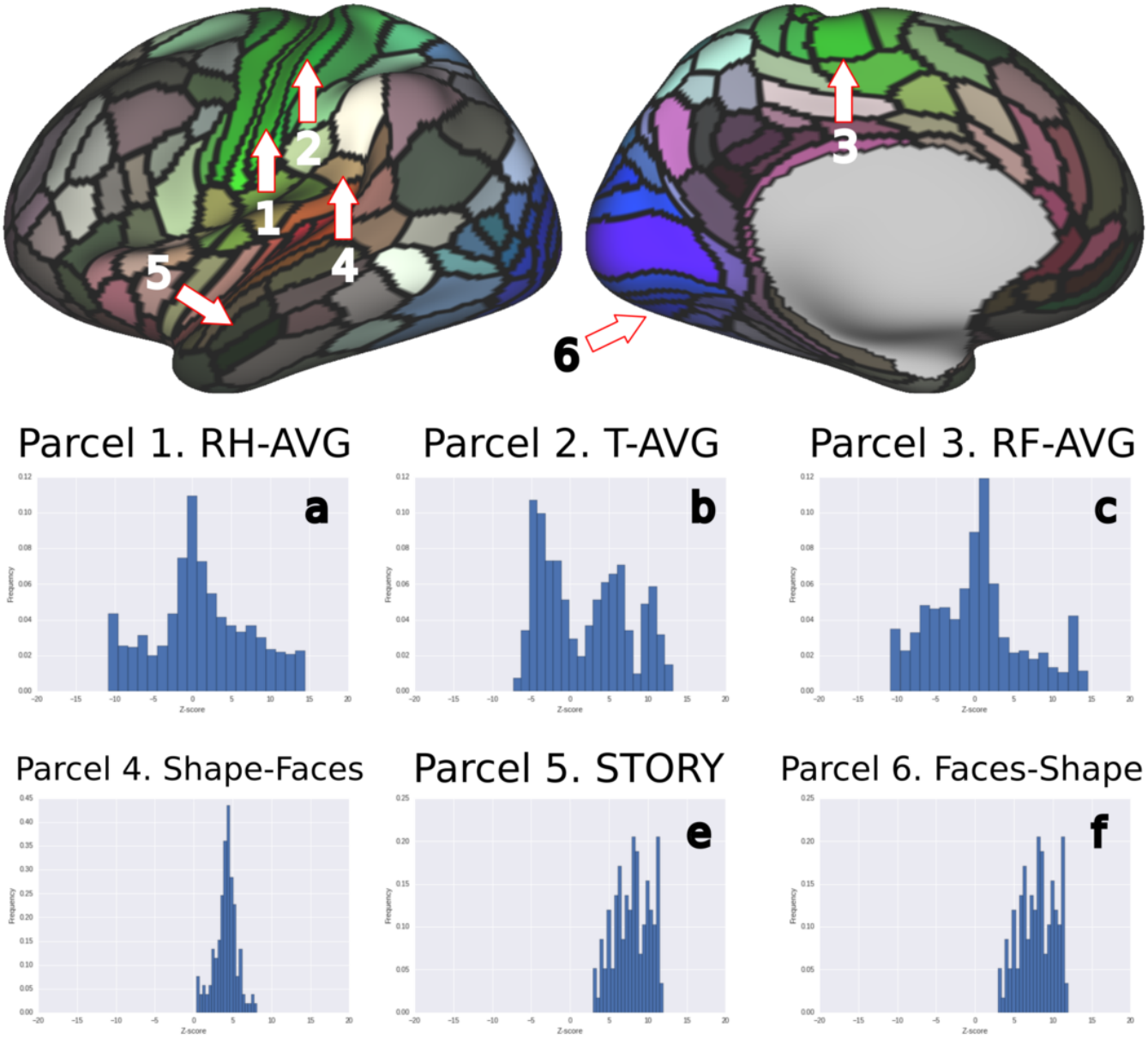

Figure 4.12: Glasser et al.[20] parcellation (upper) and histograms of z-score contained in different parcels for different functional task. (a) Histogram for parcel 1 for the contrast related to Tongue movement. (b) Histogram for parcel 2 for the contrast related to Tongue movement. (c) Histogram for parcel 3 for the contrast related to Right Foot movement. (d) Histogram for parcel 4 for the contrast Shape recognition vs Face recognition. (e) Histogram for parcel 5 for the contrast related to Story Categorization. (f) Histogram for parcel 5 for the contrast Face recognition vs Shape recognition. The histograms (d); (e) and (f) correspond to the parcels with the greatest mean z-score of their respective tasks.

(fig. 4.8). This could add evidence to the hypothesis that the Fusiform plays a role in visual tasks[38;39]. Finally, the Motor and Sensory cortex appear to be found. While the appearance of each gyri is most probably because of gyral bias[7], the parcels inside them show specific patterns of structural connectivity (fig. 4.13), and, as seen in section 3.5.2, functional specialization.

Our Results Show a Close Relationship Between Structural Connectivity and Brain Function.

We assessed the functional specialization of some of our parcels by showing how they overlap with responses to functional and cognitive tasks measured with fMRI. In particular, for all the studied tasks, the parcels contained a higher proportion of positive values than negative ones as expressed by the positive mean values reported in tables 2 and 3. For some parcels there were not even neg-

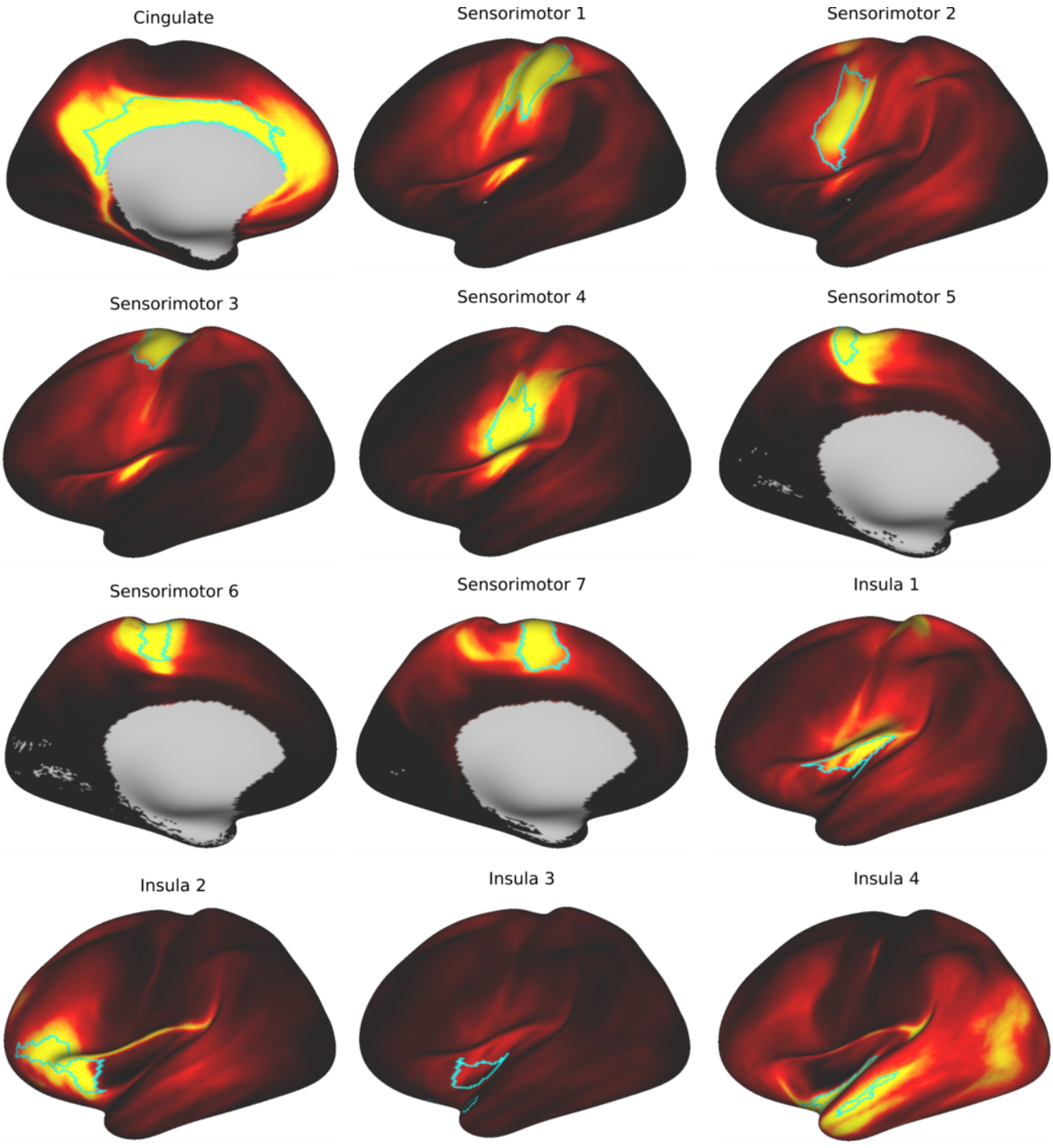

Figure 4.13: Connectivity fingerprint for different parcels in our groupwise parcellation. The names in the titles are given after the anatomical structure that they subdivide (or contain, as with the Fusiform).

ative values. Moreover, several of the histograms on figures 4.9 and 4.10 show a high frequency of z-score values greater than 5, which indicate a significant correlation with functional activation. Therefore, our results show, for some tasks, the strong relationship between extrinsic connectivity and functional specialization in the human brain cortex.

Our Parcels Are Not Similar to Those Obtained by Glasser et al. (2016) But Possess Better Functional Specialization for Motor Tasks.

Our parcels were not related to those of Glasser et al.[20]. This is shown by the obtained adjusted Rand index score between them (0.28). It's important to remark that our parcels are purely based on extrinsic connectivity, meanwhile those of Glasser et al.[20] do not use dMRI information. Glasser's parcels are mostly based on myelin and functional information. In particular, their subdivision of the sensori-motor cortex (green parcels in fig. 4.11) is mostly based in Myelin maps as shown in Figure 4.a of Glasser et al.[20]. Because of this, their parcels in the sensori-motor cortex contain a wide range of z-scores when compared with responses to functional stimuli as shown by histograms a; b and c in fig. 4.12. In contrast, our parcels in the sensori-motor cortex, for a coarser parcellation, show a good overlap with function and are in agreement with the motor strip mapping as discussed in the previous section. Also, for the case of story categorization; shape recognition and face recognition, our parcels show a similar distribution of z-scores (fig. 4.9) than those with the highest mean z-scores of Glasser et al.[20] (parcels d; e and f of fig. 4.12).

4.6. Conclusion

Understanding how the brain is structurally organized and how it constraints functionality is an open question in neuroscience. Recent advances in acquisition and modeling techniques on dMRI have facilitated to study axonal connectivity in the brain. However, parceling the whole cortex based on a structural criterion remained challenging. In this chapter we presented a connectivity model; framed tractography within our model and presented a parceling technique that allows parcellation of the whole brain in both single subject and groupwise cases.

However, a new question rises, given two single subject parcellations, how to match the parcels across them?. Even when our results show that our technique is stable across groups of subjects, some variability still exists, and finding a correspondence between two parcellations is not a trivial task. The following chapter of this thesis will work on this problem.

Bibliography

[1] G. Gallardo, R. Fick, W. Wells, R. Deriche, and D. Wassermann, "Groupwise Structural Parcellation of the Cortex: A Sound Approach Based on Logistic Models," in *MICCAI 2016 Work. Comput. Diffus. MRI*, pp. 99–112, Springer International Publishing, 2017.

[2] K. Brodmann, *Vergleichende Lokalisationslehre der Großhirnrinde in ihren Prinzipien dargestellt auf Grund des Zellaufbaues*. Leipzig: Barth, 1909.

[3] B. Thirion, G. Varoquaux, E. Dohmatob, and J. B. Poline, "Which fMRI clustering gives good brain parcellations?," *Front. Neurosci.*, vol. 8, no. 8 JUL, pp. 1–13, 2014.

[4] M. Thiebaut de Schotten, M. Urbanski, B. Batrancourt, R. Levy, B. Dubois, L. Cerliani, and E. Volle, "Rostro-caudal Architecture of the Frontal Lobes in Humans," *Cereb. Cortex*, pp. 1–15, 2016.

[5] J. D. Schmahmann and D. N. Pandya, *Fiber Pathways of the Brain*, vol. 1. Oxford University Press, apr 2006.

[6] R. E. Passingham, K. E. Stephan, and R. Kötter, "The anatomical basis of functional localization in the cortex," *Nat. Rev. Neurosci.*, vol. 3, pp. 606–616, aug 2002.

[7] D. C. Van Essen, S. Jbabdi, S. N. Sotiropoulos, C. Chen, K. Dikranian, T. Coalson, J. Harwell, T. E. Behrens, and M. F. Glasser, "Mapping Connections in Humans and Non-Human Primates," in *Diffus. MRI*, no. January 2014, pp. 337–358, Elsevier, 2014.

[8] S. Jbabdi and T. E. Behrens, "Long-range connectomics," *Ann. N. Y. Acad. Sci.*, vol. 1305, pp. 83–93, dec 2013.

[9] M. J. Clarkson, I. B. Malone, M. Modat, K. K. Leung, N. Ryan, D. C. Alexander, N. C. Fox, and S. Ourselin, *A Framework For Using Diffusion Weighted Imaging To Improve Cortical Parcellation*, vol. 6362 of *Lecture Notes in Computer Science*. Berlin, Heidelberg: Springer Berlin Heidelberg, 2010.

[10] S. Lefranc, P. Roca, M. Perrot, C. Poupon, D. Le Bihan, J.-F. Mangin, and D. Rivière, "Groupwise connectivity-based parcellation of the whole human cortical surface using watershed-driven dimension reduction," *Med. Image Anal.*, vol. 30, pp. 11–29, may 2016.

[11] P. Roca, D. Rivière, P. Guevara, C. Poupon, and J. F. Mangin, "Tractography-based parcellation of

the cortex using a spatially-informed dimension reduction of the connectivity matrix," *Lect. Notes Comput. Sci. (including Subser. Lect. Notes Artif. Intell. Lect. Notes Bioinformatics)*, vol. 5761 LNCS, no. PART 1, pp. 935–942, 2009.

[12] M. Thiebaut de Schotten, M. Urbanski, R. Valabregue, D. J. Bayle, and E. Volle, "Subdivision of the occipital lobes: An anatomical and functional MRI connectivity study," *Cortex*, vol. 56, pp. 121–137, 2014.

[13] D. Moreno-Dominguez, A. Anwander, and T. R. Knösche, "A hierarchical method for whole-brain connectivity-based parcellation," *Hum. Brain Mapp.*, vol. 35, pp. 5000–5025, oct 2014.

[14] P. Roca, A. Tucholka, D. Rivière, P. Guevara, C. Poupon, and J. F. Mangin, "Inter-subject connectivity-based parcellation of a patch of cerebral cortex," *Lect. Notes Comput. Sci. (including Subser. Lect. Notes Artif. Intell. Lect. Notes Bioinformatics)*, vol. 6362 LNCS, no. PART 2, pp. 347–354, 2010.

[15] S. Parisot, S. Arslan, J. Passerat-Palmbach, W. M. Wells, and D. Rueckert, "Tractography-Driven Groupwise Multi-scale Parcellation of the Cortex.," *Inf. Process. Med. Imaging*, vol. 24, pp. 600–12, 2015.

[16] J. F. Pendergast, S. J. Gange, M. A. Newton, M. J. Lindstrom, M. Palta, and M. R. Fisher, "A Survey of Methods for Analyzing Clustered Binary Response Data," *Int. Stat. Rev. / Rev. Int. Stat.*, vol. 64, p. 89, apr 1996.

[17] T. Yarkoni, R. A. Poldrack, T. E. Nichols, D. C. Van Essen, and T. D. Wager, "Large-scale automated synthesis of human functional neuroimaging data," *Nat. Methods*, vol. 8, pp. 665–670, jun 2011.

[18] R. S. Desikan, F. Ségonne, B. Fischl, B. T. Quinn, B. C. Dickerson, D. Blacker, R. L. Buckner, A. M. Dale, R. P. Maguire, B. T. Hyman, M. S. Albert, and R. J. Killiany, "An automated labeling system for subdividing the human cerebral cortex on MRI scans into gyral based regions of interest," *Neuroimage*, vol. 31, pp. 968–980, jul 2006.

[19] M. F. Glasser, S. N. Sotiropoulos, J. A. Wilson, T. S. Coalson, B. Fischl, J. L. Andersson, J. Xu, S. Jbabdi, M. Webster, J. R. Polimeni, D. C. Van Essen, and M. Jenkinson, "The minimal preprocessing pipelines for the Human Connectome Project," *Neuroimage*, vol. 80, pp. 105–124, oct 2013.

[20] M. F. Glasser, T. S. Coalson, E. C. Robinson, C. D. Hacker, J. Harwell, E. Yacoub, K. Ugurbil, J. Andersson, C. F. Beckmann, M. Jenkinson, S. M. Smith, and D. C. Van Essen, "A multi-modal parcellation of human cerebral cortex.," *Nature*, vol. 536, no. 7615, pp. 171–8, 2016.

[21] T. E. Behrens, M. Woolrich, M. Jenkinson, H. Johansen-Berg, R. Nunes, S. Clare, P. Matthews, J. Brady, and S. Smith, "Characterization and propagation of uncertainty in diffusion-weighted MR imaging," *Magn. Reson. Med.*, vol. 50, pp. 1077–1088, nov 2003.

[22] J. A. N. McCullagh, P., *Generalized Linear Models*. London: Chapman and Hall/CRC, 2 ed., 1989.

[23] K. M. Pohl, J. Fisher, S. Bouix, M. Shenton, R. W. McCarley, W. E. L. Grimson, R. Kikinis, and W. M. Wells, "Using the logarithm of odds to define a vector space on probabilistic atlases," *Med. Image Anal.*, vol. 11, pp. 465–477, oct 2007.

[24] J. Ward Jr., "Hierarchical Grouping to Optimize an Objective Function," *J. Am. Stat. Assoc.*, vol. 58, no. 301, pp. 236–244, 1963.

[25] D. C. Van Essen, K. Ugurbil, E. Auerbach, D. Barch, T. E. Behrens, R. Bucholz, A. Chang, L. Chen, M. Corbetta, S. W. Curtiss, S. Della Penna, D. Feinberg, M. F. Glasser, N. Harel, a. C. Heath, L. Larson-Prior, D. Marcus, G. Michalareas, S. Moeller, R. Oostenveld, S. E. Petersen, F. Prior, B. L. Schlaggar, S. M. Smith, a. Z. Snyder, J. Xu, and E. Yacoub, "The Human Connectome Project: A data acquisition perspective," *Neuroimage*, vol. 62, no. 4, pp. 2222–2231, 2012.

[26] D. M. Barch, G. C. Burgess, M. P. Harms, S. E. Petersen, B. L. Schlaggar, M. Corbetta, M. F. Glasser, S. Curtiss, S. Dixit, C. Feldt, D. Nolan, E. Bryant, T. Hartley, O. Footer, J. M. Bjork, R. Poldrack, S. Smith, H. Johansen-Berg, A. Z. Snyder, and D. C. Van Essen, "Function in the human connectome: Task-fMRI and individual differences in behavior," *Neuroimage*, vol. 80, pp. 169–189, oct 2013.

[27] J.-D. Tournier, F. Calamante, D. G. Gadian, and A. Connelly, "Direct estimation of the fiber orientation density function from diffusion-weighted MRI data using spherical deconvolution," *Neuroimage*, vol. 23, pp. 1176–1185, nov 2004.

[28] C. Reveley, A. K. Seth, C. Pierpaoli, A. C. Silva, D. Yu, R. C. Saunders, D. a. Leopold, and F. Q. Ye, "Superficial white matter fiber systems impede detection of long-range cortical connections in diffusion MR tractography," *Proc. Natl. Acad. Sci.*, vol. 112, pp. E2820–E2828, may 2015.

[29] E. Garyfallidis, M. Brett, B. Amirbekian, A. Rokem, S. van der Walt, M. Descoteaux, and I. Nimmo-Smith, "Dipy, a library for the analysis of diffusion MRI data," *Front. Neuroinform.*, vol. 8, p. 8, feb 2014.

[30] F. Murtagh and P. Contreras, "Methods of Hierarchical Clustering," *Empir. Econ.*, vol. 38, pp. 23–45, apr 2011.

[31] L. Hubert and P. Arabie, "Comparing partitions," *J. Classif.*, vol. 2, pp. 193–218, dec 1985.

[32] K. J. Gorgolewski, G. Varoquaux, G. Rivera, Y. Schwartz, V. V. Sochat, S. S. Ghosh, C. Maumet, T. E. Nichols, J. B. Poline, T. Yarkoni, D. S. Margulies, and R. A. Poldrack, "NeuroVault.org: A repository for sharing unthresholded statistical maps, parcellations, and atlases of the human brain," *Neuroimage*, vol. 124, no. April, pp. 1242–1244, 2016.

[33] D. L. Collins, A. P. Zijdenbos, V. Kollokian, J. G. Sied, N. J. Kabani, C. J. Holmes, and A. C. Evans, "Design and construction of a realistic digital brain phantom," *IEEE Trans. Med. Imaging*, vol. 17, no. 3, pp. 463–468, 1998.

[34] F. Murtagh, *Multidimensional Clustering Algorithms*. Vienna: Comps Physica Verlag, 1985.

[35] K. Beyer, J. Goldstein, R. Ramakrishnan, and U. Shaft, "When is "nearest neighbor" meaningful?," *Database Theory—ICDT'99*, pp. 217–235, 1999.

[36] B. G. N. Lance and W. T. Williams, "A general theory of classificatory sorting strategies 1 . Hierarchical systems," *Comput. J.*, vol. 9, no. 4, pp. 373–380, 1967.

[37] J. Ghaziri, A. Tucholka, G. Girard, J.-C. Houde, O. Boucher, G. Gilbert, M. Descoteaux, S. Lippe, P. Rainville, and D. K. Nguyen, "The Corticocortical Structural Connectivity of the Human Insula," *Cereb Cortex*, pp. 1–13, 2015.

[38] N. Kanwisher and G. Yovel, "The fusiform face area: a cortical region specialized for the perception of faces.," *Philos. Trans. R. Soc. Lond. B. Biol. Sci.*, vol. 361, no. 1476, pp. 2109–28, 2006.

[39] J. D. Yeatman, K. S. Weiner, F. Pestilli, A. Rokem, A. Mezer, and B. A. Wandell, "The vertical occipital fasciculus: A century of controversy resolved by in vivo measurements," *Proc. Natl. Acad. Sci.*, vol. 111, pp. E5214–E5223, dec 2014.

Chapter 5
Solving the Cross-Subject Parcel Matching Problem using Optimal Transport

5.1. Overview

Matching structural parcels across different subjects is an open problem in neuroscience. Even when produced by the same technique, parcellations tend to differ in the number, shape, and spatial localization of parcels across subjects. In this chapter, we propose a parcel matching method based on Optimal Transport. We test its performance by matching parcels of the Desikan atlas, parcels based on a functional criteria and structural parcels. We compare our technique against three other ways to match parcels which are based on the Euclidean distance, the cosine similarity, and the Kullback-Leibler divergence. Our results show that our method achieves the highest number of correct matches.

This work was presented as part of the MICCAI 2018 [1].

5.2. Introduction

Brain organization displays high variability across individuals and species. Studying brain connectivity therefore faces the challenge of locating homogeneous regions while accounting for this variability. Different techniques have been proposed to parcellate the brain based on its structural connectivity. However, matching the resulting parcels across different subjects is still an open problem in neuroscience. Even when produced by the same technique, parcellations tend to differ in the number, shape, and spatial localization of parcels across subjects [2]. Current theories hold that long-range structural connectivity, namely, extrinsic connectivity, is strongly related to brain function [3]. Therefore, being able to match parcels with similar connectivity across subjects can help to understand brain function while also enabling the comparisons of cortical areas across different species [4].

Most of the current methods to match parcels across subjects are strongly linked to the technique used to create them. For example, Moreno-Dominguez et al. [5] seek correspondences between dendrograms created by means of Hierarchical Clustering. Parisot et al. [6] impose the consistence of parcels across subjects while creating the parcellation. In recent works Mars et al. propose to use the Manhattan distance, cosine similarity [7] or the Kullback–Leibler (KL) divergence [4] to compare and match connectivity fingerprints, successfully identifying common areas across humans and primates.

In this work, we propose to match parcels based on their extrinsic connectivity fingerprint using Optimal Transportation theory. Optimal Transport (OT) is a technique that seeks the optimal way to transport mass between probability distributions. While KL divergence computes the difference between two distributions, OT computes a matching between them. In particular, our method adopts a discrete regularized version of Optimal Transport (OT), which has been presented in Gayraud et al. [8] and Courty et al. [9] as a solution to the domain adaptation problem.

We validate our method with four different experiments. In the first experiment, we test the feasibility of our method by generating parcels with synthetic connectivity fingerprints and matching them. In the second one, we show that our technique is able to match parcels of the same atlas across subjects. We use the anatomical atlas of Desikan [10] as its parcels have high spatial coherence and consistent connectivity profiles across subjects [11]. Finally, we show the capacity of our method to match parcels generated with the same criteria but have some spatial cross-subject variability. We assess this for two different situations. In the first one, we derive the parcels from functional activations [12]. We use responses to motor and visual stimuli since they have been shown to be strongly related to structural connectivity [13;14]. In the second one, we divide the Lateral Occipital Gyrus in 3 parcels using a structurally-based parcellation technique [15]. We use the Lateral Occipital Gyrus since it has been shown to have a consistent parcellation across subjects [16;15]. The outline of the last three experiments can be seen in Figure 5.1.

In each experiment, we compare our technique against three other ways to match parcels based on the Euclidean distance; the cosine similarity; and the Kullback-Leibler divergence. Our results on real data show that our method based on OT always achieves the highest number of correct matches.

5.3. Methods

Given two subjects with their respective parcellations, we compute their parcel matching by considering one as the origin and the other one as target. More formally, let $X^a = \{x_i^a\}_{i=1}^{N_a}$, $x_i^a \in \Omega^a \subset \mathbb{R}^n$ be an origin dataset where N_a denotes the number of parcels; x_i^a is the extrin-

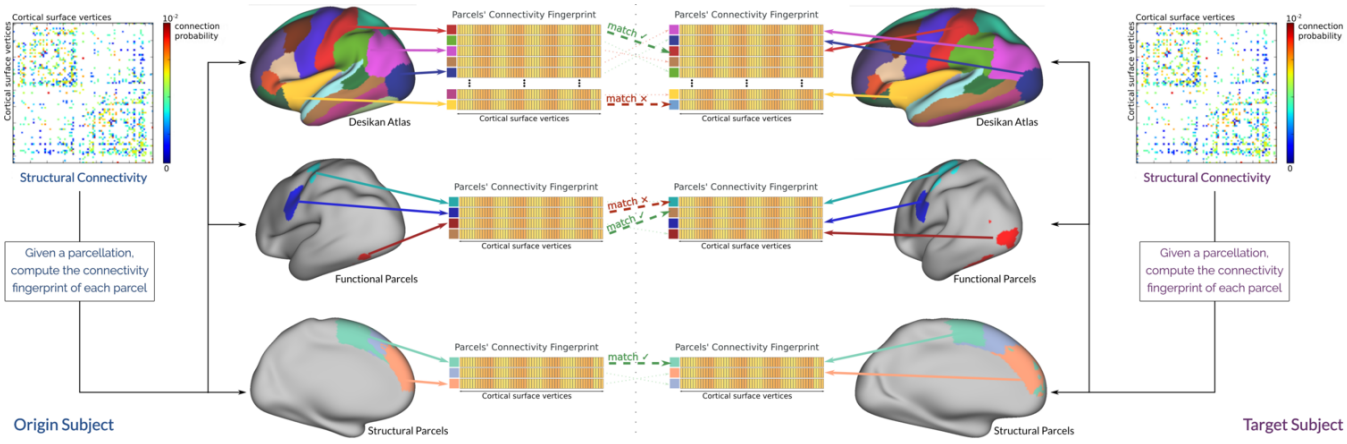

Figure 5.1: From the cortico-cortical structural connectivity matrix of a subject, we can estimate the connectivity fingerprints of each parcel in three different types of parcellations. For each parcellation we compute the amount of correct matches (green lines) that each matching technique produces.

sic connectivity fingerprint of parcel i; and n denotes its dimension. We wish to recover a matching between X^a and a target dataset $X^b = \{x_i^b\}_{i=1}^{N_b}$, $x_i^b \in \Omega^b \subset \mathbb{R}^n$.

In this section, we start by formulating our regularized discrete OT-based method and proceed by presenting three ways of computing this matching that are based on the Euclidean distance; the cosine similarity; and the KL-divergence.

Discrete Regularized Optimal Transport

Optimal Transport (OT) theory boils down to finding the optimal way to transport or redistribute mass from one probability distribution to another with respect to some cost function. In this work, since the datasets X^a and X^b are discrete datasets, we use their empirical probability distributions and apply the discrete formulation of OT[8;9] to solve the parcel matching problem. A simplified example of how our method proceeds is presented in Figure 5.2.

Assume that X^a and X^b follow probability distributions $p_a(x^a)$ and $p_b(x^b)$, respectively. We suppose that X^a has undergone a transformation $\mathbf{T} : \Omega^a \to \Omega^b$, such that $p_b(\mathbf{T}(x^a)) = p_b(x^b)$. We wish to recover $\mathbf{T}$ and use it to match the parcels of X^a and X^b. Using discrete regularized OT we compute a transport plan γ_0 between these two probability distributions. This transport plan is a doubly stochastic matrix which minimizes a certain transportation cost C over the vectors of X^a and X^b. In other words, it defines the optimal exchange of mass between the two probability distributions. We use γ_0 to compute an estimation $\hat{\mathbf{T}}$ by selecting the pairs of vectors, i.e., parcels that exchange the most mass.

Since $p_a(x^a)$ and $p_b(x^b)$ are not known, we use the corresponding empirical distributions $\mu_a = \sum_{i=1}^{N^a} p_i^a \delta_{x_i^a}$ and $\mu_b = \sum_{j=1}^{N^b} p_j^b \delta_{x_j^b}$ instead, where p_i^a and p_j^b are the probability masses associated to each sample. However, given that the dimension of our data depends on the number of vertices in the cortical mesh, the curse of dimensionality makes the estimation of μ_a and μ_b intrinsically difficult. We therefore simply assume a uniform probability distribution over all vectors, $p_i^a = \frac{1}{N^a}$ and $p_j^b = \frac{1}{N^b}$. We compute the transport plan γ_0 such that, if

$$\mathcal{B} = \left\{\gamma \in (\mathbb{R}^+)^{N_a \times N_b} \mid \gamma \mathbf{1}_{N_b} = \frac{1}{N^a}\mathbf{1}_{N_a}, \gamma^{\mathbf{T}}\mathbf{1}_{N_a} = \frac{1}{N^b}\mathbf{1}_{N_b}\right\} \tag{5.1}$$

denotes the set of all doubly stochastic matrices whose marginals are the probability measures μ_a and μ_b, where $\mathbf{1}_N$ is an N-dimensional vector of ones, then $\gamma_0 \in \mathcal{B}$ is the output of the following minimization problem.

$$\gamma_0 = arg\,min_{\gamma \in \mathcal{B}}\ \langle \gamma, C \rangle_F + \lambda \sum_{i,j} \gamma(i,j)\ \log\ \gamma(i,j) \tag{5.2}$$

The matrix C, where $C(i,j) = \|x_i^a - x_j^b\|_2^2$, represents the cost of moving probability mass from location x_j^a to location x_i^b, in terms of their squared Euclidean distance. The rightmost term is a regularization term based on the negative entropy of γ allows us to solve this optimization problem using the Sinkhorn-Knopp algorithm[17] which improves the computation time.

Matrix γ_0 contains information about the exchange of probability mass between the vectors of X^a and X^b. By construction, this exchange depends on the selected cost function. The choice of the squared euclidean distance is motivated both by the fact that it renders the optimization problem convex and because it will allow the parcels to be matched according to the vicinity of their feature vectors. Hence, the origin feature vectors will distribute

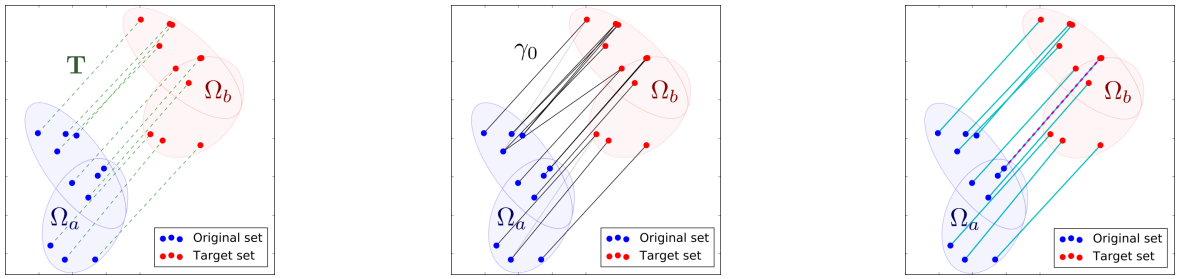

(a) Original & target datasets **(b)** Computed transport plan **(c)** Matching

Figure 5.2: A 2-d example of using OT to compute the matching between two different datasets. On the left we show the original and target datasets. The real matchings are displayed as green dashed edges. In the middle, the edge densities represent the values of the computed coupling γ_0, which denote the amount of mass that is exchanged between vectors x_i^a and x_j^b. On the right, we see the recovered matching. The blue edges represent the correct matchings, while the red dotted edges represent the incorrect ones.

their corresponding probability mass to the target feature vectors that are closest to them. Consequently, we define $\hat{\mathbf{T}} : \Omega^a \to \Omega^b$ as $\hat{\mathbf{T}}(x_i^a) = x_{\hat{j}}^b$ where $\hat{j} = \text{argmax}_j \, \gamma_0(i,j)$. Therefore, i will be matched to the parcel $\hat{j}$ that it sent the most mass to.

Matching Parcels Based on Dissimilarity Between Features

Let $d(x_i^a, x_j^b)$ be some dissimilarity measure between the elements of X^a and X^b. Then, we say that parcel i matches parcel j if $arg\,min_k d(x_i^a, x_k^b) = j$. We compare three dissimilarity measures against our method. First, we use the Euclidean distance, which can be interpreted as matching the parcel i to the parcel j whose feature vector x_j^b is the closest to x_i^a. Then, we use the cosine similarity, which is minimized when two feature vectors are colinear. Lastly, we use the Kullback-Leibler divergence, which measures the difference between two probability distributions in terms of their relative entropy. Note that we need to convert our vectors into probability vectors in order to evaluate d_{KL}.

5.4. Experiments and Results

Data and Preprocessing

For this work we randomly selected 20 subjects from the S500 group of the Human Connectome Project (HCP), all preprocessed with the HCP minimum pipeline[18]. Fiber orientation distributions functions where computed using spherical constrained deconvolution with a spherical harmonic order of 8. Probabilistic tractography was then performed using 1000 seeds per vertex of the cortical mesh provided with the HCP data. For each subject, we computed a connectivity matrix by counting the number of streamlines that connect each pair of vertices of the cortical mesh. Each row in the matrix is a vertex connectivity vector, representing the probability that a connection exists between a surface vertex and the rest of the surface's vertices.

Given a whole brain cortical parcellation, we compute the connectivity fingerprint of each parcel by averaging the connectivity fingerprint of its vertices. Because the mesh's vertices are coregistered across subjects[18], we are able to compare the connectivity fingerprints across subjects. The criterion to compute the parcel matching between two subjects is the similarity between connectivity fingerprints. That is, we match two parcels if they are connected to the rest of the brain in a similar manner. Due to the distance bias that occurs in tractography, a parcel tends to be highly connected to the vertices that compose it. To prevent the matching to be influenced by this bias, we disconnect each parcel from its own vertices.

Matching Parcels

In this section we evaluate the performance of our method by comparing it to the methods presented in Section 5.3.2. For each experiment we compute parcel matchings between all possible pairs of connectivity matrices. To quantify the result of each technique, we compute the accuracy in terms of percentage of correctly matched parcels per pairwise matching.

Matching parcels with synthetic fingerprints. In this first experiment, we test the feasibility of our method by generating parcels with synthetic connectivity fingerprints and matching them. We start by generating a connectivity matrix M using probabilistic Constrained Spherical Deconvolution based tractography to use as ground truth. Our ground truth matrix is a square matrix that represents the connectivity between the 64 parcels of the Desikan atlas in one subject of the HCP dataset. Each coefficient $M(i,j) = \theta_{ij}$ is the parameter of a random variable that follows a Bernoulli distribution $X_{ij}\ B(\theta_{ij})$. This variable X_{ij} represents the probability of a connection existing between the parcels i and j. Using M, we

generate 20 synthetic matrices in such a way that the coefficients of each synthetic connectivity matrix are random variables that follow a binomial distribution $X(i,j) \sim B(p = M(i,j), n)$. By doing this we simulate doing tractography for various values of the number n of particles. Figure 5.3a shows the performance of each method as a function of n.

Matching parcels of the Desikan Atlas. For each subject, we compute the connectivity fingerprint of each parcel in their Desikan atlas as explained in Section 5.4.1. When matching parcels across subjects, Figure 5.3b shows that on average OT achieves an accuracy of 98%±2%, followed by cosine similarity (94%±3%), KL divergence (87%±4%), and finally Euclidean distance (77%±11%).

Matching parcels created using functional criteria. Each subject in the HCP dataset possesses z-score maps representing responses to different stimuli obtained with functional MRI (fMRI)[12]. We derive parcels for each subject from the responses to motor (hand, foot and tongue movement) and visual stimuli (faces vs shape recognition). We do so by keeping only the vertices whose z-score is in the top 35%. Figure 5.3b shows that OT performs best with an average of 98%±6%. The cosine similarity, KL divergence, and Euclidean distance achieve average accuracies of 97%±6%, 92%±10%, and 90%±13% respectively.

Matching parcels created using structural criteria. For each subject, we first mask their Lateral Occipital Gyrus using the Desikan atlas. Then, we divide it into 3 parcels using the structural based parcellation technique of Gallardo et al.[15]. Once more, we can see on Figure 5.3b that optimal transport has the highest average accuracy, equal to 92%±16%. It is followed by the cosine similarity, the KL divergence, and the Euclidean distance, whose average accuracies equal 85%±17%, 84%±17%, and 75%±17%

5.5. Discussion

In this work we proposed a method to match parcels across subjects based on the connectivity fingerprint of a parcel.

We tested our method with four different experiments. In the first experiment our technique correctly matched connectivity fingerprints created in a synthetic way. Specifically, each entry in a fingerprint was sampled from a Binomial distribution, whose parameter was chosen as the corresponding value of a ground truth connectivity matrix. This can be thought as a simulation of the process of tracking in tractography with different number of streamlines.

Our second experiment shows that we can correctly match parcels of the Desikan atlas across subjects with a 98% of correct matches. The parcels of the Desikan atlas are known to have high spatial coherence and consistent connectivity profiles across subjects[11]. We therefore use this experiment as a reference point to benchmark our technique. The last two experiments show that our technique can match parcels generated with a same criteria, even when they have some spatial variability across-subjects. The first experiment uses parcels created from the functional response to specific motor and visual stimuli, known to be strongly linked to functional connectivity[13;14]. The second one, parcels created from the structural parcellation of the Lateral Occipital Gyrus, a structure documented to have a consistent structural division[16;15].

It's important to notice that our technique achieved more than a 90% of correct matches in every experiment with real data. Given that we used 20 subjects, this represents a total of 20x19=380 cross-subject matches. In the case of the Desikan atlas, which possesses 64 parcels, this translates into a total of 24320 matches, from which 98% where correctly matched. Furthermore, when tested with a paired t-test to compare the number of correct matches, our method always performs significantly better than the other three ($p < 10^{-256}$).

5.6. Conclusion

In this chapter, we proposed a novel parcel matching method based on Optimal Transport. We showed that our technique outperforms state-of-the-art matching techniques in three different baseline scenarios.

Both this chapter and the previous one are based on the fact that we can estimate brain connectivity. However, some brain pathologies can disrupt the white matter, hampering the estimation of brain connectivity. In the following chapter, we will introduce a technique to infer which tracts are affected by a pathology, even when is not possible to use tractography.

Bibliography

[1] G. Gallardo, N. Gayraud, R. Deriche, M. Clerc, S. Deslauriers-Gauthier, and D. Wassermann, "Solving the Cross-Subject Parcel Matching Problem Using Optimal Transport," *Med. Image Comput. Comput. Assist. Interv. – MICCAI 2018. Lect. Notes Comput. Sci.*, no. 11070, 2018.

[2] S. Jbabdi and T. E. Behrens, "Long-range connec-

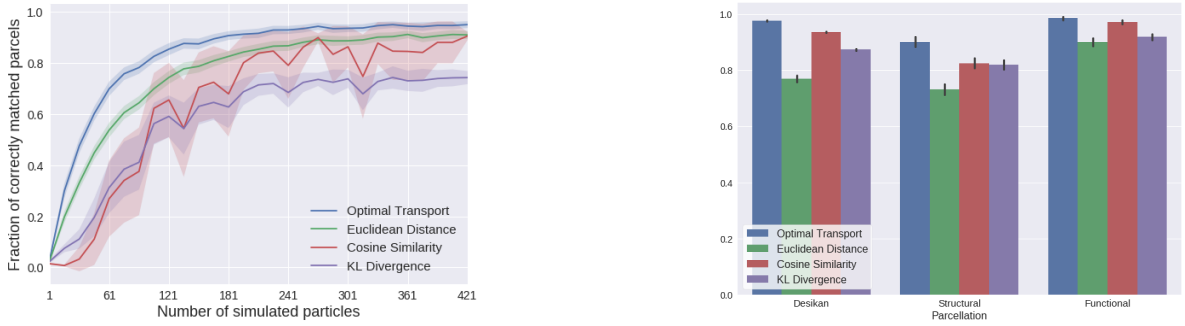

(a) Synthetic data **(b)** Real data

Figure 5.3: Proportion of parcels correctly matched by each method (see section 5.3.2) when matching: (a) synthetic connectivity fingerprints and (b) connectivity fingerprints of a cortical parcellation, for three different parcellations (as described in section 5.4.2). OT always performs significantly better.

tomics," *Ann. N. Y. Acad. Sci.*, vol. 1305, pp. 83–93, dec 2013.

[3] R. E. Passingham, K. E. Stephan, and R. Kötter, "The anatomical basis of functional localization in the cortex," *Nat. Rev. Neurosci.*, vol. 3, pp. 606–616, aug 2002.

[4] R. B. Mars, S. N. Sotiropoulos, and R. E. Passingham, "Whole brain comparative anatomy using connectivity blueprints," *bioRxiv*, p. 245209, 2018.

[5] D. Moreno-Dominguez, A. Anwander, and T. R. Knösche, "A hierarchical method for whole-brain connectivity-based parcellation," *Hum. Brain Mapp.*, vol. 35, pp. 5000–5025, oct 2014.

[6] S. Parisot, S. Arslan, J. Passerat-Palmbach, W. M. Wells, and D. Rueckert, "Tractography-Driven Groupwise Multi-scale Parcellation of the Cortex.," *Inf. Process. Med. Imaging*, vol. 24, pp. 600–12, 2015.

[7] R. B. Mars, L. Verhagen, T. E. Gladwin, F. X. Neubert, J. Sallet, and M. F. S. Rushworth, "Comparing brains by matching connectivity profiles," *Neurosci. Biobehav. Rev.*, vol. 60, pp. 90–97, 2016.

[8] N. T. Gayraud, A. Rakotomamonjy, and M. Clerc, "Optimal Transport Applied to Transfer Learning For P300 Detection," in *7th Graz Brain-Computer Interface Conf. 2017*, 2017.

[9] D. Tuia, S. Member, and A. Rakotomamonjy, "Optimal Transport for Domain Adaptation," *IEEE Trans. Pattern Anal. Mach. Intel.*, vol. 39, no. 9, pp. 1853–1865, 2017.

[10] R. S. Desikan, F. Ségonne, B. Fischl, B. T. Quinn, B. C. Dickerson, D. Blacker, R. L. Buckner, A. M. Dale, R. P. Maguire, B. T. Hyman, M. S. Albert, and R. J. Killiany, "An automated labeling system for subdividing the human cerebral cortex on MRI scans into gyral based regions of interest," *Neuroimage*, vol. 31, pp. 968–980, jul 2006.

[11] M. A. de Reus and M. P. van den Heuvel, "The parcellation-based connectome: Limitations and extensions," *Neuroimage*, vol. 80, pp. 397–404, 2013.

[12] D. M. Barch, G. C. Burgess, M. P. Harms, S. E. Petersen, B. L. Schlaggar, M. Corbetta, M. F. Glasser, S. Curtiss, S. Dixit, C. Feldt, D. Nolan, E. Bryant, T. Hartley, O. Footer, J. M. Bjork, R. Poldrack, S. Smith, H. Johansen-Berg, A. Z. Snyder, and D. C. Van Essen, "Function in the human connectome: Task-fMRI and individual differences in behavior," *Neuroimage*, vol. 80, pp. 169–189, oct 2013.

[13] D. E. Osher, R. R. Saxe, K. Koldewyn, J. D. E. Gabrieli, N. Kanwisher, and Z. M. Saygin, "Structural Connectivity Fingerprints Predict Cortical Selectivity for Multiple Visual Categories across Cortex," *Cereb. Cortex*, vol. 26, no. 4, pp. 1668–1683, 2016.

[14] W. Penfield and H. Jasper, *Epilepsy and the Functional Anatomy of the Human Brain*. 1954.

[15] G. Gallardo, W. Wells, R. Deriche, and D. Wassermann, "Groupwise structural parcellation of the whole cortex: A logistic random effects model based approach," *Neuroimage*, pp. 1–14, feb 2017.

[16] M. Thiebaut de Schotten, M. Urbanski, B. Batrancourt, R. Levy, B. Dubois, L. Cerliani, and E. Volle, "Rostro-caudal Architecture of the Frontal Lobes in Humans," *Cereb. Cortex*, pp. 1–15, 2016.

[17] M. Cuturi, "Sinkhorn Distances : Lightspeed Computation of Optimal Transport," *Adv. Neural Inf. Process. Syst.*, pp. 2292–2300, 2013.

[18] M. F. Glasser, S. N. Sotiropoulos, J. A. Wilson, T. S. Coalson, B. Fischl, J. L. Andersson, J. Xu, S. Jbabdi, M. Webster, J. R. Polimeni, D. C. Van Essen, and M. Jenkinson, "The minimal preprocessing pipelines for the Human Connectome Project," *Neuroimage*, vol. 80, pp. 105–124, oct 2013.

Chapter 6
Inferring the Localization of White-Matter Tracts using Diffusion Driven Label Fusion

6.1. Overview

In the previous chapters we studied the structural organization of the brain, and saw that it is highly related to function. White-matter pathologies disrupt the white-matter organization, that manifests as deficits in brain function. When treating such pathologies, it is of great importance to infer which pathways are affected. However, sometimes the white-matter lesions hamper the use of tractography to track fiber bundles. In this chapter, we introduce a way to infer the location of white-matter pathways, even when it is not possible to use tractography to locate them. Our technique is based on a methodology named label fusion. Particularly, we show how to add dMRI information to the label fusion in order to better estimate the location of white matter pathways.

This work was presented as part of OHBM 2018[1].

6.2. Introduction

Pathologies such as traumatic brain injury (TBI), or focal lesions disrupt the structure of white matter, resulting in cognitive deficits. Depending on the type and severity of the pathology, fiber bundles can be displaced, infiltrated or directly interrupted[2;3;4]. Inferring which pathways are closely located to the lesion or being directly affected by it is key for palliative care, and for both pre and post-treatment planning. With this knowledge, neurologists and neurosurgeons can decide if a lesion should be treated more aggressively or conservatively[3;5]. In healthy brains, tractography allows to non-invasively reconstruct the major white matter pathways in the brain[6]. However, in the presence of pathologies, tracking through the white-matter becomes challenging[7].

Four pattern types associated with brain pathologies can be identified in major tracts and Diffusion Weighted Images (DWIs) [7]. The first pattern consists of unchanged Fractional Anisotropy (FA)[8], and tract displacement[7]. In this case, a bundle is displaced by the pathology without damaging it. The second pattern is substantially decreased FA with no tract displacement, this could be an indicator of edema or small infiltration[2;3]. The third pattern is substantially decreased FA with some loss of directionality, which makes tracking hard[2;7]. Finally, the fourth pattern consists of isotropic diffusion within the area affected by the pathology, which causes a disruption of the tracts[7]. Some of these patterns denote situations in which the tracking results in interrupted or distorted tracts. This hampers the identification of which pathways are directly affected by pathology[7].

When tracking is not possible, but tracts are present, aggregating anatomical information from other subjects could help to infer tracts affected by pathology. Assuming we identified major bundles in a group of healthy subjects, we could register them to our patient's brain, and combine them using a label fusion technique. Label fusion is a family of techniques which aim is to infer the localization of a structure in a target subject, based on its characteristics in a group of control subjects[9].

One well known label fusion technique is Majority Voting[10]. Given a voxel on a brain image, each template subject "votes" for a label. The resulting label for the voxel will be that with the most votes. Majority Voting is simple to implement and has been shown to generate accurate segmentations[9], even when using few template subjects to perform the inference. Typically among the template segmentations there are more accurate ones as well as less accurate ones[11]. However, Majority Voting weights the vote of each template subject equally. To improve this, it has been proposed to weigh the vote of each subject based on a similarity measure between the template subject and the target[12]. The underlying intuition is that the label choice should be driven by those subjects who resemble the most to the one being labeled. The practical advantages of various strategies based on this idea have been demonstrated by Artaechevarria et al.[13].

Current label fusion techniques rely only on anatomical information, not taking into account the structure of white matter. In the case of white matter pathways, the presence of a path constrains the diffusion of water particles, which can be measured by dMRI. Therefore, adding diffusion information to the fusion algorithm could help to better delineate fiber bundles[14].

In this work, we introduce a label fusion technique that takes advantage of dMRI and weights the vote of each subject based on how the voted pathway is supported by the target subject's diffusion data (Fig. 6.1). Hence, if the diffusion data of the target subject is consistent with the direction of the voted pathway, the vote has a higher weight.

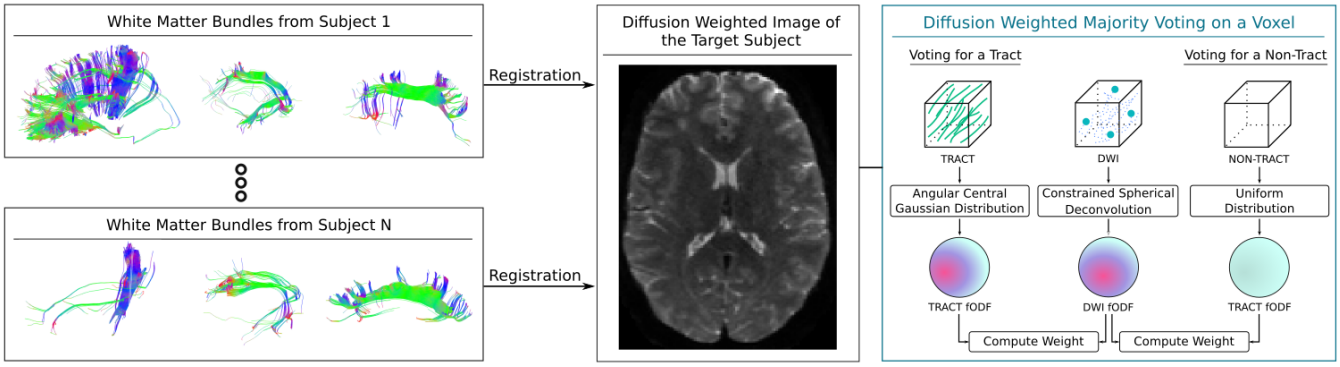

Figure 6.1: We use a label fusion technique to infer the location of white matter bundles by aggregating information of healthy subjects. After registering the tracts, each subject "votes" for either a tract or a non-tract structure (gray matter or background). Our technique adds diffusion based weights to each one of these votes. The weights are computed based on the similarity between the fiber Orientation Distribution Function of the structure being voted and the DWI of the target subject.

We first validate our technique with synthetic DWIs. Using Phantomas[15], we generate three types of synthetic DWIs: with a single fiber, with two fibers crossing, and with no fibers, representing images with isotropic diffusion. We use the synthetic DWIs to test how a vote for a tract is weighted based on the tract's directionality and the DWIs' diffusion. We show that our technique assigns higher weights to the votes for tracts aligned with the DWI's diffusion.

Then, we randomly select 10 subjects from the Human Connectome Project (HCP). On each subject, we determinate the shape and location of 4 left hemisphere tracts using whole-brain tractography and an implementation of the white matter query language (WMQL). We use these results as ground truth to benchmark the inferences made by our technique and Majority Voting on a leave-one-out cross-validation experiment. Our results show that our proposed technique has a lower sensitivity than Majority Voting, but a higher precision. Meaning, our technique obtains less false positives at the cost of obtaining more true negatives.

Finally, we simulate focal lesions with different degrees of severity in the white matter of one HCP subject. Particularly, we target a spherical region where the Superior Longitudinal Fasciculus passes by. We do so by iteratively decreasing the FA of each voxel in the spherical region, until obtaining isotropic diffusion. We show that our technique labels less voxels as the FA decreases, but is still able to label voxels around the pathology.

6.3. Methods

Majority Voting.

Let $labels = \{l_i\}$ be the set of labels representing tracts and grey matter structures the brain. Let $L_s, s \in S$ represent the labeling of a set of template subjects S, where each $L_s \in labels^{v_x \times v_y \times v_z}$ is a 3D volume with dimension (v_x, v_y, v_z) representing the labeling of template subject s. Majority Voting[11] infers the label of each voxel x in a target subject by computing:

$$L^*(x) = \underset{l \in labels}{\operatorname{argmax}} \sum_{s \in S} p(L(x) = l | L_s(x)),$$

where

$$p(L(x) = l | L_s(x)) = \begin{cases} 1, & \text{if } L_s(x) = l \\ 0, & \text{otherwise.} \end{cases} \tag{6.1}$$

In this case, it's said that each subject votes for a label, and the label with the most amount of votes is assigned to the target voxel. It is important to notice that no information from the target subject is being used to infer the label $L^*(x)$.

Diffusion Based Voting

Majority Voting (Eq. 6.1) decides the label of a target voxel based on the "votes" of template subjects, without using any information from the target subject. The aim of this work is to infer white matter pathways. Knowing that water particles diffuse along pathways, we can profit from the diffusion information to weigh the voting process. In particular, votes for tracts aligned with the diffusion of the target subject should get higher weights.

One way to characterize the directionality on a diffusion weighted image (DWI) is by means of fiber orientation distribution functions (fODFs)[16]. Now, we will first explain how to estimate a fODF from both DWI and tracts. Then, we will present how to compare the fODFs, in order to compute weights for each vote.

Fiber Orientation Density Function from dMRI Data. By fitting the diffusion information into a Con-

strained Spherical Deconvolution (CSD) model, it's possible to estimate a fiber orientation density function[17] (fODF). The fiber ODF $F_x(\theta, \phi)$ represents the estimated fraction of fibers within the voxel x that are aligned along the direction (θ, ϕ), expressed in spherical coordinates.

Fiber Orientation Density Function from Tractography. A tract can be described as a set of streamlines, where a streamline is a discretized 3-dimensional curve. Assuming that a streamline doesn't have sharp turns, we can estimate its directionality within a voxel by looking at its entry and exit points (Fig. 6.1 A). Repeating this for each streamline on a tract, we obtain a set of directional vectors, representing the directionality of the tract within the voxel. A fiber ODF can be estimated from this set of vectors by means of directional statistics. In this work, we use the Angular Central Gaussian Distribution[18] (ACGD). The ACGD models antipodal symmetric directional data, and has a closed form to estimate its parameters. Assuming a tract makes no sharp turns inside of a voxel, we can assume antipodal symmetry on its entry and exit points. Based on this symmetry, we can use the ACGD model, making both suitable and simple to estimate the directionality of a tract in a voxel[18]

Label Fusion Weighted by Diffusion Majority Voting (Eq. 6.1) decides the label of a voxel based on how many subjects "vote" for it. Given that we are inferring brain pathways, we want to introduce a weight that denotes how much the voted tract resembles the target's diffusion data:

$$L^*(x) = \underset{l \in labels}{\operatorname{argmax}} \sum_{s \in S} p(L(x) = l | L_s(x)) p(D(x) | D_{sl}(x)). \tag{6.2}$$

In our segmentation scheme, the term $p(L(x) = l|L_s(x))$ is modeled as in the voting scheme (eq. 6.1). Our second term, $p(D(x)|D_{sl}(x))$ express the probability of seeing the diffusion of our target subject, $D(x)$, on voxel x, given the diffusion of subject s generated by tract l on the same voxel, $D_{sl}(x)$. Since registering DWIs is a highly time consuming task[19], we want to avoid it. Instead, we can register tracts, for which efficient algorithms exist, and use them as an estimator of the diffusion of each template subject. Knowing that water particles in the brain diffuse along tracts, we can estimate $D_{sl}(x)$ by computing the fODF of the registered tract l. Simultaneously, we can characterize $D(x)$ with the fODF computed from the DWI of the target subject. In order to reflect how much the fODF of our target subject's diffusion resembles the fODF of the voted tract on a voxel, we model $p(D(x)|D_{sl}(x))$ as:

$$p(D(x)|D_{sl}(x)) = \begin{cases} \langle F(x), F_{sl}(x) \rangle, & \text{if } L_s(x) = l, \\ & \text{and } l \neq 0 \\ \langle F(x), U \rangle, & \text{if } L_s(x) = 0 \\ 0, & \text{otherwise} \end{cases} \tag{6.3}$$

where $F(x)$ is the fiber ODF on voxel x estimated from the target's DWI by means o CSD, and is normalized such that $\langle F(x), F(x) \rangle = 1$. $F_{sl}(x)$ is the fiber ODF of the tract l registered from subject s, estimated by means of ACGD, and normalized as $F(x)$. U is a uniformly distributed fiber ODF, this is the diffusion assumed for either the label no-tract, representing the background or a gray matter structure. By computing the inner product between normalized ODFs, we can estimate how much they look alike. In this way, we weight the vote of each subject accounting for the white-matter structure of both the voting and target subjects.

6.4. Experiments and Results

In section 6.3 we presented how to add diffusion information to Majority Voting (Eq. 6.2). This allows us to weigh the vote for a tract by how much the diffusion of the target supports it. Now, we present experiments both in synthetic data and subjects from the Human Connectome Project (HCP). We start by assessing that the computed weights correctly reflect the diffusion information in DWI phantoms. Then, we proceed to infer the location of white-matter pathways in subjects of the HCP, and compare them with their true shape. Finally, we simulate lesions in the white matter and test how our method behaves in their presence.

Data and Preprocessing

We created three types of diffusion weighted image phantoms using Phantomas[15]. The first phantom possess only one tract, traveling from one side to the other of the image horizontally (Fig. 6.2 A). The second possess two crossing tracts, forming a 90 degrees angle between them (Fig. 6.2 B). The last, has no fibers, and represents isotropic diffusion (Fig. 6.2 C). From each one of them, we generated 31 DWIs. All the DWIs were generated using a Signal to Noise Ratio of 20, and a resolution of $1mm$ per voxel. The final images are 3-dimensional matrices, with 10 voxels in each dimension. Having such small images, allows us to test how our label fusion technique behaves on a controlled environment.

To test our technique in more realistic scenarios, we randomly selected 10 subjects from the HCP500 dataset from the Human Connectome Project. For each subject, we computed whole-brain tractography using each voxel in

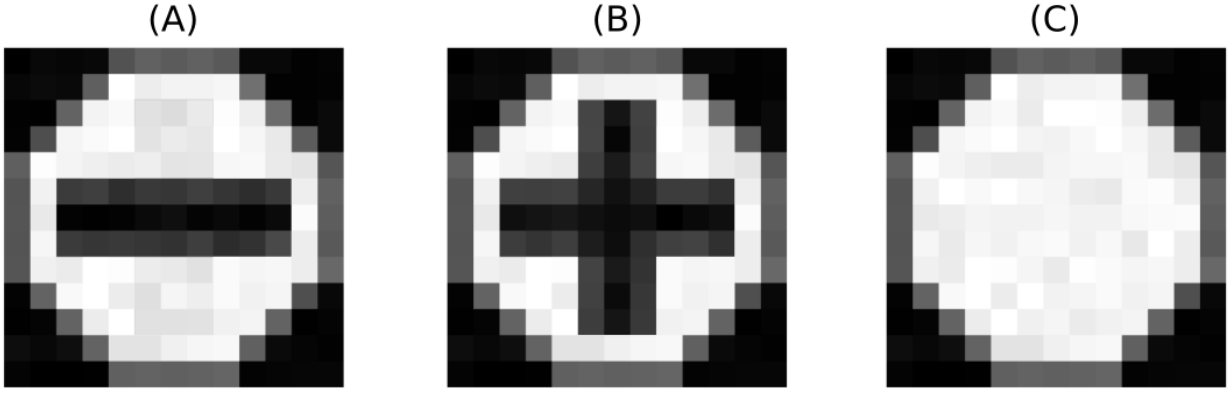

Figure 6.2: In order to test our technique, we created three types of synthetic DWIs, known as phantoms. (A) A phantom with only one tract in the white matter. (B) A phantom with two fibers crossing. (C) A phantom with no tracts, representing isotropic diffusion.

the white-matter as a seed and simulating the movement of 8 water particles per seed [20]. We extracted four tracts from the left hemisphere using the implementation of the white-matter query language (WMQL) [21]. For each subject we computed non linear registrations to the rest using as reference their T1w images [22]. Using the resulting warp transformations, we registered the tracts between every pair of subjects.

We estimated fiber ODFs in each voxels of the phantom DWIs, and in the DWI data of the HCP subjects by means of CSD using Dipy [20]. The fODFs were discretrized on a sphere with $n = 100$ vertices. A uniform fODF, U, was created by assigning to each vertex of the sphere the value $\sqrt(n)/n$, making $\langle U, U \rangle = 1$.

Assessing the Correctness of Voting Weights in Synthetic Data

In order to study how the tract's directionality influences its vote weight, we started by reconstructing the tract present in the first phantom (Fig. 6.2 A). For this, we took one of the 31 generated DWIs, and computed 1000 streamlines by means of probabilistic tracking from the voxels in which the tract passes.

In the DWIs generated from the first phantom, the reconstructed tract is the one that should generate the highest weight. At the same time, any change in its directionality, should decrease the received weight. To assess this was happening, we computed weights in 30 DWIs for the reconstructed tract, and for planar rotations of it around the central voxel. Figure 6.3 A shows the obtained weights on the first phantom. Effectively, the weight starts to rapidly decrease as the angle increments and the directionality of the tract moves away from that of the diffusion. Figure 6.3 B shows the weights obtained when computing weights of the reconstructed tract in 30 DWIs derived from the second phantom (Fig. 6.2 B), which have a fiber crossing in the central voxel. In this case, the weight is higher when the reconstructed tract aligns with one of the crossing fibers (at 0 degrees or 90 degrees), while rapidly decaying in between them. Finally, figure 6.3 C shows the weights when using 30 DWIs with isotropic diffusion (Fig. 6.2 C). In this case, the weight is always low, driven by the discrepancy between the directionality of the tract and the free diffusion present in the DWIs.

To assess that the proposed model is not overweighting tracts, we also computed the weight that a "non-tract" label would receive in each of the phantoms. As explained in section 6.3, equation 6.3, when a subject is voting for a non-tract label, a uniform fiber ODF is compared against the diffusion fODF. Figure 6.2 A, B, and C show the weight obtained in the central voxel when a subject is voting for the label "non-tract". In figure 6.2 A, we can see that the weight of "non-tract" is low, specially when compared with the high weight of the correctly aligned tracts (low angle rotations). This is driven by the highly directional underlying diffusion data of the phantom. Figure 6.2 B shows that the weight of a "non-tract" vote is similar to that of an aligned tract. Finally, figure 6.2 C shows always a higher weight for the "non-tract" than for any tract, consistent with the isotropic diffusion of our third phantom.

Inferring Tracts in Human Connectome Project Subjects To validate our technique in a more realistic but controlled scenario, we inferred single tracts in the HCP subjects. We selected the following tracts to work with: inferior part of the Superior Longitudinal Fasciculus (SLF1), Inferior Longitudinal Fasciculus (ILF), middle part of the Corpus Callosum (CC2), and External Capsule (EC). These four tracts provide a fair diversity of directionality, shape, and position in the brain.

For each tract we performed a leave-one-out cross-validation experiment. At each step, we inferred the tract of one

Figure 6.3: In order to study how a tract's directionality influences its vote weight, we estimated the fiber bundle by means of tractography in the Phantom A. Then, we computed the weights obtained by the tract and planar rotations of it in: (A) Phantom A. (B) Phantom B. (C) Phantom C. The figures show that our technique gives the highest weights to structures that are aligned with the underlying diffusion.

subject from the registered tracts of the others using both Majority Voting and our technique. Using as "ground truth" the target's bundle computed by means of tractography and WMQL, we quantified the performance of both techniques. In particular, we computed their confusion matrix. A confusion matrix is a matrix $M \in \mathbb{R}^{labels \times labels}$, where each entry M_{ij} represents the number of times the label in the ground truth was i and the technique labeled j. In this experiment, since we are only inferring one tract, we have two labels: "tract" and "non-tract". We computed the sensitivity, and precision of each confusion matrix[23]. Sensitivity measures the proportion of voxels in the ground-truth tract that were "discovered". Precision measures the proportion of voxels that were correctly labeled, over all the labeled voxels. Table 1 shows the results obtained for each technique and tract. In all of the tracts, our technique achieves a lower sensitivity than Majority Voting. This means that we label a smaller portion of the ground-truth bundle. On the other hand, our diffusion weighted label-fusion always achieve a higher precision. This is, if we only look at the labels created by the techniques, our technique has the highest proportion of correct ones. Another way to phrase it is, our technique has a lower number of false positives. Therefore, our technique is discovering less voxels, but those which are labeled can be trusted more.

Inferring Tracts in the Presence of Simulated Lesions To test how our technique behaves on an injured brain, we simulated lesions at different degrees of severity in the white matter of one of our subjects. Given that some brain lesions directly affect FA[2;3], we simulated lesions by adding isotropic signal to a set of voxels, therefore lowering their FA. We targeted the SLF bundle, in order to compare how the labeling changes with lesion of different degrees. We did so by selecting a spherical region of $4mm$ where the SLF passes, and mixing the diffusion signal there with signal from the ventricles. Since the ventricles are regions filled with cerebrospinal fluid (CSF), their diffusion is approximately isotropic. In particular, for each voxel x in the lesioned region, we chose a voxel v in the ventricle and mixed their DWI signals, $S(\cdot)$, as follows:

$$S(x) = S(x)(1-\alpha) + S(v)\alpha, \alpha \in [0,1], \tag{6.4}$$

where α manages the severity of the lesion. In this case, $\alpha = 0$ represents healthy tissue, and $\alpha = 1$ represents a total disruption of the white-matter, resulting in pure isotropic diffusion. Figure 6.4 shows that, at higher alpha (lower FA), less voxels are labeled within the lesion. This is a good behaviour, since by lowering the FA we make the diffusion more isotropic, loosing the underlying tract. In particular, for $\alpha = 1$, the diffusion is completely isotropic, meaning that there is no tract, therefore, it's correct to not label it. Since our technique still labels the surroundings of the pathology, it allows to correctly identify the affected tract.

6.5. Discussion

In this chapter we presented a label-fusion technique to infer white-matter structures in the brain. An advantage of label-fusion techniques is that they can achieve accurate segmentations even when the inference is made from few subjects[9]. In particular, our technique allows to infer white matter pathways without the need of tracking. This is specially important in the presence of brain pathologies that show no deformations. In the presence of deformations, as in tumors, segmentation becomes challenging, because the label fusion techniques rely heavily on registration, which is difficult with deformed brains.

The main contribution of this work is to add diffusion information in the process of label-fusion. Given that fiber bundles constrains the diffusion of water particles

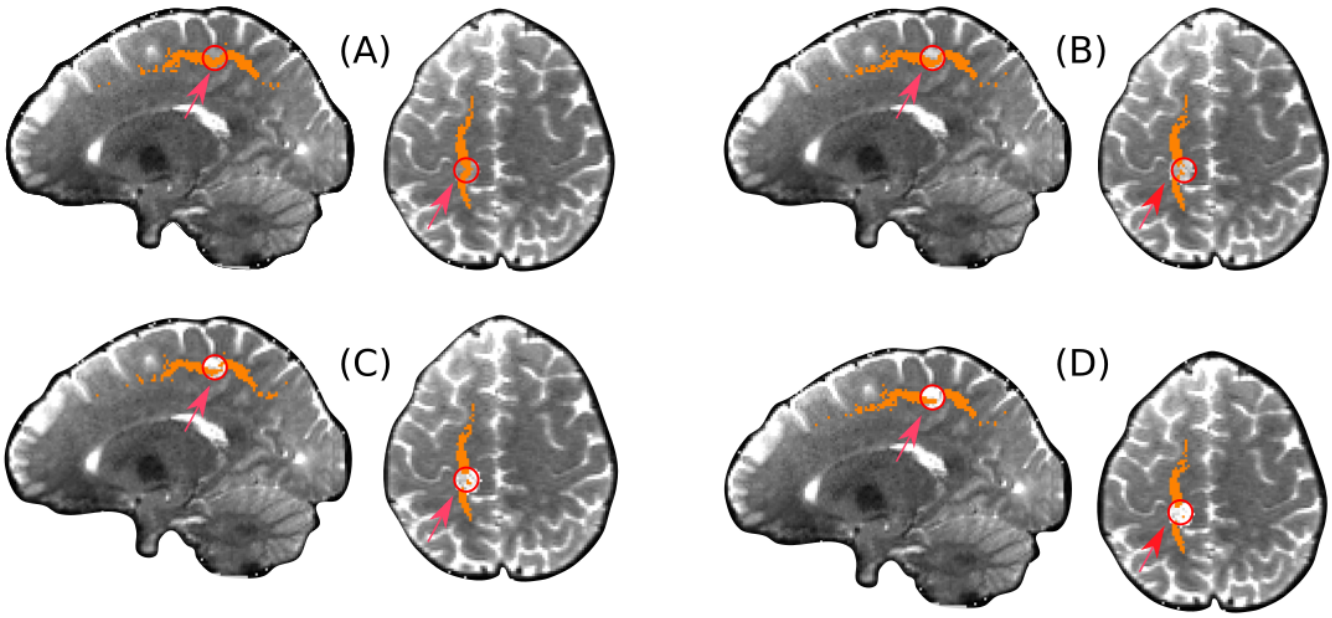

Figure 6.4: We tested how our technique behaves in the presence of simulated lesions. Lesions were simulated in a specific region (red circle) by following eq. 6.4 to lower the FA of the region. The SLF passes through such a region. The figures show the result of applying our technique in order to determine the SLF at different values of the parameter α in eq. 6.4: (A) $\alpha = 0.2$, (B) $\alpha = 0.5$, (C) $\alpha = 0.75$, and (D) $\alpha = 1$. Results show that while the value of α increases, the amount of voxels labeled within the affected region decreases.

in the brain, our technique uses diffusion information to improve Majority Voting [10]. More specifically, we weight each vote based on how the voted pathway is supported by the target's diffusion data. In this way, voted pathways that better resemble the white matter of the target subject obtain a higher weight. The weights come from comparing how much the diffusion fODF of our target subject's resembles the fODF of the voted tract on a voxel. In this way, we can compare the white-matter structure of our target subject with that of the voting subject, without having to register DWIs. Adding diffusion weights to Majority Voting, allowed us to profit from its robustness while improving the labeling of white-matter bundles, as shown by our results in synthetic data and subjects from the Human Connectome Project.

Our Technique Creates Weights Consistent With the Underlying Diffusion Data.

In order to study how the directionality of the tracts influence their vote weight, we created three different phantoms, and derived DWIs from them. This allowed us to create a controlled environment, in which we could study how the directionality of a tract affects its vote weight. Since weight variability can come from changes on the directionality of the tract, we generated many DWIs for each phantom. At the same time, we computed weights for tracts in different directions. Figure 6.2 shows the weights obtained on a phantom with a single bundle. The weights show that tracts with a directionality similar to the underlying diffusion get higher votes. However, when the alignment start to decrease, also does the weight. Particularly, when the directions differ by more than 20 degrees, the weight starts to drop rapidly, falling bellow the weight of the 'non-tract' label. The Figure 6.2 B shows that, in the presence of crossing fibers in the DWI, tracts aligned with a crossing fibers get the highest weights. It is important to notice that the highest weights are similar to those of the 'non-label' votes. This means, that tracts roughly aligned with one of the crossing fibers will compete with equal weights against the 'non-label' structures. Finally, Figure 6.2 C shows that, when there is no underlying white-matter structure in the DWI image, then the label 'no-tract' is the one that receives the highest weight. These results show that our technique is able to correctly weight each label based on diffusion directionality.

Our Technique Shows Lower Sensitivity but Higher Precision than Majority Voting.

To test our technique in realistic data, we registered tracts between different subjects of the HCP. Using these registered tracts, we inferred the position of individual tracts in each subject. Table 1 shows that in each inferred tract, our technique achieved a lower sensitivity but a higher precision. In fact, the precision, except for the External Capsule, is always higher than 0.7. This means that our technique was able to discover less voxels belonging to the tracts, but at least 70% of those labeled are correct. An-

Table 6.1: Sensitivity and precision of our proposed method (Weighted) and Majority Voting (Majority) when inferring single bundles in 9 subjects. The inferred bundles are: Superior Longitudinal Fasciculus (SLF), Inferior Longitudinal Fasciculus (ILF), Corpus Callosum (CC), and the External Capsule (EC).

	SLF		ILF		CC		EC	
	Weighted	Majority	Weighted	Majority	Weighted	Majority	Weighted	Majority
Sensitivity	0.19±0.04	**0.30±0.05**	0.33±0.02	**0.47±0.07**	0.53±0.04	**0.64±0.09**	0.06±0.02	**0.27±0.20**
Precision	**0.70±0.11**	0.58±0.10	**0.74±0.05**	0.41±0.20	**0.91±0.15**	0.82±0.17	**0.42±0.20**	0.31±0.13

other way to phrase this is that our techniques presents less false positives at the cost of more false negatives, making it more conservative than Majority Voting.

Our Technique Infers Tracts Before and After, But Not Within Voxel Affected by Pathologies

We further characterized the behaviour of our technique by simulating lesions in the white-matter of a HCP subject. Particularly, we defined a spherical region on the path of the Superior Longitudinal Fasciculus, and increased its Fractional Anisotropy until achieving isotropic diffusion. In doing so, we simulated focal lesions in the brain of a subject. As explained in the Introduction, these pathologies are characterized by a decreased FA inside the lesion, but do not deform the white-matter around it. Figure 6.4 shows that our technique labels less voxels as the FA becomes higher on the region. This is the expected behaviour in the scenario of tract disruption. Since our technique is still able to label the surroundings of the lesion, we can still identify the affected tract. It is important to notice that the simulated lesions do not include mass-effect, this is, white matter deformations. Such pathologies are difficult to simulate and study, since the process of registration from healthy subjects to the patient has to be fined tuned manually .

6.6. Conclusions

In this chapter we presented a label fusion technique that relies on dMRI data to infer the localization of white-matter tracts. The results show that our technique is well suited to create subject specific segmentation of the brain. Our method could be use in precision medicine to interrogate diffuse pathologies like TBI, even in the presence of small lesions (as shown in fig. 6.4). Our technique could be used in the study of infiltrative brain tumors, where registration is less of a problem, and in the future, could be extended to larger tumors, due to the growing advances in registration based on tumor growth models.

Bibliography

[1] G. Gallardo, B. Sylvain, and D. Wassermann, "Diffusion Driven Label Fusion for White Matter Multi-Atlas Segmentation," *OHBM 2018 - Organ. Hum. Brain Mapp.*, 2018.

[2] T. Schonberg, P. Pianka, T. Hendler, O. Pasternak, and Y. Assaf, "Characterization of displaced white matter by brain tumors using combined DTI and fMRI," *Neuroimage*, vol. 30, pp. 1100–1111, 2006.

[3] T. A. G. M. Huisman, "Tumor-like lesions of the brain," *Cancer Imaging*, pp. 10–13, 2009.

[4] Y. I. Won, C. K. Chung, C. H. Kim, C.-k. Park, B.-b. Koo, J.-m. Lee, and H.-w. Jung, "White Matter Change Revealed by Diffusion Tensor Imaging in Gliomas," *Brain Tumor Res Treat*, vol. 4, no. 2, pp. 100–106, 2016.

[5] M. J. McGirt, K. L. Chaichana, M. Gathinji, F. J. Attenello, K. Than, A. Olivi, J. D. Weingart, H. Brem, and A. redo Quiñones-Hinojosa, "Independent association of extent of resection with survival in patients with malignant brain astrocytoma," *J. Neurosurg.*, vol. 110, pp. 156–162, jan 2009.

[6] M. Catani and M. Thiebaut de Schotten, "A diffusion tensor imaging tractography atlas for virtual in vivo dissections," *Cortex*, vol. 44, no. 8, pp. 1105–1132, 2008.

[7] B. J. Jellison, A. S. Field, J. Medow, M. Lazar, M. S. Salamat, and A. L. Alexander, "Diffusion Tensor Imaging of Cerebral White Matter: A Pictorial Review of Physics, Fiber Tract Anatomy, and Tumor Imaging Patterns," 2004.

[8] P. J. Basser and C. Pierpaoli, "Microstructural and Physiological Features of Tissues Elucidated by Quantitative-Diffusion-Tensor MRI," vol. 111, pp. 209–219, 1996.

[9] A. J. Asman and B. A. Landman, "Non-local statistical label fusion for multi-atlas segmentation," *Med. Image Anal.*, vol. 17, no. 2, pp. 194–208, 2013.

[10] L. Xu, A. Krzyżak, and C. Y. Suen, "Methods of Combining Multiple Classifiers and Their Applications to Handwriting Recognition," *IEEE Trans. Syst. Man Cybern.*, vol. 22, no. 3, pp. 418–435, 1992.

[11] T. Rohlfing, D. B. Russakoff, and C. R. Maurer, "Performance-based classifier combination in atlas-based image segmentation using expectation-maximization parameter estimation," *IEEE Trans. Med. Imaging*, vol. 23, no. 8, pp. 983–994, 2004.

[12] M. R. Sabuncu, B. T. T. Yeo, K. V. Leemput, B. Fischl, and P. Golland, "A Generative Model for Image Segmentation Based on Label Fusion," *IEEE Trans. Med. Imaging*, vol. 29, no. 10, pp. 1714–1729, 2010.

[13] X. Artaechevarria, A. Muñoz-Barrutia, and C. Ortiz-de Solórzano, "Combination strategies in multi-atlas image segmentation: Application to brain MR data," *IEEE Trans. Med. Imaging*, vol. 28, no. 8, pp. 1266–1277, 2009.

[14] G. Girard, A. Daducci, L. Petit, J. P. Thiran, K. Whittingstall, R. Deriche, D. Wassermann, and M. Descoteaux, "AxTract: Toward microstructure informed tractography," *Hum. Brain Mapp.*, vol. 38, no. 11, pp. 5485–5500, 2017.

[15] E. Caruyer, A. Daducci, M. Descoteaux, J.-C. Houde, J.-P. Thiran, and R. Verma, "Phantomas: a flexible software library to simulate diffusion MR phantoms," *Ismrm*, vol. 17, p. 20013, 2014.

[16] D. S. Tuch, "Q-ball imaging," *Magn. Reson. Med.*, vol. 52, pp. 1358–1372, dec 2004.

[17] J.-D. Tournier, F. Calamante, D. G. Gadian, and A. Connelly, "Direct estimation of the fiber orientation density function from diffusion-weighted MRI data using spherical deconvolution," *Neuroimage*, vol. 23, pp. 1176–1185, nov 2004.

[18] K. V. Mardia and P. E. Jupp, *Directional Statistics*. Wiley, 1999.

[19] L. J. O'Donnell, A. Daducci, D. Wassermann, and C. Lenglet, "Advances in computational and statistical diffusion MRI," *NMR Biomed.*, no. July, p. e3805, 2017.

[20] E. Garyfallidis, M. Brett, B. Amirbekian, A. Rokem, S. van der Walt, M. Descoteaux, and I. Nimmo-Smith, "Dipy, a library for the analysis of diffusion MRI data," *Front. Neuroinform.*, vol. 8, p. 8, feb 2014.

[21] D. Wassermann, N. Makris, Y. Rathi, M. Shenton, R. Kikinis, M. Kubicki, and C.-f. Westin, "The white matter query language: a novel approach for describing human white matter anatomy," *Brain Struct. Funct.*, vol. 221, pp. 4705–4721, dec 2016.

[22] M. Jenkinson, C. F. Beckmann, T. E. Behrens, M. W. Woolrich, and S. M. Smith, "Fsl," *Neuroimage*, vol. 62, no. 2, pp. 782–790, 2012.

[23] M. Kuhn and K. Johnson, *Applied Predictive Modeling*. Springer, 2013.

Part III

Conclusion

Chapter 7
Conclusion

7.1. Overview

In this thesis we tackled the problem of parcellation the brain based on its axonal connectivity, estimated by means of Diffusion MRI. The first contribution we reported is a parcellation technique that creates both single subject and groupwise multi-scale parcellations of the brain [1] based on long range connectivity. Then, we proposed a new method to find correspondence between structural parcellations of different subjects [2]. Finally, we introduced a new label fusion technique to infer the location of white-matter bundles in patients with brain pathology [3]. In this last chapter, we discuss our three contributions in this thesis, and provide some perspectives for the field.

7.2. Discussion

Brain parcellation is a way of dimensionality reduction. Parceling the brain allows to abstract the interaction between billions of neurons into a tractable number of interacting regions. Accumulated evidence suggest that regions with distinct function or cytoarchitecture also possess distinct axonal connectivity [4;5;6;7]. Hence, understanding how the cortex is arranged based on its axonal connectivity could provide key information in unraveling brain organization. This motivates the first contribution of our thesis.

Structural Connectivity Based Parcellation

Our first contribution is a parsimonious model for the long-range axonal connectivity (extrinsic connectivity), and an efficient technique to divide the brain in regions with homogeneous extrinsic connectivity [1]. Our model assumes that the cortex is divided in patches of homogeneous extrinsic connectivity and, using logistic random effects, accounts for intra-patch and across subject variability in the connections.

Leveraging our proposed model, we presented an efficient technique to parcellate the cortex based on its extrinsic connectivity. Our parcellation technique presents many advantages. First, it works directly with the dMRI information, not needing to rely on an initial parcellation. Second, our technique can create both single subject and groupwise parcellations of the whole cortex. Third, inspired by Moreno-Dominguez et al. [8], our technique uses Hierarchical Clustering to comprise multiple granularities of the same parcellation in a dendrogram. This allows us to overcome the need to specify an expected number of clusters. Fourth, thanks to our model, we can retrieve a parcellation from the dendrogram using a simple technique: horizontal cut [9]. Finally, also thanks to our model, our technique works with tractograms in the Euclidean space [10], which allows us to use Ward clustering to compute clusters with minimum intra-cluster variance.

It is important to also point the trade-offs in which our technique incurs. First, our groupwise parcellation technique relies on anatomical seed-correspondence across subjects. Given anatomical differences across-subjects, a purely anatomical matching of seeds is probably suboptimal. However, this allows us to compute single and groupwise parcellations independently, without the need to impose constraints between both. Second, in comparing high-dimensional vectors with the Euclidean distance, we are probably affected by the curse of dimensionality [11]. However, working with the Euclidean distance allows us to generate clusters with minimum intra-cluster variance by means of Ward's Clustering.

The biggest limitations of our technique come from tractography, the tool we used to estimate the brain's extrinsic connectivity. Tractography suffers from at least three problems: gyral bias, distance bias, and false positives. The gyral bias refers to the fact that streamlines tend to terminate preferentially in gyri, in contrast with the general widely distributed connections obtained with tracers [12]. The distance bias reflects that connectivity strength that is usually inferred from tractography tends to decrease with distance between the source and target area [13]. Finally, recent studies show that state-of-the-art tractography algorithms create four times more false positives than true positives [14]. However, these limitations do not imply that tractography is plain wrong [15]. In fact, it has been shown that tractography can recover major white matter bundles [16]. Also, studies found correlation tractography-based tracts and tracer-based ones in Old World monkeys [17].

The most important point to highlight about our parcellation technique, is that it created parcels consistent with brain function. Particularly, some of our parcels showed a high spatial overlap with responses to functional and cognitive tasks measured with functional MRI. This was specially the case with motor functions as hand movement, foot movement and tongue movement. Other cognitive functions that show a good overlap were: face recognition, shape recognition and short-story categorization. These results reflect the strong relationship between

extrinsic connectivity and functional specialization in the human brain cortex.

Something noticeable in our resulting parcels is that the single subject parcellations show big variability across subjects. This is in fact not specific of our methodology, brain parcellations tend to differ in the number, shape, and spatial localization across subjects[13]. This does not necessarily reflect a problem with the parcellation methodology, human brains are different from each other, and "individual variability is not noise"[18]. Studying brain connectivity therefore faces the challenge of locating homogeneous regions while accounting for this variability. This motivates our second contribution.

Matching Structural Parcels Across-Subjects

Our second contribution, is a method to find correspondence between structural parcellations based on Optimal Transport. Given two parcellations, we aim to find the mapping between the parcels in both brains, based on their connectivity fingerprints. Particularly, our method tries to find the optimal way to transport connectivity fingerprints in one brain to the other. In this way, parcels with similar connectivity fingerprints are matched.

Our technique allows matching two parcels based on how they are connected, no matter if they do not spatially overlap after registration. The main advantages of our method is that it is highly performant, and outperforms state-of-the-art matching techniques in our experiments. Using Optimal Transport has an important advantage over existent matching techniques. Existing matching techniques define a similarity (e.g. euclidean or cosine), and match a parcel to that with the most similar connectivity fingerprint. Optimal Transport does the same, while taking into account all the parcels at the same time. In this way, the obtained match is that which maximizes the similarity between parcels globally.

The major limitation of our technique is the necessity to define coherent fingerprints across subjects. In order to compare two connectivity fingerprints, both have to be defined over the same target regions. If the first fingerprint is a 3-dimensional vector representing the connectivity to regions A, B and C, then the second fingerprint must represent the same. This limitation is not specific to our method. All current techniques that we know of have it. However, studies have shown how to define such correspondences, allowing even to match fingerprints across species[19;20].

Inferring White-Matter Tracts in the Presence of Pathology

Our third contribution is a label-fusion techniques that leverages dMRI information in order to infer white matter structures in the brain. We profit of the fact that water particles diffuse along white matter bundles to improve Majority Voting[21]. More specifically, we weight each vote based on how the voted pathway is supported by the target's diffusion data. In this way, voted pathways that better resemble the white matter of the target subject obtain a higher weight.

Our technique presents many advantages. First, our technique can achieve accurate segmentations even when inferring from few subjects. Second, our technique allows inferring white matter pathways without the need of tracking. This is specially important in the presence of diffuse brain pathologies like traumatic brain injuries. Third, while we weight the votes of each tract based on dMRI information, we do not need to register DWIs. Registering DWIs is a highly time consuming task[22]. Instead, we register tracts across subjects and use them to estimate the diffusion information. Fourth, our technique obtains a higher precision than Majority Voting, as a trade-off, our technique possess a lower sensitivity. Meaning, our technique has less false positives at the cost of more true negatives. Fifth, in our simulated experiments, out technique was able to label a tract affected by a local lesion.

As with every label-fusion technique, the main limitation of our technique is the necessity to do registration. While registration of healthy subjects is a well known and studied task, registering subject with severe brain pathologies as tumors is still an open problem. Most registering algorithms fail or return inaccurate registrations, hampered by the pathology[23]. In such cases where the registration is highly inaccurate, our technique will most probably fail.

7.3. Perspectives

We believe that some contributions from the thesis can now be applied to answer more neuroscientific questions. Our parcellation technique divides the brain in regions of homogeneous extrinsic connectivity. This can give a sound basis for studies based on connectivity. One example is the collaboration with Samuel Deslauriers-Gauthier, from Inria. Briefly, we parcelled a subject's cortex based on its extrinsic connectivity and then detect and estimate the information flow between parcels using connectivity and MEG data[24]. Given that information flows through axons, our structural parcellation is suitable to predefine the interconnected regions through which information flows. Another example is the collaboration with Matteo Frigo et al., from Inria. We parcelled 3 subjects and used the resulting parcels to filter false positives streamlines using a functionally informed COMMIT[25]. A final example is our collaboration with Gaston Zanitti, student from the University of Buenos Aires. The aim of our work is to study if specific responses to func-

tional activation measured with fMRI can be predicted using structural connectivity. For this, we define cortical regions with our parcellation technique, and see if the structural connectivity of the vertices within a region can predict its functional activation.

These applications aside, we expect to be able to use our parcellation technique to further characterize the relationship between brain structure and brain function. In particular, in further work we will try to estimate the overlap between our parcels and more functional activations from fMRI. We will also focus on studying the functional properties of the structural networks derived from our parcellation. Meaning, we will study if the structural and functional connections between regions generated by our technique are correlated. As a long term project, we expect that improvements in tractography as well as in dMRI acquisition allow us to infer an atlas of human connections in the brain. We believe this to be a doable yet arduous task, hindered presently by the limitations of tractography.

Our matching technique could have major implications in the study of brain connectivity and its relationship with brain function, allowing for the location of parcels with similar connectivity but not high spatial coherence. Also, it could improve results in the areas where matching techniques are being used. This is, our matching technique could help to better understand the link between different brain atlases, and improve the comparisons of cortical areas between higher primates.

Finally, our label-fusion technique could be use in precision medicine to interrogate diffuse pathologies like traumatic brain injuries, even in the presence of small lesions. Our technique could be used in the study of infiltrative brain tumors, where registration is less of a problem, and in the future, could be extended to larger tumors, due to the growing advances in registration based on tumor growth models.

7.4. Conclusion

In this thesis we tackled the problem of brain parcellation based on structural connectivity. During the whole thesis, We putted emphasis on the importance of the structural connectivity, and how it is strongly related to brain function. However, we fell important to conclude the thesis reminding the reader that, if a universal parcellation of the brain exists, it has not been found yet. Presently, different atlases and techniques to divide the brain coexist, each one with different and disadvantages. At the end, which parcellation to use in practice will heavily depend on the hypothesis and the goal of the study to be done.

Bibliography

[1] G. Gallardo, W. Wells, R. Deriche, and D. Wassermann, "Groupwise structural parcellation of the whole cortex: A logistic random effects model based approach," *Neuroimage*, pp. 1–14, feb 2017.

[2] G. Gallardo, N. Gayraud, R. Deriche, M. Clerc, S. Deslauriers-Gauthier, and D. Wassermann, "Solving the Cross-Subject Parcel Matching Problem Using Optimal Transport," *Med. Image Comput. Comput. Assist. Interv. – MICCAI 2018. Lect. Notes Comput. Sci.*, no. 11070, 2018.

[3] G. Gallardo, B. Sylvain, and D. Wassermann, "Diffusion Driven Label Fusion for White Matter Multi-Atlas Segmentation," *OHBM 2018 - Organ. Hum. Brain Mapp.*, 2018.

[4] R. E. Passingham, K. E. Stephan, and R. Kötter, "The anatomical basis of functional localization in the cortex," *Nat. Rev. Neurosci.*, vol. 3, pp. 606–616, aug 2002.

[5] H. Johansen-Berg, T. E. Behrens, M. D. Robson, I. Drobnjak, M. F. S. Rushworth, J. M. Brady, S. M. Smith, D. J. Higham, and P. M. Matthews, "Changes in connectivity profiles define functionally distinct regions in human medial frontal cortex.," *Proc. Natl. Acad. Sci. U. S. A.*, vol. 101, no. 36, pp. 13335–40, 2004.

[6] C. J. Honey, O. Sporns, L. Cammoun, X. Gigandet, J. P. Thiran, R. Meuli, and P. Hagmann, "Predicting human resting-state functional connectivity," *Proc. Natl. Acad. Sci.*, vol. 106, no. 6, pp. 1–6, 2009.

[7] S. B. Eickhoff, S. Jbabdi, S. Caspers, A. R. Laird, P. T. Fox, K. Zilles, and T. E. J. Behrens, "Anatomical and Functional Connectivity of Cytoarchitectonic Areas within the Human Parietal Operculum," *J. Neurosci.*, vol. 30, no. 18, pp. 6409–6421, 2010.

[8] D. Moreno-Dominguez, A. Anwander, and T. R. Knösche, "A hierarchical method for whole-brain connectivity-based parcellation," *Hum. Brain Mapp.*, vol. 35, pp. 5000–5025, oct 2014.

[9] F. Murtagh and P. Contreras, "Methods of Hierarchical Clustering," *Empir. Econ.*, vol. 38, pp. 23–45, apr 2011.

[10] K. M. Pohl, J. Fisher, S. Bouix, M. Shenton, R. W. McCarley, W. E. L. Grimson, R. Kikinis, and W. M. Wells, "Using the logarithm of odds to define a vector space on probabilistic atlases," *Med. Image Anal.*, vol. 11, pp. 465–477, oct 2007.

[11] K. Beyer, J. Goldstein, R. Ramakrishnan, and U. Shaft, "When is "nearest neighbor" meaningful?," *Database Theory—ICDT'99*, pp. 217–235, 1999.

[12] D. C. Van Essen, S. Jbabdi, S. N. Sotiropoulos, C. Chen, K. Dikranian, T. Coalson, J. Harwell, T. E. Behrens, and M. F. Glasser, "Mapping Connections in Humans and Non-Human Primates," in *Diffus. MRI*, no. January 2014, pp. 337–358, Elsevier, 2014.

[13] S. Jbabdi and T. E. Behrens, "Long-range connectomics," *Ann. N. Y. Acad. Sci.*, vol. 1305, pp. 83–93, dec 2013.

[14] K. H. Maier-hein, P. Neher, J. Christophe, and M. Alexandre, "Tractography - based connectomes are dominated by false - positive connections," *bioRxiv*, pp. 1–23, 2016.

[15] I. Asimov, *The Relativity of Wrong.* Doubleday, 1988.

[16] M. Catani and M. Thiebaut de Schotten, "A diffusion tensor imaging tractography atlas for virtual in vivo dissections," *Cortex*, vol. 44, no. 8, pp. 1105–1132, 2008.

[17] C. J. Donahue, S. N. Sotiropoulos, S. Jbabdi, M. Hernandez-Fernandez, T. E. Behrens, T. B. Dyrby, T. Coalson, H. Kennedy, K. Knoblauch, D. C. Van Essen, and M. F. Glasser, "Using Diffusion Tractography to Predict Cortical Connection Strength and Distance: A Quantitative Comparison with Tracers in the Monkey," *J. Neurosci.*, vol. 36, no. 25, pp. 6758–6770, 2016.

[18] K. Zilles and K. Amunts, "Individual variability is not noise," *Trends Cogn. Sci.*, vol. 17, pp. 153–155, apr 2013.

[19] R. B. Mars, L. Verhagen, T. E. Gladwin, F. X. Neubert, J. Sallet, and M. F. S. Rushworth, "Comparing brains by matching connectivity profiles," *Neurosci. Biobehav. Rev.*, vol. 60, pp. 90–97, 2016.

[20] R. B. Mars, S. N. Sotiropoulos, and R. E. Passingham, "Whole brain comparative anatomy using connectivity blueprints," *bioRxiv*, p. 245209, 2018.

[21] L. Xu, A. Krzyżak, and C. Y. Suen, "Methods of Combining Multiple Classifiers and Their Applications to Handwriting Recognition," *IEEE Trans. Syst. Man Cybern.*, vol. 22, no. 3, pp. 418–435, 1992.

[22] L. J. O'Donnell, A. Daducci, D. Wassermann, and C. Lenglet, "Advances in computational and statistical diffusion MRI," *NMR Biomed.*, no. July, p. e3805, 2017.

[23] E. S. Lutkenhoff, M. Rosenberg, J. Chiang, and K. Zhang, "Optimized Brain Extraction for Pathological Brains (optiBET)," *PLoS One*, pp. 1–13, 2014.

[24] G. Gallardo, D. Wassermann, R. Deriche, M. Descoteaux, and S. Deslauriers-Gauthier, "Information Flow in the White Matter During a Motor Task: A Structural Connectivity Driven Approach," in *Organ. Hum. Brain Mapp. Annu. Meet.*, 2017.

[25] M. Frigo, G. Gallardo, I. Costantini, A. Daducci, D. Wassermann, R. Deriche, and S. Deslauriers-Gauthier, "Reducing false positive connection in tractograms using joint structure-function filtering," in *Organ. Hum. Brain Mapp.*, 2018.